A Framework for Understanding Heterogeneous Differentiation of $CD4^+$ T Cells

Tian Hong

Dissertation submitted to the faculty of the Virginia Polytechnic Institute and State University in partial fulfillment of the requirements for the degree of

Doctor of Philosophy

In

Genetics, Bioinformatics and Computational Biology

John J. Tyson, Chair

Liwu Li

T. M. Murali

Jianhua Xing

Lijuan Yuan

July 10, 2013

Blacksburg, VA

Keywords: $CD4^+$ T cells, mathematical model, cell differentiation

A Framework for Understanding Heterogeneous Differentiation of $CD4^+$ T Cells

Tian Hong

ABSTRACT

$CD4^+$ T cells are a group of lymphocytes that play critical roles in the immune system. By releasing cytokines, $CD4^+$ T cells regulate other immune cells for maximizing the efficiency of the system. Naïve $CD4^+$ T cells are activated and become mature upon engagement with antigens, and the mature $CD4^+$ T cells have several subsets, which play diverse regulatory functions. For the past two decades, our understanding of $CD4^+$ T cells has been advanced through the studies on the differentiation process and the lineage specification of various subsets of these cells.

Although in most experimental studies of $CD4^+$ T cells, researchers focused on how transcription factors and signaling molecules influence the differentiation of a particular subset of these cells, many evidence have shown that the differentiation of $CD4^+$ T cells can be heterogeneous in terms of the phenotypes of the cells involved. This dissertation describes a framework that uses mathematical models of the dynamics of the signaling pathways to explain heterogeneous differentiation. We show that the mutual inhibitions among the master regulators govern the formation of multi-stability behavior, which in turn gives rise to heterogeneous differentiation. The framework can be applied to systems with two or more master regulators, and models based on the framework can make specific predictions about heterogeneous differentiations.

In addition, this dissertation describes an experimental study on $CD4^+$ T cell differentiation. Being part of the adaptive immune system, the differentiation of $CD4^+$ T cells was previously known to be induced by the signals from the innate immune cells. However, the expression of

Toll-like receptor in $CD4^+$ T cells suggests that microbial products can also influence the differentiation directly. Using an *in vitro* cell differentiation approach, we show that the differentiation and proliferation of $CD4^+$ T cells can be influenced by lipopolysaccharide under the condition that would favor the differentiation of induced regulatory T cells.

These theoretical and experimental studies give novel insights on how $CD4^+$ T cells differentiate in response to pathogenic challenges, and help to gain deeper understanding of regulatory mechanisms of the complex immune system.

We live only to discover beauty. All else is a form of waiting.

– Kahlil Gibran

ACKNOWLEDGEMENTS

This dissertation would have not been possible without the help, support and guidance of my committee, friends, family and many other people. It is with great pleasure and gratitude that I acknowledge their efforts.

I would like to thank my committee chair and my advisor Dr. John J. Tyson for instilling me qualities of being a good scientist. His intellectual insights on systems biology and excitement on teaching have been major driving forces throughout my doctoral training. I thank my committee member Dr. Jianhua Xing, who has been supporting me since my first day of the GBCB program with his intellectual richness, particularly on the topic of phenotypic heterogeneity of the cells. I thank my committee member Dr. Liwu Li, who has been generously supporting me with his resources and expertise on experimental training, and sharing his abundant knowledge on immunology with me. Most parts of this dissertation stem from the far-sighted discussion among Dr. Tyson, Dr. Xing and Dr. Li. I thank my committee member Dr. T. M. Murali, who has taught me techniques of computer science and offered me priceless advice on future careers of systems biology. I thank my committee member Dr. Lijuan Yuan, who has shared her valuable insights on immunology and experimental data from her laboratory with me.

I would like to thank Dr. David Bevan for being a respectable and caring leader of the GBCB program. I thank Ms. Dennie Munson, who has being a tremendous help for my life in the program.

I thank all members from Dr. Tyson, Dr. Xing and Dr. Li's research groups for helpful discussions and accompany. In particular, I thank Dr. Kathy Chen for the encouragement and suggestions she has offered to me, and I thank Dr. Yan Fu for discussions on modeling immune systems and her initial works on T cell models.

I thank Dr. Curtis Davey, my previous advisor at Nanyang Technological University, Singapore, for showing me the excitement and joy of doing scientific research. I thank Dr. Yuguang Mu, my advisor during my undergraduate training in Singapore, for offering me my first opportunity to learn techniques in computational biology.

I thank Dr. Jonathan Widom, a late professor at Northwestern University. His pioneering work inspired me to study computational biology in a graduate program.

I thank Dr. Robert Clewley at Georgia State University for developing PyDSTool, an excellent software package for simulating and analyzing dynamic systems. I thank Mr. John Hunter, who is the creator of Matplotlib, a python library designed for scientific plotting. These works made my life in graduate school much easier and more enjoyable.

I thank all my friends who helped me through the difficult times when I was suffering from health problems. Finally, I would like to thank my family – my mother Xiaorong Zheng and my father Xing Hong for their love, encouragement and support during my doctoral training.

ATTRIBUTION

Chapters 2 and 3 of this dissertation are published research articles.

Chapter 2 ‘A Mathematical Model for the Reciprocal Differentiation of T Helper 17 Cells and Induced Regulatory T cells’ is an article published in PLoS Computational Biology (2011, 7:e1002122)

Chapter 3 ‘A simple theoretical framework for understanding heterogeneous differentiation of $CD4^+$ T cells’ is an article published in BMC Systems Biology (2012, 6: 66)

On both Chapters 2 and 3, Dr. Jianhua Xing (an associate professor in the Department Biological Sciences at Virginia Tech), Dr. Liwu Li (a professor in the Department Biological Sciences at Virginia Tech) and Dr. John J. Tyson (a professor in the Department Biological Sciences at Virginia Tech) are co-authors. For both chapters, Dr. Xing, Dr. Li and Dr. Tyson contributed to conceiving the study and analyzing the data. Dr. Li and Dr. Tyson also contributed to the manuscript writing.

TABLE OF CONTENTS

LIST OF FIGURES

Chapter 2

Chapter 3

Chapter 4

Chapter 5

LIST OF TABLES

Chapter 2

Chapter 3

Chapter 4

CHAPTER 1

INTRODUCTION

The immune system protects the host from diseases by detecting and removing various types of pathogens, including viruses, bacteria, parasites, infected host cells and tumors. In order to perform these functions, the immune system has a wide variety of professional immune cells, known as leukocytes, or while blood cells. Different types of leukocytes have distinct roles in the system. For example, macrophages engulf and digest cell debris and pathogens; B cells release antibodies to neutralize and help the detection of pathogens; $CD8^+$ T cells kill infected cells [1]. To help to coordinate these activities, the immune system also evolved a group of regulatory cells, known as $CD4^+$ T cells. $CD4^+$ T cells can maximize the activity of macrophages, help the antibody production by B cells, and activate $CD8^+$ T cells. Moreover, they are responsible for modulating the immune activity to avoid excessive inflammatory responses, in order to protect healthy host tissues [1]. $CD4^+$ T cells perform their regulatory functions by releasing signaling molecules called cytokines. Depending on their functions and cytokine profiles, $CD4^+$ T cells can be further classified into several subsets, including T helper 1 (T_H1), T helper 2 (T_H2), T helper 17 (T_H17) and induced regulatory T (iT_{Reg}) cells [2]. Each subset of the $CD4^+$ T cells has a key transcription factor, known as a master regulator, which determines its lineage specification [3]. These subsets of cells are differentiated from a common type of precursor cells, known as naïve $CD4^+$ T cells, in peripheral tissues such as lymph nodes, and the differentiated $CD4^+$ T cells play diverse and essential roles in the immune system [2]. Studying the differentiation of $CD4^+$ T cells is critical for understanding the regulatory machineries of the immune system.

In order to understand the differentiation of $CD4^+$ T cells, it is important to identify the environmental cues that influence the differentiation of $CD4^+$ T cells. Many previous experimental studies focused on cytokines that regulate the differentiation [3,4], and these studies have shown how pathogens can influence the differentiation via the activation of cytokine-releasing cells. To further our understanding of

the extracellular regulators of $CD4^+$ cells, we asked whether microbial products can influence the differentiation of $CD4^+$ T cells directly. In this dissertation, we demonstrated that (lipopolysaccharide) LPS can influence both differentiation and proliferation of $CD4^+$ T cells under the inducing condition for iT_{Reg} cells, and the results are described in Chapter 5 of this dissertation.

Equally important is to understand how populations of naïve $CD4^+$ T cells differentiate upon pathogenic challenges. It has been shown that the differentiation of $CD4^+$ T cells can be heterogeneous both *in vivo* and *in vitro*. In other words, more than one phenotypes of $CD4^+$ T cells can be derived from a population of naïve $CD4^+$ T cells in a single differentiation event [5-8]. Chapters 2, 3 and 4 of this dissertation are about how one could understand this type of phenomena from the viewpoint of systems biology. We provide a mathematical basis for heterogeneous differentiation and specific models for $CD4^+$ T cells in these chapters.

Mathematical modeling has been applied to the field of $CD4^+$ T cells to help the understanding of their complex behaviors. Early works mainly focused on the interactions among different subsets of cells [9,10]. After the identification of the key intracellular molecules involved in the $CD4^+$ T cell differentiation, mathematical models were developed to study dynamics the signaling pathways of these cells [11-17]. Most of these models were aimed to study the robustness of lineage specifications, and none of them provided explanations for heterogeneous differentiation. This dissertation presents a framework that can explain both robust lineage commitment of a single cell and heterogeneous differentiation of a cell population. Chapter 2 of the dissertation is on a specific model of T_H17 and iT_{Reg} development, which involves heterogeneous differentiation. Chapter 3 provides a more general framework for understanding heterogeneous differentiation involving two master regulators. Chapter 4 proposes a framework for understanding heterogeneous differentiation involving three or four master regulators. This framework helps the understanding of how the $CD4^+$ T cells can be diversified with simple environmental cues, how the balance of these cell types can be broken, and how the interactions among the master regulators and other signaling molecules play a role in heterogeneous differentiation. These results take us one step

further towards linking a model of intracellular signaling pathways to the models of populations of immune cells.

References

1. Janeway CA, Travers P, Walport M, Shlomchik MJ (2001) Immunobiology, 5th edition. New York: Garland Science.

2. Zhu J, Yamane H, Paul WE (2010) Differentiation of effector CD4 T cell populations. Annu Rev Immunol 28: 445-489.

3. Zhu J, Paul WE (2010) Peripheral CD4+ T-cell differentiation regulated by networks of cytokines and transcription factors. Immunol Rev 238: 247-262.

4. O'Garra A (1998) Cytokines induce the development of functionally heterogeneous T helper cell subsets. Immunity 8: 275-283.

5. Yamashita M, Kimura M, Kubo M, Shimizu C, Tada T, et al. (1999) T cell antigen receptor-mediated activation of the Ras/mitogen-activated protein kinase pathway controls interleukin 4 receptor function and type-2 helper T cell differentiation. Proc Natl Acad Sci U S A 96: 1024-1029.

6. Lochner M, Peduto L, Cherrier M, Sawa S, Langa F, et al. (2008) In vivo equilibrium of proinflammatory IL-17+ and regulatory IL-10+ Foxp3+ RORgamma t+ T cells. J Exp Med 205: 1381-1393.

7. Zhou L, Lopes JE, Chong MM, Ivanov, II, Min R, et al. (2008) TGF-beta-induced Foxp3 inhibits T(H)17 cell differentiation by antagonizing RORgammat function. Nature 453: 236-240.

8. Ghoreschi K, Laurence A, Yang XP, Tato CM, McGeachy MJ, et al. (2010) Generation of pathogenic T(H)17 cells in the absence of TGF-beta signalling. Nature 467: 967-971.

9. Fishman MA, Perelson AS (1993) Modeling T cell-antigen presenting cell interactions. J Theor Biol 160: 311-342.

10. Fishman MA, Perelson AS (1994) Th1/Th2 cross regulation. J Theor Biol 170: 25-56.

11. Höfer T, Nathansen H, Löhning M, Radbruch A, Heinrich R (2002) GATA-3 transcriptional imprinting in Th2 lymphocytes: a mathematical model. Proc Natl Acad Sci U S A 99: 9364-9368.

12. Mariani L, Löhning M, Radbruch A, Höfer T (2004) Transcriptional control networks of cell differentiation: insights from helper T lymphocytes. Prog Biophys Mol Biol 86: 45-76.

13. Yates A, Callard R, Stark J (2004) Combining cytokine signalling with T-bet and GATA-3 regulation in Th1 and Th2 differentiation: a model for cellular decision-making. J Theor Biol 231: 181-196.

14. Mendoza L (2006) A network model for the control of the differentiation process in Th cells. Bio Systems 84: 101-114.

15. Callard RE (2007) Decision-making by the immune response. Immunol Cell Biol 85: 300-305.

16. van den Ham H-J, de Boer RJ (2008) From the two-dimensional Th1 and Th2 phenotypes to high-dimensional models for gene regulation. Int Immunol 20: 1269-1277.

17. Naldi A, Carneiro J, Chaouiya C, Thieffry D (2010) Diversity and plasticity of Th cell types predicted from regulatory network modelling. PLoS Comput Biol 6: e1000912.

CHAPTER 2

A Mathematical Model for the Reciprocal Differentiation of T Helper 17 Cells and Induced Regulatory T cells

A research article published in PLoS Computational Biology in 2011 (2011, 7:e1002122).

Tian Hong[1], Jianhua Xing[2], Liwu Li[2] and John J. Tyson[2]*

1. Genetics, Bioinformatics, and Computational Biology Program, Virginia Polytechnic Institute and State University, Blacksburg, VA, 24061, USA.
2. Department of Biological Sciences, Virginia Polytechnic Institute and State University, Blacksburg, VA, 24061, USA.

* To whom correspondence should be addressed. E-mail: tyson@vt.edu

Abstract

The reciprocal differentiation of T helper 17 (T_H17) cells and induced regulatory T (iT_{reg}) cells plays a critical role in both the pathogenesis and resolution of diverse human inflammatory diseases. Although initial studies suggested a stable commitment to either the T_H17 or the iT_{reg} lineage, recent results reveal remarkable plasticity and heterogeneity, reflected in the capacity of differentiated effectors cells to be reprogrammed among T_H17 and iT_{reg} lineages and the intriguing phenomenon that a group of naïve precursor $CD4^+$ T cells can be programmed into phenotypically diverse populations by the same differentiation signal, transforming growth factor beta. To reconcile these observations, we have built a mathematical model of T_H17/iT_{reg} differentiation that exhibits four different stable steady states, governed by pitchfork bifurcations with certain degrees of broken symmetry. According to the model, a group of precursor cells with some small cell-to-cell variability can differentiate into phenotypically distinct subsets of cells, which exhibit distinct levels of the master transcription-factor regulators for the two T cell lineages. A dynamical control system with these properties is flexible enough to be steered down alternative pathways by polarizing signals, such as interleukin-6 and retinoic acid and it may be used by the immune system to generate functionally distinct effector cells in desired fractions in response to a range of differentiation signals. Additionally, the model suggests a quantitative explanation for the phenotype with high expression levels of both master regulators. This phenotype corresponds to a re-stabilized co-expressing state, appearing at a late stage of differentiation, rather than a bipotent precursor state observed under some other circumstances. Our simulations reconcile most published experimental observations and predict novel differentiation states as well as transitions among different phenotypes that have not yet been observed experimentally.

Authors' Summary

In order to perform complex functions upon pathogenic challenges, the immune system needs to efficiently deploy a repertoire of specialized cells by inducing the differentiation of precursor cells into effector cells. In a critical process of the adaptive immune system, one common type of precursor cell can give rise to both T helper 17 cells and regulatory T cells, which have distinct phenotypes and functions. Recent discoveries have revealed a certain heterogeneity in this reciprocal differentiation system. In particular, treating precursor cells with a single differentiation signal can result in a remarkably diverse population. An understanding of such variable responses is limited by a lack of quantitative models. Our mathematical model of this cell differentiation system reveals how the control system generates phenotypic diversity and how its final state can be regulated by various signals. The model suggests a new quantitative explanation for the scenario in which the master regulators of two different T cell lineages can be highly expressed in a single cell. The model provides a new framework for understanding the dynamic properties of this type of regulatory network and the mechanisms that help to maintain a balance of effector cells during the inflammatory response to infection.

Introduction

$CD4^+$ T cells are important components of the adaptive immune system in higher vertebrates. By producing various cytokines, they perform critical functions such as helping B cells to produce antibodies, activating $CD8^+$ cytotoxic T cells, enhancing the innate immune system, and suppressing the immune response to avoid autoimmunity [1-3]. In peripheral tissues, such as lymph nodes, blood and sites of infection, antigen-inexperienced (naïve) $CD4^+$ T cells can differentiate into effector cells of specialized phenotypes upon stimulation by cognate antigen delivered to the T cell receptor by Antigen Presenting Cells (APCs). Proliferation and differentiation of activated naïve T cells depends on their particular cytokine microenvironment. These specialized effector T cells produce distinct cytokine profiles tailored for their specialized functions. Also, they express lineage-defining transcription factors ("master regulators"). In general, high expression level of a particular master regulator is observed only in cells of a particular lineage, and the overexpression of a particular master regulator induces the production of the corresponding lineage-defining cytokines [4,5].

The fate of a naïve $CD4^+$ T cell was traditionally thought to be either T helper 1 (T_H1) cell or T helper 2 (T_H2) cell [6]. In the last decade, a third type of T helper cell (T_H17), derived from naïve $CD4^+$ T cells, was discovered [7]. T_H17 cells produce IL-17A, IL-17F and IL-22 as their lineage-defining cytokines, and the retinoid-related orphan receptor gamma t (RORγt) transcription factor is considered the master regulator of this lineage [8,9]. In addition, naïve $CD4^+$ T cells were found to be able to differentiate into a fourth lineage of (regulatory) T cells, which were called induced regulatory T (iT_{reg}) cells to distinguish them from natural regulatory T (nT_{reg}) cells, which differentiate in the thymus instead of the periphery [10]. iTreg cells are characterized by producing IL-10 and transforming growth factor-β (TGF-β) and highly expressing forkhead box P3 (Foxp3) transcription factor as their master regulator [11]. T_H17 cells are pro-inflammatory because they secret cytokines that promote inflammation, whereas iT_{reg} cells are anti-inflammatory because their lineage-defining cytokines can reduce the inflammatory response.

The differentiation pathways of naïve T cells into T_H17 and iT_{reg} lineages are closely related. First, stimulation by TGF-β is necessary for the differentiation of both lineages [12]. The differentiation of T_H17 and iT_{reg} cells are reciprocally regulated in the presence of TGF-β, i.e. inhibiting the differentiation pathway of one lineage will result in activation of the pathway for the other lineage. This is due to the mutual antagonism between RORγt and Foxp3. Furthermore, polarizing signals, such as interleukin-6 (IL-6) and retinoic acid, can induce the differentiation of one lineage and repress that of the other one [12]. Nonetheless, differentiated iT_{reg} cells can be reprogrammed into T_H17 cells in an appropriate cytokine environment [13], suggesting significant plasticity of these two lineages. In addition, stable co-expression of their master regulators (RORγt and Foxp3) is observed both *in vivo* and *in vitro* [14,15]. Interestingly, these double-expressing cells were found to possess either regulatory or dual (regulatory and proinflammatory) functions *in vivo* [14,15].

Perhaps the most intriguing phenomenon is that antigen-activated naïve $CD4^+$ T cells treated with TGF-β alone give rise to a heterogeneous population, which may include three phenotypes (Foxp3-only, RORγt-only, and double-expressing cells) at an intermediate TGF-β concentration [16], or two phenotypes (RORγt-only and double-expressing cells) at a higher TGF-β concentration[15]. In combination with TGF-β, IL-6 can induce the differentiation of RORγt expressing cells, whereas all-*trans* retinoic acid (ATRA) can induce the differentiation of Foxp3 expressing cells [16,17] (Figure 1). All of these *in vitro* derived phenotypes can be observed *in vivo*, and at least some of their respective functions have been demonstrated, suggesting that these *in vitro* differentiation assays provide important clues to our understanding of the development of T_H17 and iT_{reg} cells in the body.

Mathematical modeling has contributed to our understanding of the differentiation of T_H1 and T_H2 cells [18-24]. Höfer et al. first demonstrated that the dynamics of the key transcription factors can govern the robustness of the lineage choice and maintenance [18,19]. Yates et al. later related transcription factor dynamics to the mix of T_H1 and T_H2 cells in a population of differentiating T cells [20]. Recently, Naldi et al. [25] have proposed a Boolean-network model of the comprehensive repertoire of $CD4^+$ T cell

phenotypes, including T_H17 and iT_{reg} cells. Drawing inspiration from these earlier models, we have sought to explain, with a computational model, the remarkable heterogeneity of the T_H17-iT_{reg} reciprocal-differentiation system.

In terms of this model, we show that a population of naïve $CD4^+$ T cells, with some small cell-to-cell variability, can differentiate into a heterogeneous population of effector cells with distinct phenotypes upon treatment with the primary differentiation signal (TGF-β). Polarizing signals, such as IL-6 and ATRA, can skew the differentiation to one or two phenotypes. A control system with these properties can generate functional diversity of the induced cell populations and can be regulated with great flexibility by diverse environmental cues. In addition, the model suggests how treatment with different concentrations of TGF-β may favor different responding phenotypes, and how conversions among these phenotypes may be guided. Finally, the model gives a new quantitative explanation for double-expressing cells, suggesting that they are 're-stabilized co-expressing' cells rather than transient intermediate cells in the differentiation pathway. The model predicts that double-expressing cells should appear at a relatively late stage of the differentiation process, and they may be intended for specific functions. In all, our model provides a novel mathematical framework for understanding this reciprocal differentiation system, and it gives new insights into the regulatory mechanisms that underlie the molecular control of certain immune responses.

Results

A model with symmetrical interactions predicts three differentiated phenotypes of CD4$^+$ T cells induced by TGF-β.

To illustrate our basic idea, we first construct a model of a simple and perfectly symmetrical regulatory network (Figure 2A). In the Methods section we describe how this network is converted into a pair of nonlinear ordinary differential equations (ODEs) for the time rates of change of Foxp3 and RORγt. The rate functions for this model contain 12 kinetic parameters, whose basal values are specified in the Methods section (Table 1) for the "symmetrical model without intermediates". The solution of these ODEs for the basal values, and with [TGF-β] = 0, evolves to a stable steady state where both RORγt and Foxp3 have a low level of expression (RORγt^{low}Foxp3^{low}). This steady state corresponds to a naïve CD4$^+$ T cell (Figure 3A). In the presence of a sufficient TGF-β signal, the regulatory network might evolve to one of three other steady states, namely RORγt^{high}Foxp3^{low}, RORγt^{low}Foxp3^{high} and RORγt^{high}Foxp3^{high} states, corresponding to RORγt-only, Foxp3-only and double-expressing phenotypes. Note that these stable steady states are also referred as 'cell fate attractors' in some other studies, and this concept facilitates our understanding of cell lineage choice and reprogramming (reviewed in [26]). Figure 3B shows a scenario in which the TGF-β signal triggers the formation of a tri-stable system. In this particular case, the RORγt^{low}Foxp3^{low} state is no longer a stable steady state, and naïve cell, which was previously stabilized in the RORγt^{low}Foxp3^{low} state, would differentiate into the RORγt^{high}Foxp3^{high} state, whose basin of attraction (the white region in Figure 2B) contains the naïve state of the cell.

However, cell-to-cell variability can produce other results. We interpret cell-to-cell-variability as small deviations of the parameter values from their basal settings in Table 1. The basal settings correspond to the behavior of an "average" cell, but any particular cell will deviate somewhat from this average behavior. As consequences of the changing parameter values in any particular cell, the position of the RORγt^{low}Foxp3^{low} state changes, the boundaries of the basins of attractions change, and the fate of the

naïve cell may change. The naïve T cell will differentiate into the stable steady state in whose basin of attraction it lies. That is, depending on the precise parameter values of the cell, its RORγt^{low}Foxp3^{low} state may lie in any of the three basins of attraction of the TGF-β-stimulated system. Figure 3C depicts three cells in the population that adopt three different fates because of the variability among them. With a random sample of cells, each of the three differentiated states can be populated by a significant fraction of cells (Figure 3D). Although cell-to-cell variability does not make large changes in the position of the RORγt^{low}Foxp3^{low} state, it has a dramatic influence on the basins of attraction of the stable steady states, which determines the fate of the cell once the differentiation signal is turned on.

Since the system has four distinct steady states that correspond to four distinct phenotypes, we next looked for the relationships among these steady states using bifurcation analysis of an average cell. Because of the symmetrical nature of the interactions, an average cell exhibits sub-critical pitchfork bifurcations with TGF-β concentration as the control parameter (Figure 4A). (The notion of a pitchfork bifurcation was used earlier, in references [27,28], to explain a system of hematopoietic cell differentiation in which multiple lineages might be adopted.) Notably, the RORγt^{low}Foxp3^{low} state is only stable at low TGF-β concentration. At an intermediate concentration of TGF-β (~0.25 units in Figure 3A), the system bifurcates into two lineage-specific branches, corresponding to RORγt^{high}Foxp3^{low} and RORγt^{low}Foxp3^{high} states. The fourth type of stable steady state (RORγt^{high}Foxp3^{high}) appears at higher TGF-β signal strength (> 0.37 in Figure 3A), when the autoactivation of RORγt and Foxp3 eventually overrides their mutual inhibition and makes the double-expressing state the dominant phenotype of the population.

We next checked the influence of TGF-β concentration on the fractions of responding phenotypes in a population of induced cells. For various values of [TGF-β], we simulated a population of naïve CD4$^+$ T cells with cell-to-cell variability. In agreement with the bifurcation analysis, RORγt^{high}Foxp3^{low} and RORγt^{low}Foxp3^{high} cells appeared simultaneously over an intermediate range of [TGF-β] (between ~0.2 and ~0.55 units). The fraction of RORγt^{high}Foxp3^{high} cells increases at higher TGF-β concentrations and

eventually dominates the population when [TGF-β] > 0.55. In the vicinity of 0.5 units of TGF-β, the cell population is heterogeneous, with comparable fractions of all three stable phenotypes (Figure 4A lower panel).

Although this initial model accommodates the presence of dual-positive T_H17/iT_{reg} cells, it cannot fully explain the fine regulatory effects of varying TGF-β concentrations. For example, this model predicts that double-expressing cells dominate the population when TGF-β concentration is high, and that single-expressing cells may be converted into double-expressing cells by increasing [TGF-β]. In fact, this is not necessarily true if the effects of TGF-β saturate at high [TGF-β]. To take saturation effects into account, we incorporated two intermediate signaling proteins between TGF-β and the transcription factors Foxp3 and RORγt (Figure 2B). In this case, the system can be tri-stable even at high concentrations of TGF-β, and the total conversion of single-expressing cells into double-expressing cells would not occur. Instead, co-existence of the three phenotypes in comparable fractions might be observed over a wide range of [TGF-β] (Figure 4B).

A model with asymmetrical interactions provides a better account of the regulatory functions of TGF-β during the coupled differentiation of T_H17 and iT_{reg} cells.

We next considered an asymmetrical model in which the network topology and parameter values differ from the symmetrical model. In the model with perfect symmetry, we assumed that the inhibitions between Foxp3 and RORγt are equally strong, which is not supported by existing experimental evidence. In fact, Foxp3 is better known for its inhibitory function on IL-17, a downstream effector of RORγt, as demonstrated by Williams and Rudensky [29]. Therefore, we revised our model by removing the direct inhibition of RORγt expression by Foxp3 and adding the inhibition of IL-17 expression by Foxp3. This revised model, with broken symmetry (Figure 2C, Table 1-last column, and Figure 3C) shows some new features. First, RORγt behaves ultrasensitively in response to varying [TGF-β] because of RORγt's

positive (autoregulatory) feedback loop. Secondly, Foxp3 exhibits multiple saddle-node bifurcations derived from the broken symmetries of the pitchforks. Interestingly, the four types of stable steady states observed with the symmetrical model have been retained for Foxp3, and thus for the entire system. In fact, by varying [TGF-β], it is possible to obtain all three differentiated phenotypes in significant fractions simultaneously. Doing the same analysis for the effect of [TGF-β] on the induced cell population (Figure 4C lower panel), we found that the asymmetrical model behaved similarly to the symmetrical model. At low [TGF-β], Foxp3 single-positive cells are predicted to be the dominant cell type. As [TGF-β] increases to intermediate or high levels, the RORγt single-positive cells and the double-positive cells should appear and co-exist.

These simulation results are in agreement with recently published experimental data documenting the differential effects of TGF-β on the differentiation of T_H17 and iT_{reg} cells [16]. Indeed, at certain intermediate concentrations of TGF-β, three phenotypes in comparable fractions have been observed [16]. In addition, the maximum percentage of Foxp3 single-positive cells was observed at some lower concentration of TGF-β. As [TGF-β] was increased, the percentage of Foxp3 single-positive cells decreased, accompanied by a concordant rise in the percentage of RORγt-expressing cells [16]. At higher concentrations of TGF-β, RORγt-only cells and double-expressing cells were found to coexist in comparable percentages [15].

Our model not only validates existing published data on the coexistence of two or more phenotypes in mixed T helper cell populations but also predicts that increasing TGF-β concentration will cause the transformation of Foxp3 single-positive cells into RORγt-expressing cells. Conversely, decreasing TGF-β concentration might result in the reverse transformation.

Our model accommodates the observed effect of IL-6 skewing T cells into a 'RORγt-only' phenotype.

We next simulated the influence of IL-6 on this reciprocal differentiation system. In the asymmetrical model (Figure 3C), IL-6 activates STAT3, which favors production of RORγt over Foxp3. In this model, IL-6 will not trigger differentiation in the absence of TGF-β. However, IL-6 significantly increases the fraction of RORγt-only cells over a wide range of TGF-β concentrations (Figure 4A). Also, it stimulates some of the cells in the (simulated) population to produce IL-17. These results are consistent with the observations of a few groups [13,16]. In particular, Zhou et al. observed that low level TGF-β favors the RORγt-only phenotype and IL-17 production, whereas higher concentrations of TGF-β inhibit the production of IL-17. They also reported that the decrease of IL-17 production at higher TGF-β concentration is accompanied by an increase of Foxp3-expressing cells. We see this phenomenon in our simulation, and we further suggest that the decrease of RORγt-only cells, or the increase of the double-expressing cells, accounts for the reduced production of IL-17 at high TGF-β concentration, because double-expressing cells are known to be much less effective in producing IL-17 than the RORγt-only cells, at least in this type of *in vitro* assay with TGF-β and IL-6 [15,16]. However, Zhou et al. observed a pronounced inhibition of IL-17 production at higher TGF-β concentration even when Foxp3 expression had not been remarkably raised [16]. This discrepancy suggests that high TGF-β level may trigger Foxp3-independent repression of IL-17 production.

Both the observations by Zhou et al. and our simulations demonstrate that only a minor fraction of RORγt-only cells exhibit IL-17 production even in the presence of IL-6. In fact, this is not an idiosyncratic phenomenon. Mariani et al. recently discovered that only a subset of T_H2 cells produce IL-4 due to cell-to-cell variability [30], suggesting that the production of lineage-specific cytokines in T helper cells can be controlled by stochastic mechanisms.

Our model accommodates the effect of ATRA skewing T cells into a Foxp3-expressing phenotype.

In the asymmetrical model (Figure 3C), ATRA favors production of Foxp3 over RORγt. Hence, in our simulation of TGF-β + ATRA stimulation, we found that the percentage of Foxp3-only cells and double-expressing cells significantly increased as compared to TGF-β alone (compare Figure 4B to Figure 3C). Like IL-6, ATRA did not trigger differentiation by itself. We next checked if ATRA can suppress the polarizing effect of IL-6. In our simulation, ATRA was effective in reducing the IL-6 induced production of IL-17. In addition, at high TGF-β concentration, ATRA significantly decreased the percentage of RORγt-only cells, and resulted in a population with comparable fractions of RORγt-only cells and double-expressing cells (Figure 5C). All of these simulation results are consistent with published data [13,15,17,31]. Our model suggests that ATRA can significantly increase the percentage of Foxp3-only cells at intermediate TGF-β concentration, and the percentage of double-expressing cells at high TGF-β concentration.

Our model predicts that IL-6 may reprogram iT_{reg} cells to IL-17 producing cells, while ATRA may prevent this reprogramming effect

With our model, we next checked whether IL-6 could reprogram differentiated iT_{reg} cells into T_H17 cells. We first induced a population of naïve $CD4^+$ T cells to differentiate into a population dominated by 'Foxp3-only' cells with an intermediate level of TGF-β (0.28 units). After the cells came to their Foxp3-only steady state, we raised the IL-6 signal to 10 units and continued the simulation. We found that almost all the cells expressing Foxp3 before adding IL-6 stopped producing Foxp3 upon the treatment with IL-6, and a subset of 'RORγt-only' cells dominated the population. A fraction of these RORγt-only cells produced IL-17 (Figure 6A, left panel)

When we induced the differentiation of iT_{reg} cells with TGF-β + ATRA and performed the same reprogramming simulation, we found that ATRA did not prevent the repression of Foxp3 expression by IL-6 significantly. However, ATRA prevented the formation of IL-17 producing cells (Figure 6A, right

panel). The reprogramming capability of IL-6 and the inhibitory effect of ATRA have been observed by Yang et al. [13].

Analyzing the concentration dependence of these reprogramming effects, we found that a high level of IL-6 may exclusively down-regulate Foxp3 expression (Figure 6B, left panel) whereas a high level of ATRA may predominantly prevent IL-17 expression (Figure 6B, right panel). Interestingly, when both of these factors are present in high concentration, our model predicts that, although most cells exhibit high expression of RORγt, there are almost no IL-17-producing cells in the population. Future experimental studies are warranted to confirm these intriguing predictions.

Table **1**2 summarizes the observations that are in agreement with our simulation results and the testable predictions that we have made based on the bifurcation analyses and signal-response curves.

Discussion

Previous mathematical models have shown how differentiation signals can trigger a robust switch during the development of T_H1 or T_H2 cells [18-24]. In particular, earlier modeling studies by Höfer et al. demonstrated how the interactions among transcription factors can create a memory for T_H2 lineage commitment and govern the choice of T_H1 and T_H2 lineages [18,19]. These studies focused on the dynamics of transcription factors within a single (average) cell, but the authors also pointed out that cell-to-cell variability in a $CD4^+$ T cell population can be modeled mathematically by introducing parametric variations to the ordinary differential equations (ODEs). In addition to modeling molecular interactions, the study by Yates et al. related the dynamics of transcription factors to the phenotypic composition of T_H1 and T_H2 cell populations [20]. The authors built comprehensive ODE-based models which take into account cell proliferation, intercellular communication, and cell-to-cell variability. Yates et al. modeled cell-to-cell variability by variations in initial conditions, but we consider parametric variations to be a more important source of cell-to-cell variability (see Methods).

The reciprocal differentiation of T_H17 and iT_{reg} cells, although a relatively new research field, has already been shown to exhibit many interesting and unique features, and yet it has not been studied in quantitative detail using mathematical models. The work presented here reveals some of the intriguing regulatory mechanisms of this differentiation system. We showed that the four phenotypes of cells, corresponding to four different steady states of the dynamical system, are derived from a pitchfork bifurcation with certain degree of broken symmetry. A single primary differentiation signal, TGF-β, can give rise to multiple cell types with distinct functions, while other polarizing differentiation signals, such as IL-6 and ATRA, skew the system to particular type(s) of cells. If we regard TGF-β as tossing dice for the naïve cells, those polarizing signals may load the dice, although they may not toss the dice themselves. The remarkable advantage of this system is that functionally synergic cells could be generated simultaneously in desired fractions with some simple differentiation inducers.

Our model suggests that the double-expressing phenotype is a re-stabilized co-expressing state, which should be observed in relatively late stages of cell differentiation. Previously, van den Ham and de Boer found this type of state in a similar dynamical system, although they chose parameter values to avoid this state for their system [24]. With perfectly symmetrical models, some other groups described a double-expressing state as an intermediate state before the decision making switch, corresponding to some bipotent precursor cells [27,32,33]. For the T_H17-iT_{reg} paradigm, it is also possible that these double-expressing cells are at an intermediate state that should be converted into single-expressing cells at a later stage of the differentiation process. However, we do not favor this view for the following reasons. 1) A few studies have shown that the double-expressing cells are effective in repressing effector cell growth and/or secreting pro-inflammatory and anti-inflammatory cytokines [15,34]. It is not likely that a differentiation intermediate would perform any conspicuous function in the immune system. 2) There are a few reports demonstrating the conversion from iT_{reg} cells to double-expressing cells [13,14], or from RORγt-only cells to double-expressing cells [15], and to our knowledge it is not yet established that observable double-expressing cells can be converted into single-expressing cells. Assuming that differentiation from early stage to late stage is more readily to be observed than the 'dedifferentiation' process, these results indicate that the double-expressing cells might be at a differentiation stage later than the single-expressing states. 3) As shown in this report, there is a mathematical basis to support the double-expressing state appearing only at relatively high TGF-β concentration and some late differentiation stage, and the model is in accord with most published experimental observations. In addition, we are aware that the double-expressing cells are also observed for iT_{reg}-T_H1 and iT_{reg}-T_H2 paradigms [3]. Therefore, the framework presented here may be helpful for understanding iT_{reg} cells that express T-bet or GATA3 as well. Interestingly, conversion of Foxp3-expressing iT_{reg} cells to Foxp3/T-bet double-expressing cells has been reported [35]. In fact, these double-expressing cells may play very specific and indispensable roles in controlling inflammation. Chaudhry et al. have found that iT_{reg} cells require STAT3 for their suppressive function on T_H17, and not on other lineages [36]. Koch et al. discovered that the T-bet expression is required for the function of iT_{reg} cells during T_H1-mediated

inflammation [35]. These results suggest that there are subpopulations of iT_{reg} cells expressing various master regulators of T helper cells, and they are tailored for different functions [3]. Therefore, the double-expressing cells might be terminally differentiated effectors performing specific suppressive functions. It is possible that the Foxp3-only cells, which mainly appear at low TGF-β concentration, could serve as precursors or reservoir for different terminal effectors, in addition to their general suppressive functions.

Although the detailed physiological significance of this delicate differentiation system is yet to be discovered, Lochner et al. have already demonstrated in mice that, during infections and inflammation, the number of IL-17 producing $ROR\gamma t^+$ cells and double-expressing cells increased in remarkably comparable proportions [15]. This suggests the need for balance between different cell types in response to pathogenic challenges. A single differentiation network that gives rise to multiple phenotypes might be crucial for the maintenance of such balance. Furthermore, it is worth highlighting the common features shared by the T_H17-iT_{reg} differentiation system and the differentiation control systems of hematopoietic cells and of stem cells [27,28,37]. Functionally, these systems have the potential to generate multiple phenotypes in a single differentiation event, and these phenotypes may play synergic roles under certain physiological conditions. In addition, it has been shown that cell-to-cell variability within clonal populations makes significant contributions to the stochasticity of lineage choice in stem cells [38]. This is also concordant with our basic assumptions.

Pitchfork bifurcations (with broken symmetry) may be the underlying mechanism generating variable phenotypes in these dynamical control systems. We will not be surprised if other cell differentiation systems possess similar properties. Recently, Heinz *et al* discovered that the 'priming factor' PU.1, which is required for both macrophage and B cell differentiation, is responsible for creating some of the lineage specific epigenetic markers by itself [39]. Therefore, it is possible that these priming factors not only drive the differentiation event, but also help to create a heterogeneous population of cells.

One limitation of our model is the assumption that the high concentration of TGF-β used by Lochner et al. is above the saturation concentration for TGF-β signaling [15]. We are cautious about extrapolating our model to even higher TGF-β concentration because there is no available experimental result for us to compare with. In fact, it is possible that at even higher TGF-β concentration either the RORγt-only phenotype or the double-expressing phenotype dominates the population, and the conversion between these two phenotypes might be possible by adjusting the concentration of TGF-β. Although Lochner et al. observed the conversion of RORγt-only cells into double-expressing cells at late time points of induced differentiation, we are not sure about the nature of this conversion: it could be a transition from a transient intermediate to a stable steady state; it could be a transition triggered by a slow increase of TGF-β signaling in RORγt cells, possibly mediated by paracrine signaling (see below); or it may be caused by slow fluctuations in the transcriptomes [38]. Nonetheless, when more experimental results become available, we should be able to pinpoint the missing pieces in this reciprocal differentiation system and make the mathematical model more helpful for our understanding of the system in detail.

Another limitation of this study is that we have neglected the effects of intercellular communication on the differentiation of $CD4^+$ T cells. Cytokines secreted by T_H1 and T_H2 cells are known to influence the differentiation of neighboring T cells [40], and previous modeling work has highlighted the importance of these paracrine signaling effects [20]. Relevant to our work, the cytokines secreted by T_H17 and iT_{reg} cells can influence the differentiation of a population of T cells, and this influence might be reflected in changes of the proportions of induced phenotypes. For example, both T_H17 and iT_{reg} cells can produce TGF-β [41,42], which may increase the percentage of both type of cells, or induce the transition from single-expressing cells to double-expressing cells, and this may be causative for the transition observed by Lochner et al. [15]. However, it is not yet clear how important are paracrine signals via secreted cytokines compared to exogenous cytokine signals, with respect to T_H17 and iT_{reg} differentiation. We leave the consideration of these factors for future work.

In summary, we presented a novel mathematical model of T_H17-iT_{reg} differentiation. Based on the model, we show how TGF-β can trigger the differentiation of naïve $CD4^+$ T cells into a heterogeneous population containing RORγt-only, Foxp3-only and double-expressing cells, and how polarizing signals can skew the differentiation to particular phenotype(s). The model suggests how the conversions among different phenotypes can be guided. Additionally, the model gives a new quantitative explanation for the double-expressing cells, which should appear only at a late stage of the differentiation process. Our model provides new insights into the regulatory mechanisms that underlie the molecular control of certain immune responses.

Methods

We constructed our mathematical model based on known interactions among key molecules in the differentiation system of T_H17 and iT_{reg} cells. For illustrative purposes, we first consider a 'symmetrical' model in which the lineages of T_H17 and iT_{reg} have identical corresponding interaction types and strengths. Then we added two intermediate proteins for transmitting TGF-β signals in this symmetrical model. Next, we modified our model so that it became asymmetrical, and we incorporated two other input signals. Using this last model, we compared our simulation results with some published experimental data and made several testable predictions.

In the symmetrical model (Figure 2A) TGF-β upregulates both RORγt and Foxp3, which has been demonstrated in a few published experiments [13,43]. The model includes the 'autoactivation' of both master regulators. Although there is no evidence for direct autoactivation of RORγt and Foxp3, these relationships in our model represent known positive feedback loops in their respective pathways. One origin of these positive feedback loops is the epigenetic modifications observed in the promoter regions of RORγt and Foxp3 in their respective lineages [44,45]. These epigenetic modifications recruit additional chromatin remodeling complexes that further stabilize those modifications and help to maintain the gene expression, thus forming positive feedback loops [46]. Additionally, master regulators can enhance their own production by autocrine effects. For example, RORγt can induce production of IL-21 and IL-23 which further stimulate the expression of RORγt, as suggested by Murphy and Stokinger [47]. The symmetric model also includes the cross-inhibition interactions between Foxp3 and RORγt. Inhibition of Foxp3 by RORγt is supported by the recent discovery that RORγt acts as a transcriptional repressor of Foxp3 by binding to its promoter [48]. Although a few reports suggest a functional inhibition of RORγt by Foxp3 [13,16,49], the presence of Foxp3 was shown to have no pronounced effect on the expression of RORγt [50]. Our symmetrical model includes the inhibition of RORγt by Foxp3, but we relaxed this assumption in our model with broken symmetry.

In the first version of our symmetrical model, TGF-β directly activates RORγt and Foxp3. In the second version, we added intermediate proteins between TGF-β and the master regulators. It is known that Smad2, Smad3 and Smad4 mediate the TGF-β-induced upregulation of Foxp3 [51,52], but the Smad proteins are dispensable for upregulation of RORγt. It is still unclear how the TGF-β signal is transmitted to RORγt [52]. Thus, in Figure 1B, we introduce a generalized 'Smad' intermediate between TGF-β and Foxp3 and an 'unknown intermediate' between TGF-β and RORγt.

The model with broken symmetry also includes IL-17, which is activated by RORγt and STAT3, and deactivated by Foxp3 and ATRA [8,13,16,29,53]. As a polarizing signal, IL-6 stimulates RORγt and IL-17 production, and represses Foxp3 expression through the STAT3 pathway [54]. Conversely, ATRA upregulates Foxp3, downregulates RORγt, and inhibits IL-17 production [17,31]. These relations are all included in our model with broken symmetry (Figure 2C).

To model the T_H17-iT_{reg} reciprocal-differentiation system, we use a generic form of ordinary differential equations (ODEs) that describe both gene expression and protein interaction networks [55-57]. Each ODE in our model has the form:

$$\frac{dX_i}{dt} = \gamma_i (F(\sigma_i W_i) - X_i)$$
$$F(\sigma W) = 1 \Big/ (1 + e^{-\sigma W})$$
$$W_i = (\omega_i^o + \sum_j^N \omega_{j \to i} X_j)$$
$$i = 1, \ldots, N$$

X_i is the activity or concentration of protein i. $X_i(t)$ changes on a time scale = $1/\gamma_i$. $X_i(t)$ relaxes toward a value determined by the sigmoidal function, F, which has a steepness set by σ_i. The basal value of F, in the absence of any influencing factors, is determined by ω_i^o. The coefficients $\omega_{j \to i}$ determine the

influence of protein j on protein i. N is the total number of proteins in the network. For example, the pair of ODEs for the first symmetrical model are:

$$\frac{\mathrm{d}[\mathrm{ROR}\gamma\mathrm{t}]}{\mathrm{d}t} = \gamma_{\mathrm{ROR}\gamma\mathrm{t}}\left(\frac{1}{1+e^{-\sigma_{\mathrm{ROR}\gamma\mathrm{t}}W_{\mathrm{ROR}\gamma\mathrm{t}}}} - [\mathrm{ROR}\gamma\mathrm{t}]\right)$$

$$\text{where } W_{\mathrm{ROR}\gamma\mathrm{t}} = \omega^{\mathrm{o}}_{\mathrm{ROR}\gamma\mathrm{t}} + \omega_{\mathrm{ROR}\gamma\mathrm{t}\to\mathrm{ROR}\gamma\mathrm{t}}[\mathrm{ROR}\gamma\mathrm{t}] + \omega_{\mathrm{Foxp3}\to\mathrm{ROR}\gamma\mathrm{t}}[\mathrm{Foxp3}] + \omega_{\mathrm{TGF}\beta\to\mathrm{ROR}\gamma\mathrm{t}}[\mathrm{TGF}\beta]$$

$$\frac{\mathrm{d}[\mathrm{Foxp3}]}{\mathrm{d}t} = \gamma_{\mathrm{Foxp3}}\left(\frac{1}{1+e^{-\sigma_{\mathrm{Foxp3}}W_{\mathrm{Foxp3}}}} - [\mathrm{Foxp3}]\right)$$

$$\text{where } W_{\mathrm{Foxp3}} = \omega^{\mathrm{o}}_{\mathrm{Foxp3}} + \omega_{\mathrm{Foxp3}\to\mathrm{Foxp3}}[\mathrm{Foxp3}] + \omega_{\mathrm{ROR}\gamma\to\mathrm{Foxp3}}[\mathrm{ROR}\gamma\mathrm{t}] + \omega_{\mathrm{TGF}\beta\to\mathrm{Foxp3}}[\mathrm{TGF}\beta]$$

All variables and parameters are dimensionless. One time unit in our simulations corresponds to approximately 1 hour.

All simulations and bifurcation analyses were performed with PyDSTool, a software environment for dynamical systems [58]. In the Supplementary Information we provide a Python module file (Text S1) for PyDSTool that completely defines the ODEs we are solving in each case, and an example script (Text S2) to reproduce bifurcation diagrams shown in Figure 4A.

All the experimental results to which our model has been compared were obtained with differentiation assays that lasted 2-5 days, and these results are essentially consistent from one experiment to another. Thus, we assumed that the observed, differentiated cell phenotypes after 2-5 days are representative of stable steady states in our model.

We have chosen to use generic (phenomenological) ODEs instead of a more detailed kinetic model of the biochemical reaction network because we lack sufficient mechanistic and kinetic information on the molecular interactions in the T_H17-iT_{reg} reciprocal-differentiation system. To build a detailed biochemical model, based on mass-action or Michaelis-Menten kinetics, would require us to make many assumptions on the underlying mechanism and rate constants with little or no experimental evidence to back up these assumptions. In such a case, a phenomenological model seems more appropriate to us. A similar approach has been adopted in earlier theoretical studies of T cell differentiation by Mendoza and Xenarios [22],

who used a sigmoidal function similar to our F(σW), and by van den Ham and de Boer [21], who used Hill functions in place of our F(σW). To be sure that our results are not overly dependent on our mathematical approach, we have re-formulated our 'symmetrical model without intermediates' using Hill functions and confirmed that the model exhibits four types of stable steady states as [TGFβ] is varied. The basic features of the bifurcation diagrams and signal-response curves are similar, regardless of which formalism is used (details available upon request).

To account for cell-to-cell variability in a population, we made many simulations of the system of ODEs, each time with a slightly different choice of parameter values, to represent slight differences from cell to cell. We assumed that the value of each parameter conforms to a normal distribution with CV = 0.05 (CV = coefficient of variation = standard deviation / mean). The mean value that we specified for each parameter distribution is also referred as the 'basal' value of that parameter (see Table 1). In our bifurcation analysis of the dynamical system, we consider an imaginary cell that adopts the basal value for each of its parameters, and we define this cell as the 'average' cell. Note that none of the cells in our simulated population is likely to be this average cell, because every parameter value is likely to deviate a little (CV = 5%) from the basal value. Note, in addition, that our simulations sample a volume of parameter space around the 'average' cell, thereby probing the sensitivity/robustness of the differentiation process. Because we are varying all parameters simultaneously and randomly, this procedure is more indicative of robust behavior than standard sensitivity analysis, which involves estimating the partial derivative of some output property (e.g., steady state level of Foxp3) with respect to each parameter separately.

In order to simulate the induced differentiation process, we first solved the ODEs numerically with some small initial values of [RORγt] and [Foxp3] state and with [TGF-β] = 0 (and, if applicable, other input signals, e.g. IL-6 and ATRA, = 0 as well). After a short period of time, each simulated cell will find its own, stable $ROR\gamma t^{low}Foxp3^{low}$ steady state, corresponding to a naïve $CD4^+$ T cell. Next, we changed [TGF-β] (and other input signals, if applicable) to a certain positive value and continued the numerical

simulation. By the end of the simulation, each cell arrives at its corresponding 'induced' phenotype, which might vary from cell to cell because of the parametric variability of the population. To simulate the reprogramming effect, the concentration of IL-6 was raised after the cells were stabilized in the differentiated state. We made the simple definition that a protein is expressed when its level is greater than 0.5 units.

To check the effect of TGF-β concentration on the induced phenotypes, we ran a series of simulations for a group of 1000 cells with various values of [TGF-β] and plotted the percentages of cells that adopt each terminal phenotype, in order to generate a 'signal-response' curve for a population of cells. Note that this signal-response curve could only represent a series of induced differentiation experiments with various TGF-β concentrations instead of a single experiment with increasing concentration of TGF-β.

Our simulations of cell-to-cell variability are based on the assumptions that each cell follows a deterministic trajectory but that cells differ from one another in the precise values of the kinetic parameters that govern the deterministic trajectory. A similar approach was adopted by Höfer et al. in their model of transcriptional regulation of T lymphocytes [18]. An alternative view of stochasticity assumes that all cells are identical in terms of kinetic constants but they follow unique stochastic trajectories because of random fluctuations in the numbers of molecules of the dynamic variables. The truth is most likely a combination of these effects (parameter variation and molecular fluctuations), but we have adopted the parameter-variation approach for several reasons. First of all, we lack the sort of molecular details (e.g., the numbers of molecules of regulatory species per cell) needed for accurate stochastic simulations of molecular fluctuations. Second, it is unlikely that T cells are identical with respect to parameter values, and there is experimental evidence to the contrary. Peripheral naïve T cells undergo a complex developmental process in the thymus, where they likely inherit many stable cell-to-cell differences, possibly because of the great diversity of T cell receptor specificities generated by VJ or V(D)J recombination. Experiments on T cell differentiation are done by selecting cells with some common characteristics, but they may nonetheless differ in many other respects. Even monoclonal

populations of mammalian cells (derived from a single progenitor cell) exhibit a distribution of properties that can affect cell fate determination [38]. Nonetheless, to be sure that our results are not overly dependent on our view of cell-to-cell variability, we have re-formulated our 'symmetrical model without intermediates' as a pair of stochastic differential equations with additive white noise and confirmed that the SDEs generate signal-response curves similar to our results in Fig. 4A, bottom panel (details available upon request).

It is also reasonable to attribute variability among cells to different initial conditions for each simulation of the governing ODEs, as suggested by Yates et al. [20]. Since variations of initial conditions can also bias cells toward different phenotypes, we presume that this strategy will produce results similar to our own.

References

1. Mitsdoerffer M, Lee Y, Jäger A, Kim H-J, Korn T, et al. (2010) Proinflammatory T helper type 17 cells are effective B-cell helpers. Proc Natl Acad Sci U S A 107: 14292-14297.

2. Wan YY (2010) Multi-tasking of helper T cells. Immunology 130: 166-171.

3. Zhu J, Yamane H, Paul WE (2010) Differentiation of effector CD4 T cell populations. Annu Rev Immunol 28: 445-489.

4. O'Shea JJ, Paul WE (2010) Mechanisms underlying lineage commitment and plasticity of helper CD4+ T cells. Science 327: 1098-1102.

5. Zhu J, Paul WE (2010) Heterogeneity and plasticity of T helper cells. Cell research 20: 4-12.

6. Mosmann TR, Coffman RL (1989) TH1 and TH2 cells: different patterns of lymphokine secretion lead to different functional properties. Annu Rev Immunol 7: 145-173.

7. Murphy Ca, Langrish CL, Chen Y, Blumenschein W, McClanahan T, et al. (2003) Divergent pro- and antiinflammatory roles for IL-23 and IL-12 in joint autoimmune inflammation. J Exp Med 198: 1951-1957.

8. Ivanov II, McKenzie BS, Zhou L, Tadokoro CE, Lepelley A, et al. (2006) The orphan nuclear receptor RORgammat directs the differentiation program of proinflammatory IL-17+ T helper cells. Cell 126: 1121-1133.

9. Ouyang W, Kolls JK, Zheng Y (2008) The biological functions of T helper 17 cell effector cytokines in inflammation. Immunity 28: 454-467.

10. Curotto de Lafaille MA, Kutchukhidze N, Shen S, Ding Y, Yee H, et al. (2008) Adaptive Foxp3+ regulatory T cell-dependent and -independent control of allergic inflammation. Immunity 29: 114-126.

11. Fontenot JD, Gavin MA, Rudensky AY (2003) Foxp3 programs the development and function of CD4+CD25+ regulatory T cells. Nat Immunol 4: 330-336.

12. Bettelli E, Carrier Y, Gao W, Korn T, Strom TB, et al. (2006) Reciprocal developmental pathways for the generation of pathogenic effector TH17 and regulatory T cells. Nature 441: 235-238.

13. Yang XO, Nurieva R, Martinez GJ, Kang HS, Chung Y, et al. (2008) Molecular antagonism and plasticity of regulatory and inflammatory T cell programs. Immunity 29: 44-56.

14. Voo KS, Wang Y-H, Santori FR, Boggiano C, Wang Y-H, et al. (2009) Identification of IL-17-producing FOXP3+ regulatory T cells in humans. Proc Natl Acad Sci U S A 106: 4793-4798.

15. Lochner M, Peduto L, Cherrier M, Sawa S, Langa F, et al. (2008) In vivo equilibrium of proinflammatory IL-17+ and regulatory IL-10+ Foxp3+ RORgamma t+ T cells. J Exp Med 205: 1381-1393.

16. Zhou L, Lopes JE, Chong MMW, Ivanov II, Min R, et al. (2008) TGF-beta-induced Foxp3 inhibits T(H)17 cell differentiation by antagonizing RORgammat function. Nature 453: 236-240.

17. Mucida D, Park Y, Kim G, Turovskaya O, Scott I, et al. (2007) Reciprocal TH17 and regulatory T cell differentiation mediated by retinoic acid. Science 317: 256-260.

18. Höfer T, Nathansen H, Löhning M, Radbruch A, Heinrich R (2002) GATA-3 transcriptional imprinting in Th2 lymphocytes: a mathematical model. Proc Natl Acad Sci U S A 99: 9364-9368.

19. Mariani L, Löhning M, Radbruch A, Höfer T (2004) Transcriptional control networks of cell differentiation: insights from helper T lymphocytes. Prog Biophys Mol Biol 86: 45-76.

20. Yates A, Callard R, Stark J (2004) Combining cytokine signalling with T-bet and GATA-3 regulation in Th1 and Th2 differentiation: a model for cellular decision-making. J Theor Biol 231: 181-196.

21. Mendoza L (2006) A network model for the control of the differentiation process in Th cells. Bio Systems 84: 101-114.

22. Mendoza L, Xenarios I (2006) A method for the generation of standardized qualitative dynamical systems of regulatory networks. Theor Biol Med Model 3: 13.

23. Callard RE (2007) Decision-making by the immune response. Immunol Cell Biol 85: 300-305.

24. van den Ham H-J, de Boer RJ (2008) From the two-dimensional Th1 and Th2 phenotypes to high-dimensional models for gene regulation. Int Immunol 20: 1269-1277.

25. Naldi A, Carneiro J, Chaouiya C, Thieffry D (2010) Diversity and plasticity of Th cell types predicted from regulatory network modelling. PLoS Comput Biol 6: e1000912.

26. Graf T, Enver T (2009) Forcing cells to change lineages. Nature 462: 587-594.

27. Huang S, Guo Y-P, May G, Enver T (2007) Bifurcation dynamics in lineage-commitment in bipotent progenitor cells. Dev Biol 305: 695-713.

28. Laslo P, Spooner CJ, Warmflash A, Lancki DW, Lee H-J, et al. (2006) Multilineage transcriptional priming and determination of alternate hematopoietic cell fates. Cell 126: 755-766.

29. Williams LM, Rudensky AY (2007) Maintenance of the Foxp3-dependent developmental program in mature regulatory T cells requires continued expression of Foxp3. Nat Immunol 8: 277-284.

30. Mariani L, Schulz EG, Lexberg MH, Helmstetter C, Radbruch A, et al. (2010) Short-term memory in gene induction reveals the regulatory principle behind stochastic IL-4 expression. Mol Syst Biol 6: 359.

31. Elias KM, Laurence A, Davidson TS, Stephens G, Kanno Y, et al. (2008) Retinoic acid inhibits Th17 polarization and enhances FoxP3 expression through a Stat-3 / Stat-5 independent signaling pathway. Blood 111: 1013-1020.

32. Guantes R, Poyatos JF (2008) Multistable decision switches for flexible control of epigenetic differentiation. PLoS Comput Biol 4: e1000235.

33. Huang S (2009) Reprogramming cell fates: reconciling rarity with robustness. BioEssays 31: 546-560.

34. Ayyoub M, Deknuydt F, Raimbaud I, Dousset C, Leveque L, et al. (2009) Human memory FOXP3+ Tregs secrete IL-17 ex vivo and constitutively express the T(H)17 lineage-specific transcription factor RORgamma t. Proc Natl Acad Sci U S A 106: 8635-8640.

35. Koch MA, Tucker-Heard G, Perdue NR, Killebrew JR, Urdahl KB, et al. (2009) The transcription factor T-bet controls regulatory T cell homeostasis and function during type 1 inflammation. Nat Immunol 10: 595-602.

36. Chaudhry A, Rudra D, Treuting P, Samstein RM, Liang Y, et al. (2009) CD4+ regulatory T cells control TH17 responses in a Stat3-dependent manner. Science 326: 986-991.

37. Orkin SH, Zon LI (2002) Hematopoiesis and stem cells: plasticity versus developmental heterogeneity. Nat Immunol 3: 323-328.

38. Chang HH, Hemberg M, Barahona M, Ingber DE, Huang S (2008) Transcriptome-wide noise controls lineage choice in mammalian progenitor cells. Nature 453: 544-547.

39. Heinz S, Benner C, Spann N, Bertolino E, Lin YC, et al. (2010) Simple combinations of lineage-determining transcription factors prime cis-regulatory elements required for macrophage and B cell identities. Mol Cell 38: 576-589.

40. O'Garra A (1998) Cytokines induce the development of functionally heterogeneous T helper cell subsets. Immunity 8: 275-283.

41. Gutcher I, Donkor Moses K, Ma Q, Rudensky Alexander Y, Flavell Richard A, et al. (2011) Autocrine Transforming Growth Factor-β1 Promotes In Vivo Th17 Cell Differentiation. Immunity 34: 396-408.

42. Curotto de Lafaille MA, Lafaille JJ (2009) Natural and adaptive foxp3+ regulatory T cells: more of the same or a division of labor? Immunity 30: 626-635.

43. Zhu J, Paul WE (2010) Peripheral CD4+ T-cell differentiation regulated by networks of cytokines and transcription factors. Immunol Rev 238: 247-262.

44. Josefowicz SZ, Rudensky A (2009) Control of regulatory T cell lineage commitment and maintenance. Immunity 30: 616-625.

45. Wei G, Wei L, Zhu J, Zang C, Hu-Li J, et al. (2009) Global mapping of H3K4me3 and H3K27me3 reveals specificity and plasticity in lineage fate determination of differentiating CD4+ T cells. Immunity 30: 155-167.

46. Dodd IB, Micheelsen MA, Sneppen K, Thon G (2007) Theoretical analysis of epigenetic cell memory by nucleosome modification. Cell 129: 813-822.

47. Murphy KM, Stockinger B (2010) Effector T cell plasticity: flexibility in the face of changing circumstances. Nat Immunol 11: 674-680.

48. Burgler S, Mantel PY, Bassin C, Ouaked N, Akdis CA, et al. (2010) RORC2 is involved in T cell polarization through interaction with the FOXP3 promoter. J Immunol 184: 6161-6169.

49. Zhang F, Meng G, Strober W (2008) Interactions among the transcription factors Runx1, RORgammat and Foxp3 regulate the differentiation of interleukin 17-producing T cells. Nat Immunol 9: 1297-1306.

50. Gavin Ma, Rasmussen JP, Fontenot JD, Vasta V, Manganiello VC, et al. (2007) Foxp3-dependent programme of regulatory T-cell differentiation. Nature 445: 771-775.

51. Feng X-H, Derynck R (2005) Specificity and versatility in tgf-beta signaling through Smads. Annu Rev Cell Dev Biol 21: 659-693.

52. Yoshimura A, Wakabayashi Y, Mori T (2010) Cellular and molecular basis for the regulation of inflammation by TGF-beta. J Biochem 147: 781-792.

53. Okamoto K, Iwai Y, Oh-Hora M, Yamamoto M, Morio T, et al. (2010) IkappaBzeta regulates T(H)17 development by cooperating with ROR nuclear receptors. Nature 464: 1381-1385.

54. Kimura A, Kishimoto T (2010) IL-6: Regulator of Treg/Th17 balance. Eur J Immunol 40: 1830-1835.

55. Wilson HR, Cowan JD (1972) Excitatory and Inhibitory Interactions in Localized Populations of Model Neurons. Biophys J 12: 1-24.

56. Mjolsness E, Sharp DH, Reinitz J (1991) A connectionist model of development. J Theor Biol 152: 429-453.

57. Tyson JJ, Novåk B (2010) Functional motifs in biochemical reaction networks. Annu Rev Phys Chem 61: 219-240.

58. Clewley R, Sherwood WE, LaMar MD, Guckenheimer JM (2007) PyDSTool, a software environment for dynamical systems modeling. http://pydstool.sourceforge.net. Accessed: August 10 2010.

Figure Legends

Figure 1. Induction of differentiation from naïve $CD4^+$ T cells to T_H17 and iT_{reg}. A population of antigen-activated naïve $CD4^+$ T cells (white) can be induced by different types of cytokine micro-environment to produce corresponding differentiated cell populations. T_H17 cells (red) express the RORγt transcription factor, and iT_{reg} cells (green) express the Foxp3 transcription factor. Some cells (yellow) express both master regulators and may possess both regulatory and pro-inflammatory functions.

Figure 2. Influence diagrams of the mathematical models. A. Symmetrical model without intermediates. **B.** Symmetrical model with intermediates. **C.** Asymmetrical model with three input signals: TGF-β, ATRA, and IL-6.

Figure 3. Phase plane analysis of the symmetrical model without intermediates. X and Y axes: dimensionless quantities that represent the intracellular concentrations of master regulators Foxp3 and RORγt respectively. Value = 1 indicates the maximum intracellular concentration of the master regulator, and value = 0 indicates the absence of the master regulator. Red Line: nullcline for RORγt. Green line: nullcline for Foxp3. Steady states, at the intersections of red and green nullclines, are labeled as 'u' (unstable) or 's' (stable). Magenta dashed line with arrow: trajectory of a time-course simulation. Semi-transparent red and green areas: the basins of attractions for $ROR\gamma t^{high}Foxp3^{low}$ and $ROR\gamma t^{low}Foxp3^{high}$ states, respectively. **A.** Phase plane for the average cell with [TGF-β] = 0. Magenta circle: $ROR\gamma^{low}Foxp3^{low}$ steady state. **B.** Phase plane for the average cell with [TGF-β] = 0.5 units. Magenta circle is the location of the steady state in Panel A. **C.** Overlaid phase planes and trajectories for three cells adopting distinct fates. **D.** Simulation trajectories for a population of 30 cells on the plane of RORγt and Foxp3.

Figure 4. Bifurcation diagrams and signal-response curves for three models. Upper and middle panels: one-parameter bifurcation diagrams for the average cell. Steady state levels of RORγt and Foxp3 are plotted as functions of TGF-β concentration. Solid line: stable steady states. Dashed line: unstable

steady states. Lower panels: signal-response curves. For each point on the abscissa (for [TGF-β] = constant), we simulate induced differentiation of a population of 1000 cells. Percentages of cells at the alternative steady states are plotted as functions of TGF-β concentration used for induction. Red line: RORγt-only cells. Green line: Foxp3-only cells. Yellow line: double-expressing cells. Blue marker: Foxp3-expressing cells. Magenta marker: IL-17 producing cells. **A.** Symmetrical model without intermediates. **B.** Symmetrical model with intermediates. **C.** Asymmetric model. Dotted vertical lines denote representative experimental levels of TGF-β.

Figure 5. Effects of polarizing signals on the induced differentiation. Simulation of the asymmetric model (Figure 1C). Upper and middle panels: one-parameter bifurcation diagrams for the average cell. RORγt and Foxp3 steady state levels are plotted as functions of TGF-β concentration. See the legend to Figure 3 for the interpretation of the curves. **A.** Cells treated with [IL-6] = 10 units together with the indicated amount of TGF-β. **B.** Cells treated with [ATRA] = 1.5 units together with the indicated amount of TGF-β. **C.** Cells treated with [IL-6] = 10 units and [ATRA] = 1.5 units together with the indicated amount of TGF-β.

Figure 6. Reprogramming from iT_{reg} to T_H17 in the presence of TGF-β. A. Time course trajectories of simulated reprogramming effects. 1 time unit ≈ 1 h. [TGF-β] = 0 for $t < 10$, and [TGF-β] = 0.28 for $t > 10$. [IL-6] = 0 for $t < 80$, and [IL-6] = 10 for $t > 80$. At each time point, we plot the percentages of cells at the alternative steady states, using the same color scheme as in Figure 3. Left panel: no ATRA added. Right panel: 1.5 units of ATRA added together with TGF-β. **B.** Analysis of concentration dependencies for simulations described in Panel A. X axis: amount of IL-6 used for reprogramming. Y axis: amount of ATRA used for initial induction of differentiation. Percentages of cells at steady state are shown according to a color gradient. Left panel: percentage of Foxp3-expressing cells at steady state. Right panel: percentage of IL-17-producing cells at steady state.

Figures

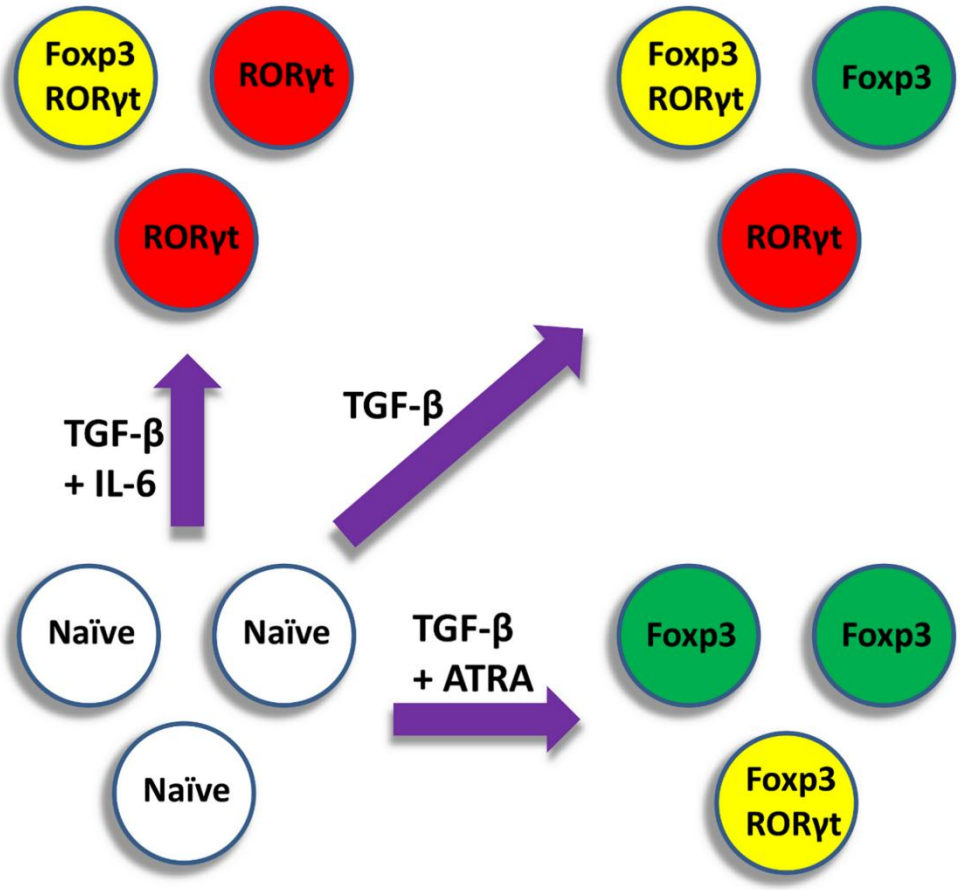

Figure 1. Induction of differentiation from naïve $CD4^+$ T cells to T_H17 and iT_{reg}

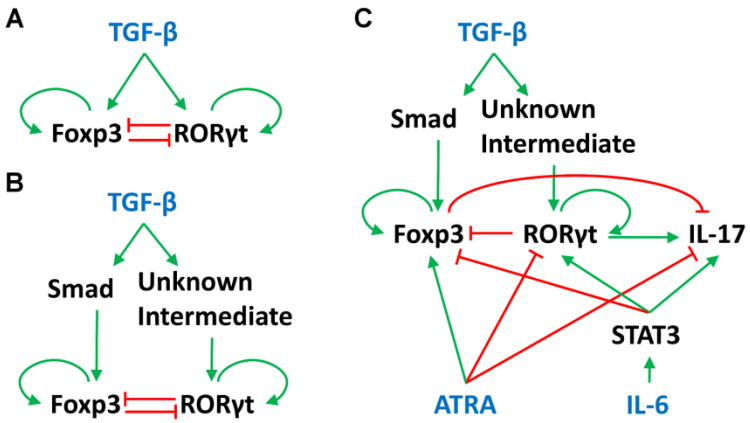

Figure 2. Influence diagrams of the mathematical models

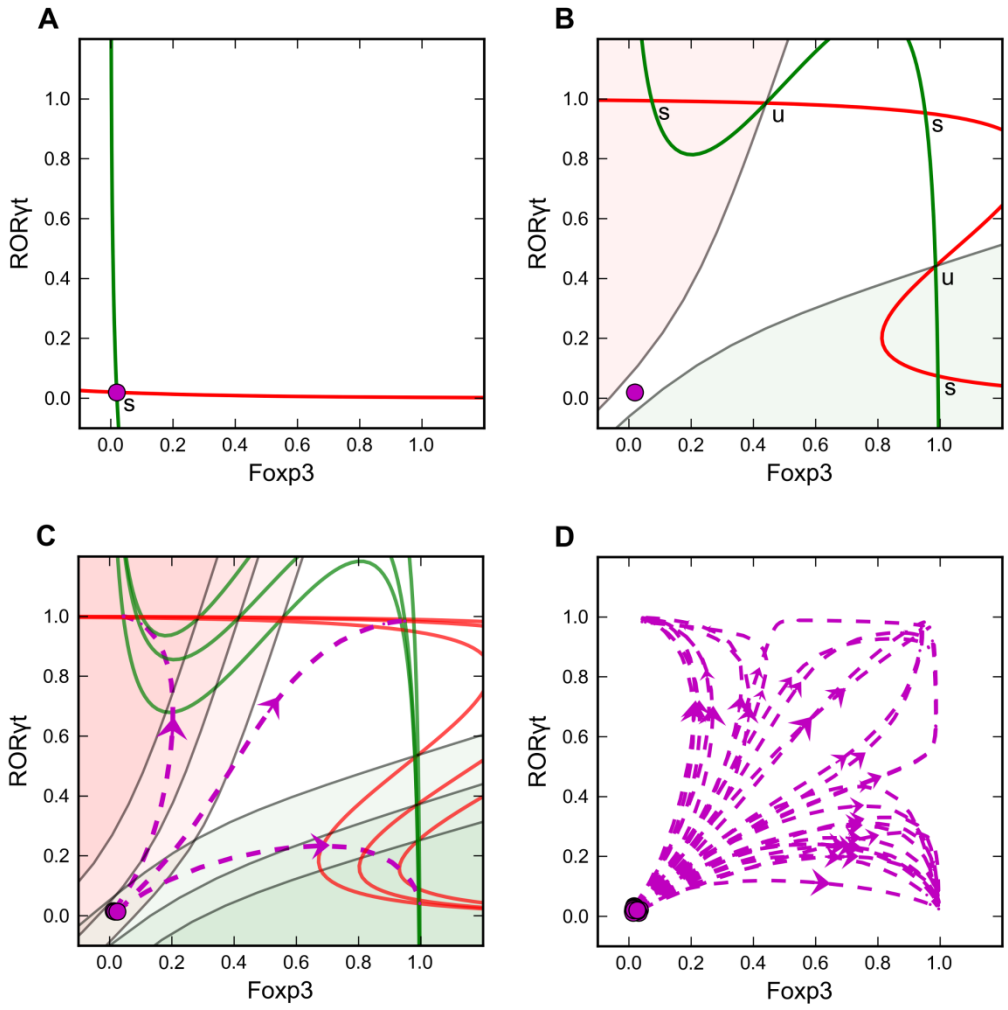

Figure 3. Phase plane analysis of the symmetrical model without intermediates

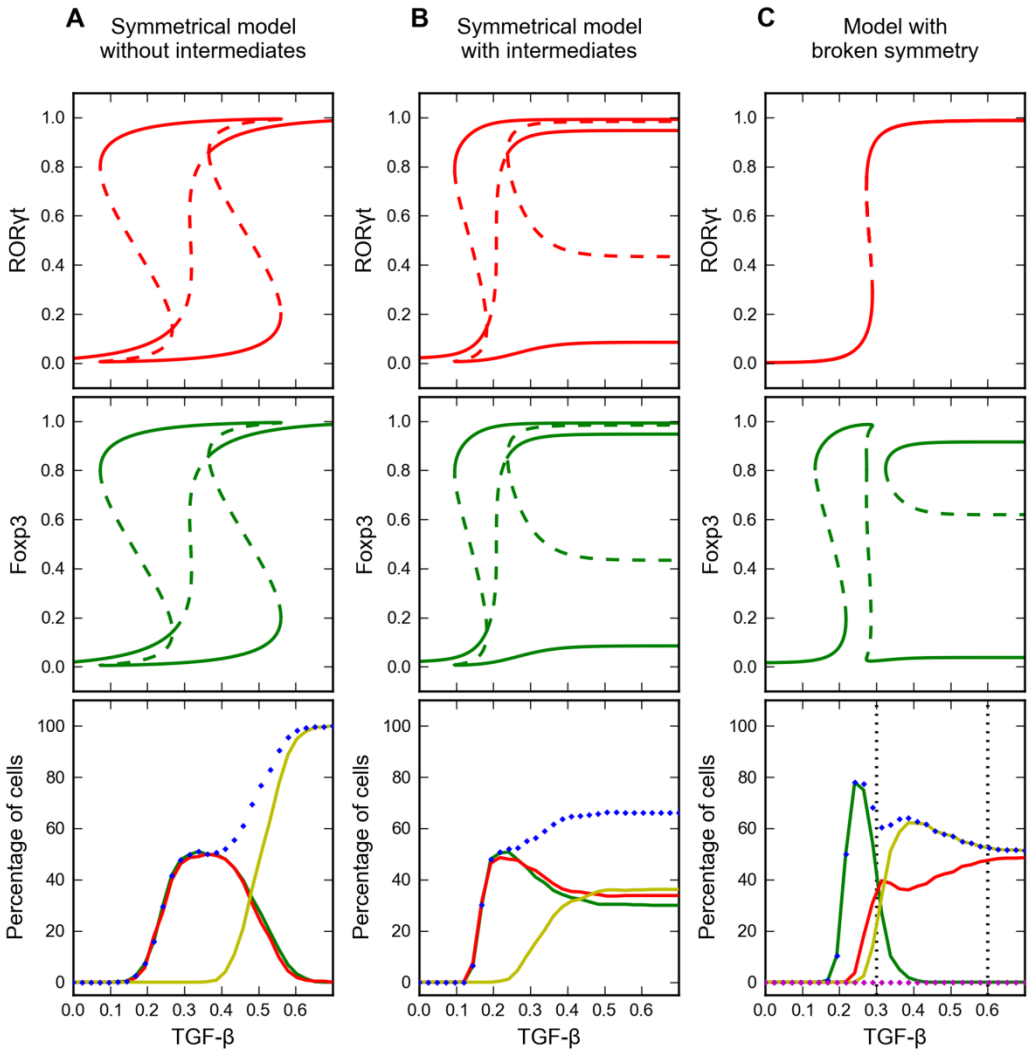

Figure 4. Bifurcation diagrams and signal-response curves for three models

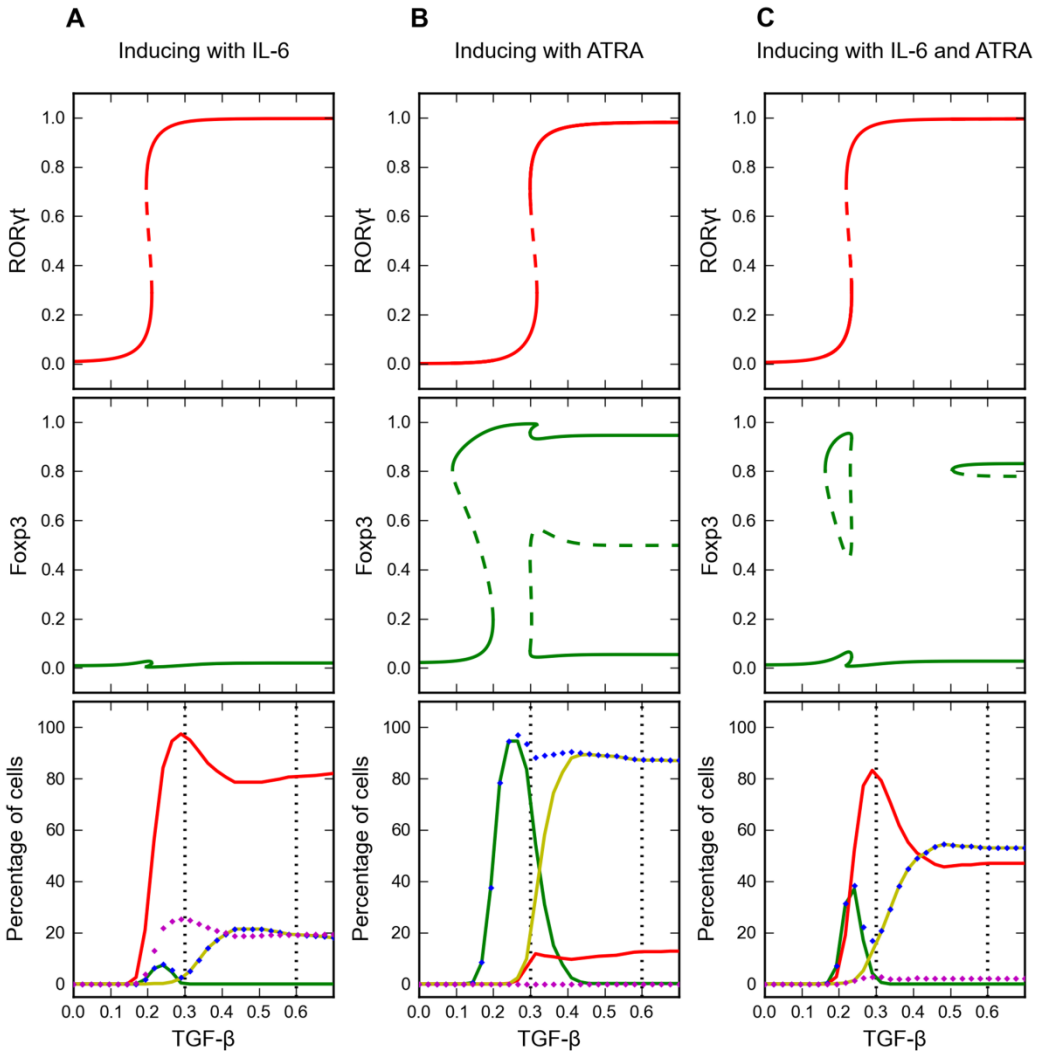

Figure 5. Effects of polarizing signals on the induced differentiation

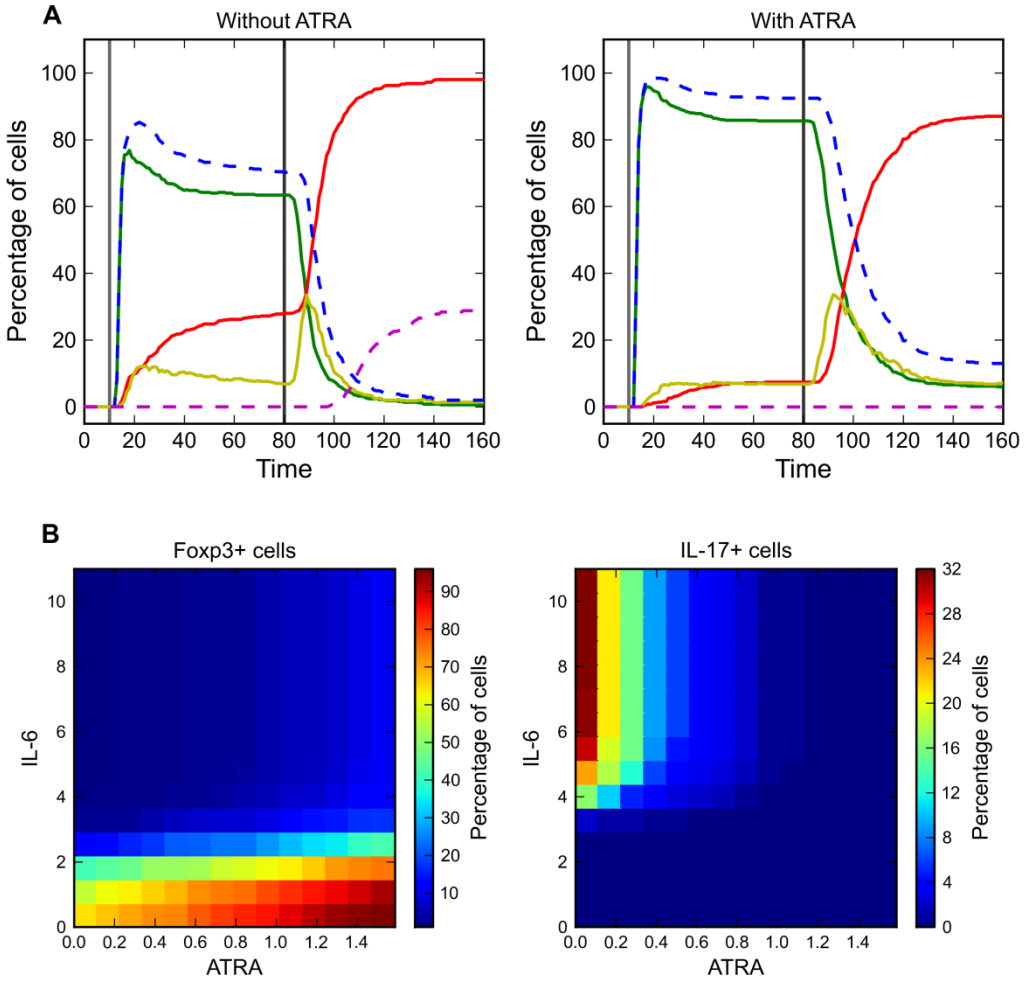

Figure 6. Reprogramming from iT_{reg} to T_H17 in the presence of TGF-β

Tables

Table 1 Descriptions and basal values of parameters

Parameter name	Description	Basal value in symmetrical model without intermediates	Basal value in symmetrical model with intermediates	Basal value in model with broken symmetry
$\gamma_{\mathrm{RORγt}}$	Relaxation rate of RORγt	1	1	1
γ_{Foxp3}	Relaxation rate of Foxp3	1	1	1
$\sigma_{\mathrm{RORγt}}$	Steepness of sigmoidal function for RORγt	5	5	7
σ_{Foxp3}	Steepness of sigmoidal function for Foxp3	5	5	5
$\omega^{o}_{\mathrm{RORγt}}$	Basal activation state of RORγt	-0.8	-0.8	-0.84
$\omega^{o}_{\mathrm{Foxp3}}$	Basal activation state of Foxp3	-0.8	-0.8	-0.92
$\omega_{\mathrm{RORγt\rightarrow RORγt}}$	Weight of autoactivation of RORγt	1.24	1.2	0.7
$\omega_{\mathrm{Foxp3\rightarrow RORγt}}$	Weight of inhibition on RORγt by Foxp3	-0.4	-0.4	NA
$\omega_{\mathrm{Foxp3\rightarrow Foxp3}}$	Weight of autoactivation of Foxp3	1.24	1.2	1.28
$\omega_{\mathrm{RORγt\rightarrow Foxp3}}$	Weight of inhibition on Foxp3 by RORγt	-0.4	-0.4	-0.54
$\omega_{\mathrm{TGFβ\rightarrow RORγt}}$	Weight of activation on RORγt by TGF-β	1.2	NA	NA
$\omega_{\mathrm{TGFβ\rightarrow Foxp3}}$	Weight of activation on Foxp3 by TGF-β	1.2	NA	NA
γ_{UI}	Relaxation rate of unknown intermediate (UI)	NA	1	1
γ_{Smad}	Relaxation rate of Smad	NA	1	1
σ_{UI}	Steepness of sigmoidal function for UI	NA	10	12
σ_{Smad}	Steepness of sigmoidal function for Smad	NA	10	20
ω^{o}_{UI}	Basal activation state of UI	NA	-0.2	-0.23
$\omega^{o}_{\mathrm{Smad}}$	Basal activation state of Smad	NA	-0.2	-0.225
$\omega_{\mathrm{UI\rightarrow RORγt}}$	Weight of activation on RORγt by UI	NA	0.62	0.86
$\omega_{\mathrm{Smad\rightarrow Foxp3}}$	Weight of activation on Foxp3 by Smad	NA	0.62	0.68
$\omega_{\mathrm{TGFβ\rightarrow UI}}$	Weight of activation on UI by TGF-β	NA	1.2	1
$\omega_{\mathrm{TGFβ\rightarrow Smad}}$	Weight of activation on Smad by TGF-β	NA	1.2	1
$\omega_{\mathrm{ATRA\rightarrow RORγt}}$	Weight of inhibition on RORγt by ATRA	NA	NA	-0.04
$\omega_{\mathrm{ATRA\rightarrow Foxp3}}$	Weight of activation on Foxp3 by ATRA	NA	NA	0.035
γ_{IL17}	Relaxation rate of IL-17	NA	NA	1
σ_{IL17}	Steepness of sigmoidal function for IL-17	NA	NA	30
$\omega^{o}_{\mathrm{IL17}}$	Basal activation state of IL-17	NA	NA	-0.82
$\omega_{\mathrm{RORγt\rightarrow IL17}}$	Weight of activation on IL-17 by RORγt	NA	NA	0.22
$\omega_{\mathrm{Foxp3\rightarrow IL17}}$	Weight of inhibition on IL-17 by Foxp3	NA	NA	-0.8
$\omega_{\mathrm{STAT3\rightarrow IL17}}$	Weight of activation on IL-17 by STAT3	NA	NA	0.6
$\omega_{\mathrm{ATRA\rightarrow IL17}}$	Weight of inhibition on IL-17 by ATRA	NA	NA	-0.1
γ_{STAT3}	Relaxation rate of STAT3	NA	NA	0.1
σ_{STAT3}	Steepness of sigmoidal function for STAT3	NA	NA	10
$\omega^{o}_{\mathrm{STAT3}}$	Basal activation state of STAT3	NA	NA	-0.4
$\omega_{\mathrm{STAT3\rightarrow RORγt}}$	Weight of activation on RORγt by STAT3	NA	NA	0.2
$\omega_{\mathrm{STAT3\rightarrow Foxp3}}$	Weight of inhibition on Foxp3 by STAT3	NA	NA	-0.1
$\omega_{\mathrm{IL6\rightarrow STAT3}}$	Weight of activation on STAT3 by IL-6	NA	NA	0.2

[IL6]	Concentration of IL-6	NA	NA	C
[ATRA]	Concentration of ATRA	NA	NA	C
[TGFβ]	Concentration of TGF-β	C	C	C

C: Values are specified in each simulation and might be changed at certain times during the simulation. These parameters are not subject to cell-to-cell variations.

Table 2 Simulation results and comparisons with published experimental results

Experimental/simulation condition	TGF-β concentration	Simulation result	Evidence
Inducing differentiation from naïve $CD4^+$ T cells with TGF-β alone	Intermediate	Three phenotypes in comparable fractions	Observed [16]
	Low-intermediate	Low concentration of TGF-β gives greater percentage of Foxp3 expressing cells than intermediate concentration.	Observed [16]
	High	RORγt-only and double-expressing phenotypes in comparable fractions	Observed [15]
	Low	Foxp3-only phenotype is the major differentiated phenotype	Prediction
	From low to high	Transition from Foxp3-only phenotype to RORγt-only and double-expressing phenotypes	Prediction
	From high to low	Transition from RORγt-only or double-expressing phenotype to Foxp3-only phenotype	Prediction
Inducing differentiation from naïve $CD4^+$ T cells with TGF-β and IL-6	Intermediate	Mostly RORγt phenotype, with a fraction of cells producing IL-17	Observed [16]
	High	RORγt (major fraction) and double-expressing (minor fraction) phenotypes	Observed [15]
	Low-intermediate-high	Higher concentration of TGF-β inhibits IL-17 production	Observed in more extent [16]
Inducing differentiation from naïve $CD4^+$ T cells with TGF-β and ATRA	Intermediate	More Foxp3 expressing cells than with TGF-β alone	Observed [17]
	Intermediate	Foxp3-only phenotype is the major differentiated phenotype	Prediction
	High	Double-expressing phenotype is the major differentiated phenotype	Prediction
Inducing differentiation from naïve $CD4^+$ T cells with TGF-β, IL-6 and ATRA	High	RORγt-only and double-expressing phenotypes in comparable fractions. IL-17 production is much lower than with TGF-β and IL-6	Observed [15]
Inducing differentiation from naïve $CD4^+$ T cells to iT_{reg} cells with TGF-β, and reprogramming the differentiated iT_{reg} cells with IL-6	Intermediate	Foxp3 expressing cells are reduced, and IL-17 producing cells appear in significant fraction.	Observed [13]
Inducing differentiation from naïve $CD4^+$ T cells to iT_{reg} cells with TGF-β and ATRA, and reprogramming the iT_{reg} cells with IL-6	Intermediate	Foxp3 expressing cells are reduced, and no significant number of IL-17 producing cells can be observed.	Observed [13]
	Intermediate	Most cells are in 'poised' state at which RORγt expression is high, but no IL-17 is produced.	Prediction

Supplementary Texts

Text S1

```
# This module file contains full list of equations and parameters for three
# models discussed in the paper
# They can be used as inputs for simulations with PyDSTool

pars = {} # parameters
varspecs = {} # ODEs
fnspecs = {} # helper functions

# Symmetrical model without intermediates
pars['sym_1'] = {
        'tgf'               : 0,
        'w_Foxp3_ROR'       : -0.4,
        'w_ROR_Foxp3'       : -0.4,
        'w_Foxp3_Foxp3'     : 1.24,
        'w_ROR_ROR'  : 1.24,
        'w_Foxp3_O'     : -0.8,
        'w_ROR_O'       : -0.8,
        'w_Foxp3_tgf'   : 1.2,
        'w_ROR_tgf'     : 1.2,
        'sigma_Foxp3'   : 5,
        'sigma_ROR'     : 5,
        'gamma_Foxp3' : 1,
        'gamma_ROR'   : 1,
}

varspecs['sym_1'] = {
        'Foxp3' : \
                'gamma_Foxp3 * ( hbt(sigma_Foxp3, w_Foxp3_O + \
                w_Foxp3_Foxp3 * Foxp3 + \
                w_Foxp3_ROR * ROR + w_Foxp3_tgf * tgf)\
                 - Foxp3 )',
        'ROR'   : \
                'gamma_ROR * ( hbt(sigma_ROR, w_ROR_O + \
                w_ROR_ROR * ROR + \
                w_ROR_Foxp3 * Foxp3 + w_ROR_tgf * tgf)\
                 - ROR )'
}

fnspecs['sym_1'] = {
        'hbt': \
        (['sigma', 'sum_omega'],'1 / (1 + exp(-sigma * sum_omega))')
}


# Symmetrical model with intermediates
pars['sym_2'] = {
        'tgf'               : 0,
```

```
        'w_Foxp3_ROR'           : -0.4,
        'w_ROR_Foxp3'           : -0.4,
        'w_Foxp3_Foxp3'         : 1.2,
        'w_ROR_ROR' : 1.2,
        'w_Foxp3_O'     : -0.8,
        'w_ROR_O'       : -0.8,
        'w_Foxp3_Smad'          : 0.62,
        'w_ROR_UI'      : 0.62,
        'sigma_Foxp3'   : 5,
        'sigma_ROR'     : 5,
        'gamma_Foxp3' : 1,
        'gamma_ROR'   : 1,
        'gamma_Smad'  : 1,
        'sigma_Smad'    : 15,
        'w_Smad_O'      : -0.21,
        'w_Smad_tgf'    : 1.2,
        'gamma_UI'      : 1,
        'sigma_UI'      : 15,
        'w_UI_O'        : -0.21,
        'w_UI_tgf'      : 1.2,
}

varspecs['sym_2'] = {
        'Foxp3' : \
                'gamma_Foxp3 * ( hbt(sigma_Foxp3, w_Foxp3_O + \
                w_Foxp3_Foxp3 * Foxp3 + w_Foxp3_ROR * ROR +\
                w_Foxp3_Smad * Smad)\
                 - Foxp3 )',
        'Smad'  : \
                'gamma_Smad * ( hbt(sigma_Smad, w_Smad_O + w_Smad_tgf * tgf)\
                 - Smad )',
        'UI'    : \
                'gamma_UI * ( hbt(sigma_UI, w_UI_O + w_UI_tgf * tgf) \
                 - UI)',
        'ROR'   : \
                'gamma_ROR * ( hbt(sigma_ROR, w_ROR_O + \
                w_ROR_ROR * ROR + \
                w_ROR_Foxp3 * Foxp3 + w_ROR_UI * UI)\
                 - ROR )',
}

fnspecs['sym_2'] = {
        'hbt': \
        (['sigma', 'sum_omega'],'1 / (1 + exp(-sigma * sum_omega))')
}

# Asymetric Model
pars['asym'] = {
        'tgf'           : 0,
        'il6'           : 0,
        'atra'          : 0,
```

```
        'w_Foxp3_ROR'           : -0.54,
        'w_ROR_Foxp3'           : 0,
        'w_Foxp3_Foxp3'         : 1.28,
        'w_ROR_ROR' : 0.7,
        'w_Foxp3_O'     : -0.84,
        'w_ROR_O'       : -0.92,
        'w_Foxp3_Smad'          : 0.68,
        'w_ROR_UI'      : 0.86,
        'sigma_Foxp3'   : 5,
        'sigma_ROR'     : 7,
        'gamma_Foxp3' : 1,
        'gamma_ROR'   : 1,
        'w_ROR_STAT3'           : 0.2,
        'w_Foxp3_STAT3'         : -0.1,
        'w_ROR_atra'    : -0.04,
        'w_IL17_atra'   : -0.1,
        'w_Foxp3_atra' : 0.035,
        'sigma_IL17'    : 30,
        'gamma_IL17'    : 1,
        'w_IL17_O'      : -0.82,
        'w_IL17_STAT3'          : 0.59,
        'w_IL17_ROR'  : 0.22,
        'w_IL17_Foxp3'          : -0.8,
        'gamma_Smad'  : 1,
        'sigma_Smad'    : 20,
        'w_Smad_O'      : -0.225,
        'w_Smad_tgf'    : 0.8*3.8/3,
        'gamma_UI'      : 1,
        'sigma_UI'      : 12,
        'w_UI_O'        : -0.23,
        'w_UI_tgf'      : 0.8*3.8/3,
        'gamma_STAT3'           : 0.1,
        'sigma_STAT3' : 10,
        'w_STAT3_O'   : -0.4,
        'w_STAT3_il6' : 0.2,
}


varspecs['asym'] = {
        'Foxp3' : \
                'gamma_Foxp3 * ( hbt(sigma_Foxp3, w_Foxp3_O + \
                w_Foxp3_Foxp3 * Foxp3 + w_Foxp3_ROR * ROR +\
                w_Foxp3_atra * atra  \
                + w_Foxp3_Smad * Smad +\
                 w_Foxp3_STAT3 * STAT3)\
                 - Foxp3 )',
        'Smad'  : \
                'gamma_Smad * ( hbt(sigma_Smad, w_Smad_O + w_Smad_tgf * tgf\
                 )\
                 - Smad )',
        'UI'    : \
```

```
                'gamma_UI * ( hbt(sigma_UI, w_UI_O + w_UI_tgf * tgf\
                 )\
                 - UI)',
        'ROR'   : \
                'gamma_ROR * ( hbt(sigma_ROR, w_ROR_O + \
                w_ROR_ROR * ROR + w_ROR_atra * atra + \
                w_ROR_Foxp3 * Foxp3 + w_ROR_UI * UI + \
                w_ROR_STAT3 * STAT3)\
                 - ROR )',
        'STAT3'         : \
                'gamma_STAT3 * ( hbt(sigma_STAT3, w_STAT3_O + \
                w_STAT3_il6 * il6)\
                - STAT3)',
        'IL17'  : \
                'gamma_IL17 * ( hbt(sigma_IL17,  w_IL17_STAT3 * STAT3 \
                 + w_IL17_O +\
                 w_IL17_ROR * ROR \
                 + w_IL17_atra * atra + w_IL17_Foxp3 * Foxp3) - IL17)'
}

fnspecs['asym'] = {
        'hbt': \
        (['sigma', 'sum_omega'],'1 / (1 + exp(-sigma * sum_omega))')
}


class Model_specs:
        def __init__(self, name):
                self.name = name
        def pars(self):
                return pars[self.name]
        def varspecs(self):
                return varspecs[self.name]
        def fnspecs(self):
                if fnspecs.has_key(self.name):
                        return fnspecs[self.name]
                else:
                        return {}
        def load_model_specs(self, args_obj):
                args_obj.pars = self.pars()
                args_obj.varspecs = self.varspecs()
                args_obj.fnspecs = self.fnspecs()
                # initialize every state varialbe with 0.001
                args_obj.ics = {}
                for key in self.varspecs():
                        args_obj.ics[key] = 0.001
```

Text S2

```
# This script produces the 1-parameter bifurcation diagrams shown in Figure 4A
# It requires a module file 'Model_specs.py' which contains equations for each
# model

import Model_specs
import PyDSTool
import matplotlib.pyplot as plt
from pylab import show
from sys import exit
from matplotlib import mpl
from matplotlib.ticker import NullFormatter

# Figure format
mpl.rcParams['font.sans-serif'] =  'Arial'
mpl.rcParams['mathtext.default'] = 'regular'
mpl.rcParams['xtick.labelsize'] = 8
mpl.rcParams['ytick.labelsize'] = 8
mpl.rcParams['figure.subplot.left'] = 0.2
mpl.rcParams['figure.subplot.right'] = 0.95
mpl.rcParams['figure.subplot.bottom'] = 0.08
mpl.rcParams['figure.subplot.wspace'] = 0.3
mpl.rcParams['figure.subplot.hspace'] = 0.03
text_ROR = 'ROR' + r"$\gamma$" + 't'
text_TGF = 'TGF-' + r"$\beta$"
nullfmt = NullFormatter()

# load the model specs from Model_specs.py
DSargs = PyDSTool.args(name='T_cell') # arbitary name
model_specs = Model_specs.Model_specs(name='sym_1') # Model name in Model_specs.py
model_specs.load_model_specs(DSargs) # load DSargs with functions and parameters

# set initial state
naive_state = {
        'ROR'   : 0.0001,
        'Foxp3' : 0.0001,
}
DSargs.ics = naive_state

# setup generator
ode = PyDSTool.Generator.Dopri_ODEsystem(DSargs)

ctrl_par = 'tgf' # control parameter
PyCont = PyDSTool.ContClass(ode)
PCargs = PyDSTool.args(name='EQ1', type='EP-C') # first branch
PCargs.freepars = [ctrl_par]

# Continuation numerics
PCargs.MaxNumPoints = 450
PCargs.MaxStepSize     = 0.02
```

```
PCargs.MinStepSize      = 1e-3
PCargs.StepSize         = 1e-2
PCargs.LocBifPoints     = 'all'
PCargs.SaveEigen        = True

# Compute first branch
PyCont.newCurve(PCargs)
PyCont['EQ1'].forward()

if PyCont['EQ1'].getSpecialPoint('BP1') is not None:
        PCargs.name = 'EQ2' # second branch
        PCargs.initpoint = 'EQ1:BP1'
        PCargs.initdirec = PyCont['EQ1'].getSpecialPoint('BP1')\
                .labels['BP']['data'].branch

        # Compute second branch
        PyCont.newCurve(PCargs)
        PyCont['EQ2'].forward()


# Plotting two 1-parameter bifurcation diagrams

fig = plt.figure(figsize=(4,8))
ax_ROR = fig.add_subplot(2,1,1)
PyCont.display([ctrl_par, 'ROR'], stability='true',\
          linewidth=1.5, color='r', axes=ax_ROR, figure=fig)
title = '1-parameter bifurcation\ndiagram'
size = 10
fp = mpl.font_manager.FontProperties(size=size)
ax_ROR.set_title(title)
ax_ROR.set_xlabel('')
ax_ROR.set_ylabel(text_ROR, fontproperties=fp)
ax_ROR.set_ylim([-0.1, 1.1])
ax_ROR.set_xlim([0.0, 0.7])
ax_ROR.xaxis.set_major_formatter(nullfmt)

ax_Foxp3 = fig.add_subplot(2,1,2)
PyCont.display([ctrl_par, 'Foxp3'], stability='true',\
          linewidth=1.5, color='g', axes=ax_Foxp3, figure=fig)
ax_Foxp3.set_xlabel(text_TGF)
ax_Foxp3.set_ylabel('Foxp3', fontproperties=fp)
ax_Foxp3.set_ylim([-0.1, 1.1])
ax_Foxp3.set_xlim([0.0, 0.7])


show()
exit()
```

CHAPTER 3

A simple theoretical framework for understanding heterogeneous differentiation of $CD4^+$ T cells

A research article published in BMC Systems Biology in 2012 (2012, 6: 66)

Tian Hong[1]

Email: hongtian@vt.edu

Jianhua Xing[2]

Email: jxing@vt.edu

Liwu Li[2]

Email: lwli@vt.edu

John J Tyson[2,*]

Email: tyson@vt.edu

[*] Corresponding author

[1]Genetics, Bioinformatics, and Computational Biology Program, Virginia Polytechnic Institute and State University, Blacksburg VA, 24061, USA

[2] Department of Biological Sciences, Virginia Polytechnic Institute and State University, Blacksburg VA, 24061, USA

[*]Corresponding author. Department of Biological Sciences, Virginia Polytechnic Institute and State University, Blacksburg VA, 24061, USA

Abstract

Background

$CD4^+$ T cells have several subsets of functional phenotypes, which play critical yet diverse roles in the immune system. Pathogen-driven differentiation of these subsets of cells is often heterogeneous in terms of the induced phenotypic diversity. *In vitro* recapitulation of heterogeneous differentiation under homogeneous experimental conditions indicates some highly regulated mechanisms by which multiple phenotypes of $CD4^+$ T cells can be generated from a single population of naïve $CD4^+$ T cells. Therefore, conceptual understanding of induced heterogeneous differentiation will shed light on the mechanisms controlling the response of populations of $CD4^+$ T cells under physiological conditions.

Results

We present a simple theoretical framework to show how heterogeneous differentiation in a two-master-regulator paradigm can be governed by a signaling network motif common to all subsets of $CD4^+$ T cells. With this motif, a population of naïve $CD4^+$ T cells can integrate the signals from their environment to generate a functionally diverse population with robust commitment of individual cells. Notably, two positive feedback loops in this network motif govern three bistable switches, which in turn, give rise to three types of heterogeneous differentiated states, depending upon particular combinations of input signals. We provide three prototype models illustrating how to use this framework to explain experimental observations and make specific testable predictions.

Conclusions

The process in which several types of T helper cells are generated simultaneously to mount complex immune responses upon pathogenic challenges can be highly regulated, and a simple signaling network motif can be responsible for generating all possible types of heterogeneous populations with respect to a

pair of master regulators controlling $CD4^+$ T cell differentiation. The framework provides a mathematical basis for understanding the decision-making mechanisms of $CD4^+$ T cells, and it can be helpful for interpreting experimental results. Mathematical models based on the framework make specific testable predictions that may improve our understanding of this differentiation system.

Background

$CD4^+$ T helper cells serve as key players in host immune responses by regulating and coordinating a large repertoire of immune cells, such as macrophages, B cells and $CD8^+$ T cells. Consequently, $CD4^+$ T helper cells are critical in human health ranging from homeostasis to pathogenesis of diseases [1,2]. Central to the functions of $CD4^+$ T cells is their ability to produce a wide range of extracellular immunomodulating agents including cytokines and chemokines [3]. In order to correctly direct the immune response to antigen stimulation, $CD4^+$ T cells have to secrete appropriate types of cytokines in appropriate amounts, and they achieve this by differentiating into various subtypes of functional $CD4^+$ T cells from a pool of precursor cells, known as naïve $CD4^+$ T cells. These subsets primarily include T helper 1 (T_H1), T helper 2 (T_H2), T helper 17 (T_H17) and induced regulatory T (iT_{Reg}) cells. Each subtype of $CD4^+$ T cells produces a distinctive spectrum of cytokines, and in each of these subtypes there is typically one key transcription factor, or master regulator, that is highly expressed and controls the expression of downstream genes, including those encoding the lineage specific cytokines. The master regulators for the four functional subsets are T-bet, GATA3, RORγt and Foxp3, respectively [3].

The differentiation of $CD4^+$ T cells is a highly controlled process, and the lineage specificity of the differentiation process is determined by integrating micro-environmental cues that activate various signaling pathways. These pathways include the T cell receptor (TCR) pathway and the Signal Transducer and Activator of Transcription (STAT) pathways [4,5], which are activated by cognate antigens and cytokines, respectively. Other pathways, such as those associated with Notch and Toll-like receptors (TLRs), are also involved in differentiation of $CD4^+$ T cells into distinct lineages [6-8].

In a few types of chronic infections, the dominance of one subtype of $CD4^+$ T cells can be observed [9]. However, most immune responses elicit balanced phenotypes of functional $CD4^+$ T cells and their

effector molecules, suggesting the importance of maintaining the diversity and flexibility of functional $CD4^+$ T cells [10,11]. The importance of balancing the phenotypic composition is further corroborated by the fact that inappropriate dominance of particular subtype(s) of $CD4^+$ T cells is often associated with inflammatory disorders [12-14]. It is not surprising to observe the balanced phenotypes of $CD4^+$ T cells *in vivo*, given the plausible heterogeneous micro-environments of the naïve $CD4^+$ T cells, which may stimulate the differentiation into multiple subtypes of functional $CD4^+$ T cells. Interestingly, however, highly purified naïve $CD4^+$ T cells can be induced to differentiate into multiple subtypes simultaneously in certain homogeneous *in vitro* experimental conditions [15-21]. Also interesting are the observations that optimum experimental conditions for generating homogeneous subsets of $CD4^+$ T cells often include conditions that block the differentiation of undesired subsets [3]. These observations suggest that some highly regulated mechanisms, intrinsic to naïve $CD4^+$ T cells, generate and maintain phenotypic heterogeneity of functional $CD4^+$ T cells. *In vitro* assays showing heterogeneous differentiation recapitulate, at least in part, the balanced $CD4^+$ T cell populations observed *in vivo*. Understanding situations of induced heterogeneous differentiation will shed light on the mechanisms controlling the response of populations of $CD4^+$ T cells under physiological conditions.

Although the overexpression of one type of master regulator is generally considered the hallmark of the differentiation of one subtype of $CD4^+$ T cells, it has been recently discovered that cells highly expressing two types of master regulators exist *in vivo* [16,17,22-26], and some of these 'double-positive' phenotypes have been shown to be important in responding to pathogens [16,17,26]. Consistent with *in vivo* studies showing that the numbers of single-positive and double-positive $CD4^+$ T cells can be increased in comparable proportions upon pathogenic challenges [16], *in vitro* induction of the differentiation of double-positive $CD4^+$ T cells often requires heterogeneous differentiation, which is accompanied by the differentiation of single-positive phenotypes [15-17]. Some double-positive $CD4^+$ T cells can be generated by reprogramming the single-positive phenotypes, which also results in a heterogeneous population containing both single-positive and double-positive cells [23,24]. These experiments provide

us with the clues to the conditions for generating double-positive phenotypes and highlight the intimate link between the double-positive phenotype and heterogeneous differentiation.

In most experiments demonstrating induction of heterogeneous differentiation, the expression levels of master regulators controlling two population subsets are examined at the single cell level. Despite the limited scope of these experiments in terms of the number of subsets considered, significant diversity of heterogeneous differentiation has been revealed. In a particular differentiation event, one can obtain one of the following types of heterogeneous populations (Figure 1): a population containing two types of single-positive cells [18], a population containing one type of single-positive cells and double-positive cells [17], and a population containing two types of single-positive cells and double-positive cells [15]. The diversity of heterogeneous differentiation in this minimum paradigm might be only the tip of an iceberg of complexity involving heterogeneous differentiation of all subsets of $CD4^+$ T cells, but understanding a minimal system with only two classical subtypes is surely the place to start.

Previously, mathematical modeling has advanced our understanding of $CD4^+$ T cell differentiation [27-32]. In particular, Höfer et al. [27] used a mathematical model to explain T_H2 cell fate memory created by positive feedbacks in the signaling network; Mariani et al. [28] used a similar model to demonstrate the robust lineage choice between T_H1 and T_H2 cells; Yates et al. [29] linked the dynamics of master regulators to the phenotypic composition of T_H1 and T_H2 cells during differentiation and reprogramming; van den Ham et al. [30] used a generic model to describe the switches among all $CD4^+$ T cell lineages; and Naldi et al. [32] developed a Boolean-network model that takes all four lineages of $CD4^+$ T cells into consideration. We recently used a mathematical model to study the reciprocal differentiation of T_H17 and iT_{Reg} cells, in which heterogeneous differentiation is observed [33]. It is unclear, however, how a broader spectrum of $CD4^+$ T cells can be involved in heterogeneous differentiation and what determines the observed types of differentiated states.

Here, we propose a simple theoretical framework for understanding the heterogeneous differentiation of $CD4^+$ T cells. We analyze the dynamic properties of a signaling network motif common to all $CD4^+$ T cell lineages. We show that, at the level of cell populations, this motif can generate all possible homogeneous and heterogeneous phenotypic compositions with respect to a pair of master regulators, and at the single-cell level it ensures the robust commitment of a particular choice of differentiated state. Two types of positive feedback loops in this network motif govern three types of bistable switches, which in turn, result in three types of heterogeneous differentiation upon receiving appropriate combinations of input signals. This framework facilitates not only an intuitive understanding of the complex process by which $CD4^+$ T cells integrate multiple signals to give rise to multiple functional phenotypes, but also the construction of more detailed mathematical models for studying $CD4^+$ T cell differentiation. We provide three prototype models illustrating how to use this framework to explain experimental observations and make specific testable predictions.

Results and Discussion

A basal signaling network motif is proposed to govern the differentiation of all lineages of $CD4^+$ T cells

To consider the heterogeneous differentiation of $CD4^+$ T cells, we introduce a minimal model based on a pair of master regulators (proteins X and Y). We neglect the influence of other master regulators during the differentiation process. In the undifferentiated (naïve) cell, the expression levels of X and Y are both low, and the stable expression of either X or Y marks the differentiation event. Three phenotypes can be observed upon differentiation: X single-positive (XSP) cell, Y single-positive (YSP) cell, and double-positive (DP) cell (Figure 1A). In the model, heterogeneous differentiation is defined as the process in which more than one functional (non-naïve) phenotypes can be observed upon uniform treatment of a population of simulated naïve cells (see Methods).

In this minimum paradigm, three types of heterogeneous differentiation can be induced: 1) two different types of single-positive cells are differentiated simultaneously from naïve precursors; 2) one type of single-positive cells differentiates simultaneously with double-positive cells; and 3) both types of single-positive cells differentiate simultaneously with double positive cells (Figure 1B). We define these three scenarios as Type 1, 2 and 3 heterogeneous differentiations, respectively.

We next propose a basal network motif that governs cell differentiation in this minimal model. Based on known molecular interactions, we notice that the four master regulators of $CD4^+$ T cells are all involved in signaling networks of similar topologies (Figure 2A-C). From these examples, we introduce a 'basal motif' (Figure 2D). In the basal motif, two master regulators (X and Y) mutually inhibit each other's expression, while activating their own production. Two types of signals are responsible for activating the expression of the master regulators: a 'primary signal' (S1) which is sufficient to fully upregulate at least

one master regulator, and two polarizing signals (S2 and S3) which favor the expression of one master regulator or the other (X and Y, respectively) but are not sufficient to upregulate their expression in the absence of a primary signal (Figure 2D). Each influence relationship in this basal motif has direct biological meaning, but some components in this motif may represent different biological entities in different dual-master-regulator networks. For example, in the T_H1-T_H2 network (Figure 2B) the primary signal represents the TCR ligands, whereas in the iT_{Reg}-T_H17 network (Figure 2C) it represents a combined treatment of TCR ligands and TGFβ, which is justified by the fact that both TCR and TGF-β signaling pathways activate both Foxp3 and RORγt. Note that the signals, which are treated as parameters in our models, represent exogenous cytokine doses only, not endogenous cytokines produced by T cells upon activation. The latter are represented in part by the auto-activation relations.

In Table 1, we list the generic signaling components and their corresponding biological entities for each prototype model. Note that a TCR ligand is a typical example of a primary signal, and certain groups of cytokines correspond to polarizing signals. In Table 2, we list the evidences for all molecular influences of each prototype model.

Table 1 Signaling components in basal motif and their corresponding biological components in prototype models

Model	Generic signaling component	Corresponding biological component
Prototype 1	Primary signal (S1)	TCR signal
Prototype 1	Polarizing signal 1 (S2)	Exogenous IL-12
Prototype 1	Polarizing signal 2 (S3)	Exogenous IL-4
Prototype 1	Master regulator 1 (X)	T-bet
Prototype 1	Master regulator 2 (Y)	GATA3
Prototype 2	Primary signal (S1)	TCR signal
Prototype 2	Polarizing signal 1 (S3-1)	Exogenous IL-23 + IL-1 signal
Prototype 2	Polarizing signal 2 (S3-2)	Exogenous TGF-β + IL-6 signal
Prototype 2	Master regulator 1 (X)	T-bet
Prototype 2	Master regulator 2 (Y)	RORγt
Prototype 3	Primary signal (S1)	TCR + Exogenous TGF-β signal
Prototype 3	Polarizing signal 1 (S2)	Exogenous ATRA/IL-2 signal
Prototype 3	Polarizing signal 2 (S3)	Exogenous IL-6 signal
Prototype 3	Master regulator 1 (X)	Foxp3
Prototype 3	Master regulator 2 (Y)	RORγt

Table 2 Evidences for molecular influences in prototype models

Model	Molecular Influence	Evidence
Prototype 1	TCR signal upregulates T-bet expression	[34]
Prototype 1	TCR signal upregulates GATA3 expression	[35]
Prototype 1	IL-12 signal upregulates T-bet expression in the presence of TCR signal	[34]
Prototype 1	IL-4 signal upregulates GATA3 expression in the presence of TCR signal	[18,36]
Prototype 1	T-bet inhibits GATA3 expression	[37]
Prototype 1	GATA3 inhibits T-bet expression	[38]
Prototype 1	T-bet promotes its own expression	[39]
Prototype 1	GATA3 promotes its own expression	[40]
Prototype 2	TCR signal upregulates T-bet expression	[34]
Prototype 2	TCR signal upregulates RORγt expression in the presence of TGF-β	[41,42]
Prototype 2	IL-23 + IL-1 signal upregulates RORγt expression in the presence of TCR signal	[17]
Prototype 2	TGF-β signal upregulates RORγt expression in the presence of TCR signal	[17]
Prototype 2	TGF-β signal downregulates T-bet expression	[43]
Prototype 2	T-bet inhibits RORγt expression	[44]
Prototype 2	RORγt inhibits T-bet expression	[45]
Prototype 2	T-bet promotes its own expression	[39]
Prototype 2	RORγt promotes its own expression	[11,46]
Prototype 3	TCR signal upregulates Foxp3 expression in the presence of TGF-β	[41,42]
Prototype 3	TCR signal upregulates RORγt expression in the presence of TGF-β	[41,42]
Prototype 3	TGF-β signal upregulates Foxp3 expression in the presence of TCR signal	[41,42]
Prototype 3	TGF-β signal upregulates RORγt expression in the presence of TCR signal	[41,42]
Prototype 3	IL-6 upregulates RORγt expression	[47]
Prototype 3	IL-6 downregulates Foxp3 expression	[47]
Prototype 3	ATRA/IL-2 upregulates Foxp3 expression	[48,49]
Prototype 3	ATRA/IL-2 downregulates RORγt expression	[48,49]
Prototype 3	Foxp3 inhibits RORγt expression	[50]
Prototype 3	RORγt inhibits Foxp3 expression	[51]
Prototype 3	Foxp3 promotes its own expression	[11]
Prototype 3	RORγt promotes its own expression	[11,46]

We first analyze Type 1 heterogeneous differentiation using the core motif, in the absence of auto-activation, and then we use the full version of the basal motif to explain all three types of heterogeneous differentiation.

The basal motif without auto-activations can generate Type 1 heterogeneous differentiation

The symmetric case

Consider first the case of perfectly symmetrical parameter settings (Additional file 1: Table S1 Generic Model 1) for the core motif without self-activations. (See the Methods section for a description of our mathematical model of the signaling motifs.) In the absence of exogenous signals, the system persists in the stable 'double-negative' state corresponding to naïve cells (Figure 3A). Small positive values of the primary signal ($0 < S1 < 0.704$) drive the expression of modest amounts of both master regulators in a single cell. Larger values ($0.704 < S1 < 2.396$) destabilize the co-expression state and give rise to two new (alternative) stable steady states: the X-high-Y-low state and the X-low-Y-high state, which correspond to XSP and YSP cells, respectively (Figure 3B). The basins of attraction of these two states are separated by the diagonal line ($X = Y$) through the state space. When the primary signal is extremely strong ($S1 > 2.396$), the system is attracted to a unique stable steady state (X-high-Y-high), corresponding to a DP cell (Figure 3C). Bifurcation analysis on these steady states shows that the system undergoes pitchfork bifurcations at $S1 = 0.704$ and at $S1 = 2.396$ (Figure 3D), a typical type of bifurcation obtained for dynamical systems with perfect symmetry [52-54]. Saturation of the primary signal may prevent cells from reaching the DP state (Additional file 2: Figure S1A and B).

The presence of a polarizing signal breaks the symmetry of the system, resulting in a pitchfork bifurcation with broken symmetry (Additional file 3: Figure S2A and B). To analyze the influence of polarizing signals on this dynamical system, we plot two-parameter bifurcation diagrams with respect to the primary signal and to each of the polarizing signals (e.g., Figure 3E, for S1 and S2). In Figure 3F we plot a 'bidirectional' two-parameter bifurcation diagram, with S2 versus S1 plotted 'up' and S3 versus S1 plotted 'down' (see Methods for details). In Figure 3F we see a bistable region (bounded by the red curves) for moderate values of the primary signal strength (0.7-2.3 units) and for low values (0–0.35 units) of either of the polarizing signal strengths. Within the bistable region are found the two types of

single-positive states. Outside the bistable region are found unique steady state solutions that vary continuously from the naïve state on the left to the double-positive state on the right, through intermediate region ($0.7 < S1 < 2.3$) dominated by XSP cells (for $S2 > 0$) or by YSP cells (for $S3 > 0$). Because of the perfect symmetry of the parameters, both of the cusps of the bistable region lie on the X-axis.

In order to predict the response of this regulatory system to changing stimuli (S1 and S2, or S1 and S3), we must be careful in interpreting the effects of trajectories crossing the two-parameter bifurcation diagram in Figure 3F. If we fix the polarizing signals at $S3 = 0$, $S2 = 0.1$ and increase the primary signal from 0 to 3, as in Additional file 3: Figure S2A and B, we see that the regulatory system passes smoothly from the naïve state (X-low-Y-low) to the XSP state (X-high-Y-low) to the DP state (X-high-Y-high). The regulatory system passes over the bistable region without undergoing any abrupt changes of the state (bifurcation) or exhibiting hysteresis effects. On the other hand, if we fix the primary signal at $S1 = 1.5$ and increase one of the polarizing signals (either S2 or S3), as in Additional file 3: Figure S2 C and D, we see that the regulatory system starts in one of the single-positive state and jumps abruptly to another single-positive state at a saddle-node bifurcation point. Also, the system exhibit hysteresis because, if the polarizing signal is reduced to zero after the jump occurs, the regulatory system remains stuck in the stable 'flipped' state (XSP if S2 increases/decreases, YSP if S3 increases/decreases). We call this type of response a 'reprogramming' switch, because the control system flips irreversibly between alternative single-positive states. On the contrary, transitions from the naïve or the DP state to either one of the single-positive states are smooth and reversible (they do not invoke reprogramming).

We next show that this network motif can generate heterogeneous differentiation and identify the parameter region in which a heterogeneous population can be obtained. To this end we simulate the induced differentiation process in a group of cells (with small cell-to-cell variability) exposed to various combinations of primary (S1) and polarizing signals (either S2 or S3). For each combination of S1 and S2 (or S3), we compute the percentages of cells of different phenotypes in the final (steady state) differentiated population. We plot these percentages (as heat maps) over the coordinates of the

bidirectional two-parameter bifurcation diagram (see Additional file 4: Figure S3A-D). We summarize these results with a 'heterogeneity score' (see Methods) to highlight the region of parameter space that can generate heterogeneous populations (Figure 3G). Not surprisingly, in the absence of strong polarizing signals ($S2 \approx 0$ and $S3 \approx 0$), the primary signal can induce heterogeneous differentiation of two single-positive phenotypes (Figure 3G, bright area). This is because of the close proximity of the naïve states to the separatrix, and the presence of cell-to-cell variability which can bias individual cells towards different phenotypes (Additional file 4: Figure S3E). The polarizing signal, on the other hand, makes the differentiation into one single-positive phenotype more likely, which can result in homogeneous differentiation once it is sufficiently strong (Figure 3G, dark area).

We next explore how the cell population responds to sequential stimuli rather than simultaneous stimuli. If the population is stimulated first by a polarizing signal and then, after the cells have reached their steady states, the simulations are continued in the presence of primary signal, we find that the response to sequential stimuli is very similar to the response to simultaneous stimuli (Figure 3H). But when we switch the sequence of the stimuli, the polarizing signal fails to influence cell fate in the bistable region, resulting in heterogeneous populations in this region (Figure 3I). This is due to a hysteresis effect, which prevents reprogramming by polarizing signals that are insufficiently strong. These results suggest that polarizing signals can influence cell fate determination until the induction of differentiation, after which their influence is greatly reduced.

Broken symmetry

The preceding analysis is based on a set of perfectly symmetrical parameters in the signaling network, although the exogenous polarizing signals can act as 'symmetry breakers'. How differently does the regulatory system behave if its intrinsic kinetic parameters are not perfectly symmetrical? For illustrative purposes, we use a representative set of asymmetrical parameter values (Additional file 1: Table S1 Generic Model 2). Because of the asymmetries, the primary signal upregulates the two master regulators

at different thresholds (Figure 4A and B), and the bistable region of the bidirectional two-parameter bifurcation diagram is re-oriented so that its cusps are located on different sides of the X-axis (Figure 4C). When we stimulate cell populations with combinations of primary and polarizing signals, we find that the parameter region that gives rise to heterogeneous populations is not coincident with the X-axis. Instead, the 'heterogeneous' region forms a patch that intersects the X-axis (Figure 4D). In this situation, the system requires a specific range of primary signal strength to generate a heterogeneous population. On the other hand, the primary signal now gains some control over cell fate determination, in addition to its ability to trigger the differentiation. For a similar network in B cells, Sciammas et al. [55] recently showed that the strength of the B cell receptor signal (primary signal) can determine cell fate because of the asymmetry of the network.

The effects of sequential stimuli in the asymmetrical model are similar to their effects in the symmetrical model (Figure 4E and F).

Up to this point, we have assumed that the relaxation rates of X and Y are identical ($\gamma_X = \gamma_Y = 5$). Breaking this symmetry changes the parameter combinations that generate heterogeneous differentiation without changing the bifurcation diagram (Additional file 5: Figure S4). This result, together with the responses to sequential stimuli discussed earlier, shows that although the bistable region is critical to obtaining heterogeneous differentiation, the exact phenotypic composition within the bistable region also depends on the kinetics of the signal inputs and the intrinsic relaxation rates of the master regulators.

We suggest that biological signaling networks of this type (i.e., those resembling the basal motif) may have evolved to take advantage of either symmetrical or asymmetrical types of behavior. A typical asymmetrical design is found in the T_H1 and T_H2 paradigm, in which TCR signaling not only triggers the heterogeneous differentiation of both T_H1 and T_H2, but also regulates their phenotypic compositions depending on signal strength (discussed in detail in later section). With this understanding, one can design

experiments to study more detailed signal-control principles of a particular signaling network governing heterogeneous differentiation.

The basal network motif with additional positive feedback loops can generate all types of heterogeneous differentiation

Previously, mathematical modelers found that interconnected positive feedback loops can give rise to complex multistability in $CD4^+$ T cell differentiation [28] and elsewhere [54]. It is still not clear, however, how these different multistable regions depend on the interconnection of multiple positive feedback loops, nor how one can use biologically relevant signals to guide cells into various multistable regions, where heterogeneous differentiation might occur. In this section, we show that our basal motif can give rise to complex multistability, we clarify the effects of the additional positive feedback loops using bifurcation analysis, and we explain the biological meaning of each parameter region in the context of the heterogeneous differentiation of $CD4^+$ T cells.

For illustrative purpose, we first choose another set of perfectly symmetrical parameters (Additional file 1: Table S1 Generic Model 3). This model differs from Generic Model 1 in that the double-negative feedback (mutual inhibition) is not strong enough to create bistability. Nonetheless, with the addition of symmetrical increase of auto-activation loops, a bistable region first appears in the intermediate range ($1.7 < S1 < 2.4$) of the primary signal (Additional file 6: Figure S5A), similar to the case of Generic Model 1 (Figure 3D). Further increase of the auto-activation weights enlarges the bistable region, and at a critical point (weights = 1.8), the pitchfork bifurcation changes from supercritical (Additional file 6: Figure S5A, weights = 1.5) to subcritical (Additional file 6: Figure S5B, weights = 3.2). Beyond the transition from supercritical to subcritical, each pitchfork bifurcation gives rise to two saddle-node bifurcation points (Additional file 6: Figure S5B and C). On the bidirectional (S1-S2-S3) two-parameter bifurcation diagram (Figure 5A), each cusp region 'folds back' to form three interconnected cusp regions, which govern two new bistable regions and one tristable region (Figure 5A). Further increase of the auto-

activation weights enlarges the original bistable region as well as the newly formed multistable regions. Eventually, the plane on the bidirectional two-parameter bifurcation diagram is divided into 11 regions with distinct stability features (Figure 5B).

We clarify this unique two-parameter bifurcation diagram as follows. If the autoactivation loops are absent or weaker, the parameter region outside of the reprogramming switchbistable region (Figure 3F) is continuous and monostable, although it can represent four types of steady states. Essentially, strong auto-activation loops create folding in this monostable region so that it is divided into four monostable regions separated by four new bistable regions. This structure effectively creates an additional level of robustness of cell fate commitment, which is rendered by two new types of bistable switches, in addition to the reprogramming switch. One type of switch consists of the two bistable regions located at lower range of the primary signal (Figure 5B, light blue areas), which controls differentiation/dedifferentiation commitment, i.e. the switches from or to the naïve state (Additional file 6: Figure S5D and E). Another type of switch consists of the two bistable regions located at higher range of the primary signal (Figure 5B, light yellow areas), which controls co-expression commitment, i.e. the switches from or to the double-positive state (Additional file 6: Figure S5D and E). We define these two switches as the 'differentiation switch' and the 'co-expression switch' respectively. The tri-stable regions in this diagram are the overlapping areas between the bistable regions governed by the reprogramming switch and either the differentiation or the co-expression switch. In fact, extremely high weights (>4) of auto-activation may give rise to a tetra-stable region, where the three types of the bistable regions overlap (Additional file 6: Figure S5C).

In summary, the positive feedback loop involving mutual inhibition of the master regulators can create the reprogramming switch, and additional feedback loops involving auto-activation can enhance the robustness of the reprogramming switch and create the differentiation switch and the co-expression switch. The features of the three bistable switches are listed in Table 3.

Table 3 Features of three bistable switches obtained with the basal motif

Bistable switch	Phenotypic transition controlled by the switch	Underlying positive feedback loops	Type of related heterogeneous differentiation
Differentiation	Naïve ⇔ XSP or YSP	Auto-activation	NA
Reprogramming	XSP ⇔ YSP	Created by mutual inhibition and enhanced by auto-activation	Type 1
Co-expression	XSP or YSP ⇔ DP	Auto-activation	Type 2

We next ran simulations to check whether these regions of multistability are correlated to various types of heterogeneous differentiation. Our results show that Type 1 heterogeneous differentiation can be induced in the reprogramming switch region (Figure 5C) (this is consistent with the results obtained with the core motif), Type 2 heterogeneous differentiation can be induced in the co-expression bistable switch regions (Figure 5D and E), and Type 3 heterogeneous differentiation can be induced in the tri-stable region consisting of three functional (non-naïve) states (Figure 5F). These types of heterogeneous differentiations are all robust in terms of single cell commitment because the corresponding parameter regions admit a variety of stable steady states.

Positive feedback loops have long been recognized as mechanisms for biological switches [56-58]. We have demonstrated that two types of positive feedback in the $CD4^+$ T cell differentiation network underlie three types of bistable switches that govern the transitions among different phenotypes of those T cells. In addition to ensuring the robust commitment, the multistability created by positive feedback loops may be used to generate phenotypic diversities of various types. In this context, the biological functions of the positive feedback loops are seen as more versatile than giving rise to simple on-or-off switches.

Our theoretical analysis of the basal regulatory motif (Figure 2D) started with symmetrical parameter values and then considered the effects of broken symmetries. In the next section, we show how non-symmetrical prototype models of heterogeneous differentiation among real lines of $CD4^+$ T cells can be studied within this unifying framework despite their diverse features.

Mathematical models based on the theoretical framework can be used to understand experimental results and make testable predictions

In this section we discuss three prototype models for studying heterogeneous differentiation of $CD4^+$ T cells. The first two models are aimed to explain some interesting biological phenomena that were not studied previously with mathematical modeling. The third one is a simplified version of our previous model [33], but we have made it more accessible by using the framework presented here. Because of their limited scope, none of these models are intended to provide a comprehensive understanding of the corresponding biological systems. Rather, our intention is to illustrate how to use the modeling framework to explain observed heterogeneous differentiation and make testable predictions.

Prototype Model 1: Heterogeneous differentiation of T_H1 and T_H2 cells

Previous mathematical models successfully described the dynamic behavior and the underlying molecular control system of the reciprocal differentiation of T_H1 and T_H2 cells [27-31]. However, heterogeneous differentiation of T_H1 and T_H2 cells and its underlying molecular controls were not studied with these models. Yamashita et al. [18] discovered that the heterogeneous differentiation of T_H1 and T_H2 cells can be obtained with antigenic stimulations. Similar observations were obtained by Hosken et al. [20], and Messi et al. [21]. We have built a mathematical model, based on the influence diagram in Figure 2A, to describe heterogeneous differentiation of T_H1 and T_H2 cells. The parameter values for the model are listed in Additional file 1: Table S2.

Figure 6A shows the bidirectional two-parameter bifurcation diagram, and Figure 6B shows the simulation results as the heterogeneity score with respect to the two single-positive phenotypes. Our simulation results suggest that exogenous polarizing signals, i.e. IL-4 and IL-12, are not sufficient to trigger differentiation. They must be accompanied by a sufficiently high dose of antigenic stimulant (TCR signal) to trigger the differentiation into the corresponding phenotypes. This conclusion is in agreement

with previous experimental results [18]. High strength of TCR signal alone (>1 unit) or with intermediate level of IL-4 (0.3 unit) was sufficient to induce the differentiation of two single-positive phenotypes. With increasing strengths of TCR signal, our simulations show a spectrum of heterogeneous populations with increasing percentages of T_H2 cells and decreasing percentage of T_H1 cells. The following experimental findings are consistent with our simulation. Messi et al. [21] observed the heterogeneous differentiation of T_H1 and T_H2 with IL-4 and antigenic stimulant. Yamashita et al. [18] observed a similar pattern of heterogeneous populations with increasing doses of antigenic stimulant in the presence of an intermediate level of IL-4. Hosken et al. [20] also observed such pattern with a different type of antigenic stimulant, although only a narrow range of stimulant concentrations could give rise to heterogeneous populations. Clearly, our model predicts that in order to achieve comparable proportions of T_H1 cells and T_H2 cells, one would need a higher dose of antigenic stimulant without exogenous IL-4 as compared to with exogenous IL-4. Based on the bifurcation diagram, we also predict that a slow increase of stimulant concentration favors the differentiation of T_H1 cells. Additionally, the simulation results and bifurcation analysis show that the double-positive phenotype can be obtained in the presence of T_H1 polarizing signals. Hegazy et al. [24] have discovered that exogenous T_H1 polarizing signals can reprogram T_H2 cells into T-bet$^+$GATA3$^+$ cells in the presence of antigenic stimulant. Our model predicts that the differentiation of such double-positive phenotype can be directly induced by high dose of antigenic stimulant (>2 units) in the presence of exogenous T_H1 polarizing signals (0.5 unit), and the differentiation is likely to be heterogeneous with the concurrent induction of two types of single-positive cells, in addition to the double-positive cells. If we reduce the auto-activation weight of GATA3 (see Methods), then the TCR signal primarily triggers the differentiation of T_H1 cells instead of a heterogeneous population (Figure 6C and D). Maruyama et al. [59] demonstrated that TCR signal alone can induce a significant fraction of GATA3$^+$ cells (this is consistent with the experimental findings mentioned above), and blocking the auto-activation feedback between GATA3 and IL-4 prevents the induction of GATA3$^+$ cells. Our model predicts that the population may be dominated by T_H1 cells under this condition.

Table 4 summarizes the published observations consistent with our simulation results and new predictions based on the bifurcation analyses and simulation results.

Table 4 Summary of simulation results of Prototype Model 1

Conditions of differentiation induction	Induced cell population	Evidence
Exogenous polarizing signals alone	No induction of differentiation	[18]
Low dose of antigenic stimulant (TCR signal <1 units) and exogenous polarizing signals	Homogeneous differentiation (induced phenotype corresponds to type polarizing signal)	[18]
Antigenic stimulant in the presence of IL-4	Heterogeneous differentiation of T_H1 and T_H2	[18,21]
Increasing strengths of TCR signal	A spectrum of heterogeneous populations with increasing percentages of T_H2 cells and decreasing percentage of T_H1 cells.	[20]
Increasing strengths of TCR signal in the presence of IL-4	A spectrum of heterogeneous populations with increasing percentages of T_H2 cells and decreasing percentage of T_H1 cells.	[18]
TCR signal alone vs. TCR signal with IL-4	Stronger TCR signal is required to achieve a balanced population of T_H1 and T_H2 in condition without IL-4 than in condition with IL-4	Prediction
TCR signal + T_H1 polarizing signals	Double-positive phenotype can be observed (via reprogramming from T_H2 cells)	[24]
TCR signal + T_H1 polarizing signals	Direct induction of double-positive phenotype can be achieved with strong TCR signal and T_H1 polarizing condition	Prediction
Blocking GATA3-IL4 feedback by antibodies against IL-4 and inducing with TCR signal	No T_H2 cells are observed	[59]
Blocking GATA3-IL4 feedback by antibodies against IL-4 and inducing with TCR signal	Homogeneous differentiation of T_H1 cells	Prediction

Prototype Model 2: Heterogeneous differentiation of T_H1 and T_H17 cells

We build a prototype model to study the heterogeneous differentiation of T_H1 and T_H17 cells that was recently demonstrated by Ghoreschi et al. [17]. The influence diagram of the model is shown in Figure 2B, and the parameter values are listed in Additional file 1: Table S3. In the presence of TCR signal alone, the simulated population is dominated by T_H1 cells (Figure 7A and B). When the TCR signal is combined with IL-23 + IL-1 polarizing signal, the induced population contains both the T-bet$^+$RORγt$^-$ single-positive phenotype and the T-bet$^+$RORγt$^+$ double positive phenotype (Figure 7A and B). When the

TCR signal is combined with TGF-β (another polarizing signal), the population is dominated by the T-bet$^-$RORγt$^+$ single-positive phenotype (Figure 7C and D). These results are consistent with the observations of Ghoreschi et al. [17]. Our model predicts that lowering the TCR signal strength may result in the reprogramming from T-bet$^+$RORγt$^+$ double positive phenotype to T-bet$^+$RORγt$^-$ single positive phenotype even in the presence of a strong IL-23 + IL-1 signal and that when low dose of TGF-β + IL-6 (≈0.4 unit) is used, one may observe the heterogeneous differentiation of T_H1 and T_H17 cells. Also, the model recapitulates the scenario in which knocking out T-bet genes resulted in the homogeneous differentiation into T-bet$^-$RORγt$^+$ single-positive phenotype when either of the polarizing signals is used (Additional file 7: Figure S6) [17].

Simulation results with testable predictions are summarized in Table 5.

Table 5 Summary of simulation results of Prototype Model 2

Conditions of differentiation induction	Induced cell population	Evidence
TCR signal alone`	The cell population is dominated by the T_H1 cells	[17]
TCR signal and IL-23 + IL-1 signal	Heterogeneous differentiation of T-bet$^+$RORγt$^-$ cells and T-bet$^+$RORγt$^+$ cells.	[17]
TCR signal and TGF-β + IL-6 signal	The cell population is dominated by T-bet$^-$RORγt$^+$ cells	[17]
Lowering TCR signal after differentiation	Reprogramming from T-bet$^+$RORγt$^+$ cells to T-bet$^+$RORγt$^-$ cells	Prediction
TCR signal and low dose of TGF-β + IL-6 (≈0.4 unit)	Heterogeneous differentiation of T_H1 and T_H17 cells	Prediction
Knocking out T-bet genes and inducing with TCR signal	Homogeneous differentiation of T-bet$^-$RORγt$^+$ cells with either TGF-β signal or IL-23 + IL-1 signal	[17]

Prototype Model 3: Heterogeneous differentiation of iT_{Reg} and T_H17 cells

Heterogeneous differentiation of iT_{Reg} and T_H17 cells has been observed in many experiments [15,16,19]. Here we present a prototype model based on the influence diagram (Figure 2C) and the parameter values (Additional file 1: Table S4). The model shows that a combination of TGF-β and TCR signal can drive a heterogeneous population containing Foxp3$^+$RORγt$^-$, Foxp3$^-$RORγt$^+$ and Foxp3$^+$RORγt$^+$ phenotypes (Figure 8A and B, tri-stable region at TCR + TGF-β signal ≈ 1.8). Raising the strength of TGF-β + TCR

signal or adding IL-6 (a T_H17 polarizing signal) can skew the population into $Foxp3^-ROR\gamma t^+$ and $Foxp3^+ROR\gamma t^+$ phenotypes (Figure 8A and B, bistable region in the upper plot at highest level of TCR + TGF-β signal). These results are in agreement with previous experimental observations [15,16]. Predictions made from the model include: 1) an intermediate TGF-β + TCR signal (1–1.5 units) favors heterogeneous differentiation of $Foxp3^+ROR\gamma t^-$ and $Foxp3^-ROR\gamma t^+$ populations; 2) an intermediate level of TGF-β + TCR signal (1–1.5 units) with an iT_{Reg} polarizing signal produces a homogeneous $Foxp3^+ROR\gamma t^-$ population; and 3) a high level of TGF-β + TCR signal (>2 units) with an iT_{Reg} polarizing signal induces heterogeneous $Foxp3^+ROR\gamma t^-$ and $Foxp3^+ROR\gamma t^+$ populations.

Simulation results with testable predictions are summarized in Table 6.

Table 6 Summary of simulation results of Prototype Model 3

Conditions of differentiation induction	Induced cell population	Evidence
Intermediate TGF-β + TCR signal (1.5-2 units)	Heterogeneous differentiation of $Foxp3^+ROR\gamma t^-$, $Foxp3^-ROR\gamma t^+$ and $Foxp3^+ROR\gamma t^+$ cells	[15]
High TGF-β + TCR signal (2.5 units)	Heterogeneous differentiation of $Foxp3^-ROR\gamma t^+$ and $Foxp3^+ROR\gamma t^+$ cells	[16]
Low-Intermediate TGF-β + TCR signal (1–2 units) and IL-6 signal	Heterogeneous differentiation of $Foxp3^-ROR\gamma t^+$ and $Foxp3^+ROR\gamma t^+$ cells	[15]
Low TGF-β + TCR signal (1–1.5 units)	Heterogeneous differentiation of $Foxp3^+ROR\gamma t^-$, $Foxp3^-ROR\gamma t^+$ cells	Prediction
Low-intermediate level of TGF-β + TCR signal (1–2 units) and IL-2 or ATRA	Homogeneous differentiation of $Foxp3^+ROR\gamma t^-$ cells	Prediction
High TGF-β + TCR signal (2.5 units) and IL-2 or ATRA	Heterogeneous differentiation of $Foxp3^+ROR\gamma t^-$ and $Foxp3^+ROR\gamma t^+$ cells	Prediction

Conclusions

In this study, we have demonstrated that a simple signaling network motif can be responsible for generating all possible types of heterogeneous populations with respect to a pair of master regulators controlling $CD4^+$ T cell differentiation. We showed how naïve $CD4^+$ T cells can integrate multiple types of signals to differentiate into populations of diverse phenotypes. We illustrate the theoretical framework with three specific cases and made testable predictions.

It is becoming evident that certain signals can drive the differentiation of multiple lineages of T cells, whereas other environmental cues can skew the outcome to specific phenotypes [60]. Because the proposed basal motif appears commonly in the signaling networks controlling $CD4^+$ T cell differentiation, biological examples of this framework are clearly not limited to the prototype models we presented here. For example, it has been recently demonstrated that STAT3 activation is required for T_H2 differentiation [61]. This gives the possibility that IL-6, which upregulates RORγt via STAT3 activation [62], can act as a primary signal giving rise to heterogeneous T_H2 and T_H17 populations if the cells are primed with certain amount of other signals, such as TCR, TGF-β and IL-4.

Our study suggests the importance of regulated cell-to-cell variations that can be exploited to generate phenotypic diversity in $CD4^+$ T cells. The significance of such variations in some other biological systems has been highlighted by other groups. Feinerman et al. [63] discovered that the cell-to-cell variations in the expression levels of some key co-receptors in $CD8^+$ T cells can be critical for achieving diversity in TCR responses. Similarly, Chang et al. [64] demonstrated that variations in the expression of stem cell markers can influence the fate of the cell. We have used a simple generic form to account for cell-to-cell variability in this study (i.e. parametric variations), it would be interesting to study which specific variable factors in naïve $CD4^+$ T cells can be predictive of the phenotypic compositions in an induced population. Harnessing such factors might be useful for fine-tuning the immune system to prevent and treat diseases.

Our modeling approach has the advantage of describing non-linear responses in biochemical reactions without knowing detailed biochemical mechanisms and kinetics, which are generally unavailable for T cell differentiation. It has the disadvantage that parameters in the equations are phenomenological and cannot be related to biochemical reaction rate constants. We expect that other modeling approaches, such as ordinary differential equations with Hill function nonlinearities, will produce results similar to ours.

We are aware of the following limitations of this framework. First, all master regulators of $CD4^+$ T cell may influence each other during differentiation. Thus considering only a pair of master regulators may not be sufficient to describe all important components governing the heterogeneous differentiation of $CD4^+$ T cells. Secondly, cell-to-cell communication is neglected in our models of cell population. We assume that our models describe the initial phase of differentiation and that the phenotypic compositions of the population do not change significantly during the differentiation process. The validity of this assumption needs to be examined in future studies.

Methods

Dynamical model

We modeled the signaling network motifs with a generic form of ordinary differential equations (ODEs) that describe both gene expression and protein interaction networks [65-67]. Each ODE in our model has the form:

$$\frac{dX_i}{dt} = \gamma_i (F(\sigma_i W_i) - X_i)$$
$$F(\sigma W) = 1 \Big/ (1 + e^{-\sigma W})$$
$$W_i = (\omega_i^o + \sum_j^N \omega_{j \to i} X_j)$$
$$i = 1, \ldots, N$$

X_i is the activity or concentration of protein i. On a time scale = 1/ $_i$, $X_i(t)$ relaxes toward a value determined by the sigmoidal function, F, which has a steepness set by σ_i. The basal value of F, in the absence of any influencing factors, is determined by ω_i^0. The coefficients $\omega_{j \to i}$ determine the influence of protein j on protein i. N is the total number of proteins in the network.

All variables and parameters are dimensionless. One time unit in our simulations corresponds to 1.5 days. Parameter values are listed in supplementary tables.

All simulations and bifurcation analyses were performed with PyDSTool, a software environment for dynamical systems [68].

Bifurcation diagrams

In order to visualize the response of the T cell differentiation network to multiple signals (a primary differentiation signal and two types of polarizing signals), we have employed bidirectional two-parameter bifurcation diagrams, as in [69]. The two two-parameter bifurcation diagrams share the same primary bifurcation parameter (the primary differentiation signal, S1) on the horizontal axis. The secondary bifurcation parameters (the polarizing signals, S2 and S3) are plotted on the vertical axis: one in the upward direction and the other in the downward direction. The bidirectional two-parameter bifurcation diagram allows one to analyze the response of the regulatory system to the primary signal alone or in combination with either of the polarizing signals. Although this two-dimensional representation does not allow a full analysis of the responses to all three types of signals simultaneously, it is very useful in understanding the complex interplay between signals and responses in these heterogeneous differentiation systems. We ran simulations for a population of naïve $CD4^+$ T cells, and we overlaid the simulation results on the bidirectional two-parameter bifurcation diagrams, allowing one to visualize the bifurcation analyses and simulation results simultaneously (detailed below).

Cell-to-cell variability

To account for cell-to-cell variability in a population, we made many simulations of the system of ODEs, each time with a slightly different choice of parameter values, to represent slight differences from cell to cell. We allowed all of the parameters in our model to change simultaneously, and we assumed that the value of each parameter conforms to a normal distribution with $CV = 0.05$ ($CV =$ coefficient of variation $=$ standard deviation / mean). The mean value that we specified for each parameter distribution is also referred as the 'basal' value of that parameter. In our bifurcation analysis of the dynamical system, we considered an imaginary cell that adopts the basal value for each of its parameters, and we defined this cell as the 'average' cell. Note that none of the cells in our simulated population is likely to be this average cell, because every parameter value is likely to deviate a little ($CV = 5$ %) from the basal value.

In order to simulate the induced differentiation process, we first solved the ODEs numerically with some small initial values of master regulator concentrations in the absence of any exogenous signals. After a short period of time, each simulated cell will find its own, stable 'double-negative' steady state, corresponding to a naïve $CD4^+$ T cell. Next, we changed the primary and/or polarizing signals to certain positive values and continued the numerical simulation. If needed, we continued the simulation again with a second change of primary and/or polarizing signals. By the end of the simulation, each cell arrives at its corresponding 'induced' phenotype, which might vary from cell to cell because of the parametric variability of the population. We repeated this simulation 200 times for a given set of exogenous signals to represent the responses of 200 cells in a population. We made the simple definition that a protein is expressed when its level is greater than 0.5 units. The simulations for a cell population were repeated 40x40 times with primary and polarizing signals of various strengths, and we overlaid the final steady state phenotypic composition on the point with corresponding coordinates on the bidirectional two-parameter bifurcation diagram.

Mutant simulation

The experiment of knocking out GATA3-IL-4 feedback was simulated with reduced weight of auto-activation of GATA-3 to one-tenth of the original value. The experiment of knocking out T-bet genes was simulated by setting $\omega^{o}_{\text{T-bet}} = -17$ (10 times its value in the basal model)

Heterogeneity score

To summarize simulations results with multiple phenotypes and to highlight heterogeneous and homogeneous populations in parameter space, we compute a 'heterogeneity score' for a simulation as follows.

$$S_H\left(P_1,\ldots,P_n\right)=\frac{\sum_{i=1}^{n-1}\sum_{j=i+1}^{n}\left(C_{P_i}+C_{P_j}-2\left|C_{P_i}-C_{P_j}\right|\right)}{\left(n-1\right)N}$$

The scoring function takes a list of 'phenotypes of interest' ($P_1,\ldots,P_n$), and computes the sum of the pairwise heterogeneities, which are based on the numbers of cells of any two different phenotypes (C_{P_i} and C_{P_j}). The score is normalized with respect to the number of phenotypes of interest (n) and the total number of cells in the population (N). $S_H \approx 1$ when there are comparable numbers of cells of the phenotypes of interest in the population, $S_H \approx -1$ when the population is dominated by one phenotype out of all the phenotypes of interest, and $S_H \approx 0$ when there are few cells with the phenotypes of interest in the population, or the degree of heterogeneity is moderate.

Authors' Contributions

Conceived and designed the experiments: TH JX LL JJT. Performed the experiments: TH. Analyzed the data: TH JX LL JJT. Wrote the paper: TH LL JJT. All authors read and approved the final manuscript.

Acknowledgements

TH was supported by a Transdisciplinary Team Science Fellowship from the Virginia Bioinformatics Institute, and by an NIH Grant (R01 GM078989-05) to JJT. LL was partially supported by grants from NIH (R0164414) and the American Heart Association. JX was supported by an NSF grant (DMS-0969417) and an NIAID grant 1R03AI099120. The funders had no role in study design, data collection and analysis, decision to publish, or preparation of the manuscript.

Competing Interests

The authors declare that they have no competing interests.

References

1. Dranoff G, Jaffee E, Lazenby A, Golumbek P, Levitsky H, Brose K, Jackson V, Hamada H, Pardoll D, Mulligan RC: Vaccination with irradiated tumor cells engineered to secrete murine granulocyte-macrophage colony-stimulating factor stimulates potent, specific, and long-lasting anti-tumor immunity.*ProcNatlAcadSci U S A* 1993, 90:3539–3543.

2. Moir S, Chun TW, Fauci AS: Pathogenic mechanisms of HIV disease.*Annu Rev Pathol* 2011, 6:223–248.

3. Zhu J, Yamane H, Paul WE: Differentiation of effector CD4 T cell populations.*Annu Rev Immunol* 2010, 28:445–489.

4. Nakayama T, Yamashita M: The TCR-mediated signaling pathways that control the direction of helper T cell differentiation.*SeminImmunol* 2010, 22:303–309.

5. O'Shea JJ, Lahesmaa R, Vahedi G, Laurence A, Kanno Y: Genomic views of STAT function in CD4+ T helper cell differentiation.*Nat Rev Immunol* 2011, 11:239–250.

6. Fang TC, Yashiro-Ohtani Y, Del Bianco C, Knoblock DM, Blacklow SC, Pear WS: Notch directly regulates Gata3 expression during T helper 2 cell differentiation.*Immunity* 2007, 27:100–110.

7. Reynolds JM, Pappu BP, Peng J, Martinez GJ, Zhang Y, Chung Y, Ma L, Yang XO, Nurieva RI, Tian Q, Dong C: Toll-like receptor 2 signaling in CD4(+) T lymphocytes promotes T helper 17 responses and regulates the pathogenesis of autoimmune disease.*Immunity* 2010, 32:692–702.

8. Amsen D, Blander JM, Lee GR, Tanigaki K, Honjo T, Flavell RA: Instruction of distinct CD4 T helper cell fates by different notch ligands on antigen-presenting cells.*Cell* 2004, 117:515–526.

9. Sher A, Coffman RL: Regulation of immunity to parasites by T cells and T cell-derived cytokines.*Annu Rev Immunol* 1992, 10:385–409.

10. O'Shea JJ, Paul WE: Mechanisms underlying lineage commitment and plasticity of helper CD4+ T cells.*Science* 2010, 327:1098–1102.

11. Murphy KM, Stockinger B: Effector T cell plasticity: flexibility in the face of changing circumstances.*Nat Immunol* 2010, 11:674–680.

12. Littman DR, Rudensky AY: Th17 and regulatory T cells in mediating and restraining inflammation.*Cell* 2010, 140:845–858.

13. Romagnani S: Immunologic influences on allergy and the TH1/TH2 balance.*J Allergy ClinImmunol* 2004, 113:395–400.

14. Mauri C, Williams RO, Walmsley M, Feldmann M: Relationship between Th1/Th2 cytokine patterns and the arthritogenic response in collagen-induced arthritis.*Eur J Immunol* 1996, 26:1511–1518.

15. Zhou L, Lopes JE, Chong MM, Ivanov II, Min R, Victora GD, Shen Y, Du J, Rubtsov YP, Rudensky AY, *et al*: TGF-beta-induced Foxp3 inhibits T(H)17 cell differentiation by antagonizing RORgammat function.*Nature* 2008, 453:236–240.

16. Lochner M, Peduto L, Cherrier M, Sawa S, Langa F, Varona R, Riethmacher D, Si-Tahar M, Di Santo JP, Eberl G: In vivo equilibrium of proinflammatory IL-17+ and regulatory IL-10+ Foxp3+ RORgamma t + T cells.*J Exp Med* 2008, 205:1381–1393.

17. Ghoreschi K, Laurence A, Yang XP, Tato CM, McGeachy MJ, Konkel JE, Ramos HL, Wei L, Davidson TS, Bouladoux N, *et al*: Generation of pathogenic T(H)17 cells in the absence of TGF-beta signalling.*Nature* 2010, 467:967–971.

18. Yamashita M, Kimura M, Kubo M, Shimizu C, Tada T, Perlmutter RM, Nakayama T: T cell antigen receptor-mediated activation of the Ras/mitogen-activated protein kinase pathway controls interleukin 4 receptor function and type-2 helper T cell differentiation.*ProcNatlAcadSci U S A* 1999, 96:1024–1029.

19. Molinero LL, Miller ML, Evaristo C, Alegre ML: High TCR stimuli prevent induced regulatory T cell differentiation in a NF-kappaB-dependent manner.*J Immunol* 2011, 186:4609–4617.

20. Hosken NA, Shibuya K, Heath AW, Murphy KM, O'Garra A: The effect of antigen dose on CD4+ T helper cell phenotype development in a T cell receptor-alpha beta-transgenic model.*J Exp Med* 1995, 182:1579–1584.

21. Messi M, Giacchetto I, Nagata K, Lanzavecchia A, Natoli G, Sallusto F: Memory and flexibility of cytokine gene expression as separable properties of human T(H)1 and T(H)2 lymphocytes.*Nat Immunol* 2003, 4:78–86.

22. Ayyoub M, Deknuydt F, Raimbaud I, Dousset C, Leveque L, Bioley G, Valmori D: Human memory FOXP3+ Tregs secrete IL-17 ex vivo and constitutively express the T(H)17 lineage-specific transcription factor RORgamma t.*ProcNatlAcadSci U S A* 2009, 106:8635–8640.

23. Voo KS, Wang YH, Santori FR, Boggiano C, Arima K, Bover L, Hanabuchi S, Khalili J, Marinova E, Zheng B, *et al*: Identification of IL-17-producing FOXP3+ regulatory T cells in humans.*ProcNatlAcadSci U S A* 2009, 106:4793–4798.

24. Hegazy AN, Peine M, Helmstetter C, Panse I, Frohlich A, Bergthaler A, Flatz L, Pinschewer DD, Radbruch A, Lohning M: Interferons direct Th2 cell reprogramming to generate a stable GATA-3(+)T-bet(+) cell subset with combined Th2 and Th1 cell functions.*Immunity* 2010, 32:116–128.

25. Zhu J, Paul WE: Peripheral CD4+ T-cell differentiation regulated by networks of cytokines and transcription factors.*Immunol Rev* 2010, 238:247–262.

26. Abromson-Leeman S, Bronson RT, Dorf ME: Encephalitogenic T cells that stably express both T-bet and ROR gamma t consistently produce IFNgamma but have a spectrum of IL-17 profiles.*J Neuroimmunol* 2009, 215:10–24.

27. Hofer T, Nathansen H, Lohning M, Radbruch A, Heinrich R: GATA-3 transcriptional imprinting in Th2 lymphocytes: a mathematical model.*ProcNatlAcadSci U S A* 2002, 99:9364–9368.

28. Mariani L, Lohning M, Radbruch A, Hofer T: Transcriptional control networks of cell differentiation: insights from helper T lymphocytes.*ProgBiophysMolBiol* 2004, 86:45–76.

29. Yates A, Callard R, Stark J: Combining cytokine signalling with T-bet and GATA-3 regulation in Th1 and Th2 differentiation: a model for cellular decision-making.*J TheorBiol* 2004, 231:181–196.

30. van den Ham HJ, de Boer RJ: From the two-dimensional Th1 and Th2 phenotypes to high-dimensional models for gene regulation.*IntImmunol* 2008, 20:1269–1277.

31. Mendoza L, Xenarios I: A method for the generation of standardized qualitative dynamical systems of regulatory networks.*TheorBiol Med Model* 2006, 3:13.

32. Naldi A, Carneiro J, Chaouiya C, Thieffry D: Diversity and plasticity of Th cell types predicted from regulatory network modelling.*PLoSComputBiol* 2010, 6:e1000912.

33. Hong T, Xing J, Li L, Tyson JJ: A mathematical model for the reciprocal differentiation of T helper 17 cells and induced regulatory T cells.*PLoSComputBiol* 2011, 7:e1002122.

34. Placek K, Gasparian S, Coffre M, Maiella S, Sechet E, Bianchi E, Rogge L: Integration of distinct intracellular signaling pathways at distal regulatory elements directs T-bet expression in human CD4+ T cells.*J Immunol* 2009, 183:7743–7751.

35. Yamane H, Zhu J, Paul WE: Independent roles for IL-2 and GATA-3 in stimulating naive CD4+ T cells to generate a Th2-inducing cytokine environment.*J Exp Med* 2005, 202:793–804.

36. Zhu J, Guo L, Watson CJ, Hu-Li J, Paul WE: Stat6 is necessary and sufficient for IL-4's role in Th2 differentiation and cell expansion.*J Immunol* 2001, 166:7276–7281.

37. Usui T, Preiss JC, Kanno Y, Yao ZJ, Bream JH, O'Shea JJ, Strober W: T-bet regulates Th1 responses through essential effects on GATA-3 function rather than on IFNG gene acetylation and transcription.*J Exp Med* 2006, 203:755–766.

38. Zhu J, Jankovic D, Grinberg A, Guo L, Paul WE: Gfi-1 plays an important role in IL-2-mediated Th2 cell expansion.*ProcNatlAcadSci U S A* 2006, 103:18214–18219.

39. Mullen AC, High FA, Hutchins AS, Lee HW, Villarino AV, Livingston DM, Kung AL, Cereb N, Yao TP, Yang SY, Reiner SL: Role of T-bet in commitment of TH1 cells before IL-12-dependent selection.*Science* 2001, 292:1907–1910.

40. Ouyang W, Lohning M, Gao Z, Assenmacher M, Ranganath S, Radbruch A, Murphy KM: Stat6-independent GATA-3 autoactivation directs IL-4-independent Th2 development and commitment.*Immunity* 2000, 12:27–37.

41. Yang XO, Nurieva R, Martinez GJ, Kang HS, Chung Y, Pappu BP, Shah B, Chang SH, Schluns KS, Watowich SS, *et al*: Molecular antagonism and plasticity of regulatory and inflammatory T cell programs.*Immunity* 2008, 29:44–56.

42. Yang L, Anderson DE, Baecher-Allan C, Hastings WD, Bettelli E, Oukka M, Kuchroo VK, Hafler DA: IL-21 and TGF-beta are required for differentiation of human T(H)17 cells.*Nature* 2008, 454:350–352.

43. Gorelik L, Constant S, Flavell RA: Mechanism of transforming growth factor beta-induced inhibition of T helper type 1 differentiation.*J Exp Med* 2002, 195:1499–1505.

44. Lazarevic V, Chen X, Shim JH, Hwang ES, Jang E, Bolm AN, Oukka M, Kuchroo VK, Glimcher LH: T-bet represses T(H)17 differentiation by preventing Runx1-mediated activation of the gene encoding RORgammat.*Nat Immunol* 2011, 12:96–104.

45. Mukasa R, Balasubramani A, Lee YK, Whitley SK, Weaver BT, Shibata Y, Crawford GE, Hatton RD, Weaver CT: Epigenetic instability of cytokine and transcription factor gene loci underlies plasticity of the T helper 17 cell lineage.*Immunity* 2010, 32:616–627.

46. Gutcher I, Donkor MK, Ma Q, Rudensky AY, Flavell RA, Li MO: Autocrine transforming growth factor-beta1 promotes in vivo Th17 cell differentiation.*Immunity* 2011, 34:396–408.

47. Kimura A, Kishimoto T: IL-6: regulator of Treg/Th17 balance.*Eur J Immunol* 2010, 40:1830–1835.

48. Elias KM, Laurence A, Davidson TS, Stephens G, Kanno Y, Shevach EM, O'Shea JJ: Retinoic acid inhibits Th17 polarization and enhances FoxP3 expression through a Stat-3/Stat-5 independent signaling pathway.*Blood* 2008, 111:1013–1020.

49. Mucida D, Park Y, Kim G, Turovskaya O, Scott I, Kronenberg M, Cheroutre H: Reciprocal TH17 and regulatory T cell differentiation mediated by retinoic acid.*Science* 2007, 317:256–260.

50. Gavin MA, Rasmussen JP, Fontenot JD, Vasta V, Manganiello VC, Beavo JA, Rudensky AY: Foxp3-dependent programme of regulatory T-cell differentiation.*Nature* 2007, 445:771–775.

51. Burgler S, Mantel PY, Bassin C, Ouaked N, Akdis CA, Schmidt-Weber CB: RORC2 is involved in T cell polarization through interaction with the FOXP3 promoter.*J Immunol* 2010, 184:6161–6169.

52. Laslo P, Spooner CJ, Warmflash A, Lancki DW, Lee HJ, Sciammas R, Gantner BN, Dinner AR, Singh H: Multilineage transcriptional priming and determination of alternate hematopoietic cell fates.*Cell* 2006, 126:755–766.

53. Huang S, Guo YP, May G, Enver T: Bifurcation dynamics in lineage-commitment in bipotent progenitor cells.*DevBiol* 2007, 305:695–713.

54. Guantes R, Poyatos JF: Multistable decision switches for flexible control of epigenetic differentiation.*PLoSComputBiol* 2008, 4:e1000235.

55. Sciammas R, Li Y, Warmflash A, Song Y, Dinner AR, Singh H: An incoherent regulatory network architecture that orchestrates B cell diversification in response to antigen signaling.*MolSystBiol* 2011, 7:495.

56. Griffith JS: Mathematics of cellular control processes. II. Positive feedback to one gene.*J TheorBiol* 1968, 20:209–216.

57. Thomas R: Logical analysis of systems comprising feedback loops.*J TheorBiol* 1978, 73:631–656.

58. Roessler OE: Basic circuits for fluid automata and relaxation systems.*Z Naturforsch* 1972, 27:333–343.

59. Maruyama T, Li J, Vaque JP, Konkel JE, Wang W, Zhang B, Zhang P, Zamarron BF, Yu D, Wu Y, *et al*: Control of the differentiation of regulatory T cells and T(H)17 cells by the DNA-binding inhibitor Id3.*Nat Immunol* 2011, 12:86–95.

60. Powell JD, Delgoffe GM: The mammalian target of rapamycin: linking T cell differentiation, function, and metabolism.*Immunity* 2010, 33:301–311.

61. Stritesky GL, Muthukrishnan R, Sehra S, Goswami R, Pham D, Travers J, Nguyen ET, Levy DE, Kaplan MH: The transcription factor STAT3 is required for T helper 2 cell development.*Immunity* 2011, 34:39–49.

62. Dong C: TH17 cells in development: an updated view of their molecular identity and genetic programming.*Nat Rev Immunol* 2008, 8:337–348.

63. Feinerman O, Veiga J, Dorfman JR, Germain RN, Altan-Bonnet G: Variability and robustness in T cell activation from regulated heterogeneity in protein levels.*Science* 2008, 321:1081–1084.

64. Chang HH, Hemberg M, Barahona M, Ingber DE, Huang S: Transcriptome-wide noise controls lineage choice in mammalian progenitor cells.*Nature* 2008, 453:544–547.

65. Wilson HR, Cowan JD: Excitatory and inhibitory interactions in localized populations of model neurons.*Biophys J* 1972, 12:1–24.

66. Mjolsness E, Sharp DH, Reinitz J: A connectionist model of development.*J TheorBiol* 1991, 152:429–453.

67. Tyson JJ, Novak B: Functional motifs in biochemical reaction networks.*Annu Rev PhysChem* 2010, 61:219–240.

68. Clewley R, Sherwood WE, LaMar MD, Guckenheimer JM: *PyDSTool, a software environment for dynamical systems modeling*, :; : [http://pydstool.sourceforge.net].

69. Tyson JJ, Novak B: Temporal organization of the cell cycle.*CurrBiol* 2008, 18:R759–R768.

Figure Legends

Figure 1 Induced heterogeneous differentiation of $CD4^+$ T cells with respect to a pair of master regulators (X and Y). A. Diversity of cell phenotypes during induced differentiation. In the undifferentiated cell, the expression levels of both X and Y are low. When the cell is differentiated, three possible functional phenotypes can be obtained: X single-positive cell, Y single-positive cell and double-positive cell. **B.** Three types of induced heterogeneous differentiation. In a differentiation event, a group of naive cells can be differentiated into two types of single-positive cells (Type 1), one type of single-positive cell and DP cell (Type 2) or all three functional phenotypes (Type 3).

Figure 2 Basal network motif controlling heterogeneous differentiation in the two master regulator paradigm. Solid green arrow: activation influence in which the activator alone can switch on the expression of the target protein. Dashed green arrow: activation influence in which the activator alone cannot switch on the expression of the target protein. Red arrow: inhibition influence. Protein name in parenthesis: possible intermediate protein for the positive feedback loop. **A.** Prototype Model 1: heterogeneous differentiation of T_H1 and T_H2. **B.** Prototype Model 2: heterogeneous differentiation of T_H1 and T_H17. **C.** Prototype Model 3: heterogeneous differentiation of iT_{Reg} and T_H17. **D.** The basal network motif.

Figure 3 Analyses of the core motif with symmetrical parameters. A-C. Phase plane portraits for three values of primary signal strength (zero, intermediate, high), in the absence of polarizing signals ($S2 = S3 = 0$). Green curve: X nullcline; red curve: Y nullcline; blue arrow: representative vector in the phase space; closed circle: stable steady state; open circle: unstable steady state; gray curve: separatrix. **D.** One-parameter bifurcation diagram for steady state level of X as a function of primary signal S1. Solid curve: stable steady state; dashed curve: unstable steady state. **E.** Two-parameter bifurcation diagram with respect to primary signal S1 and polarizing signal S2, with $S3 = 0$. Solid curve: locus of pitchfork bifurcation points. The pitchfork bifurcation points coalesce and disappear at $S2 = 0.357$. **F.** Bidirectional

two-parameter bifurcation diagram with respect to primary signal S1 and polarizing signals S2 and S3. Top half: S1—S2 diagram, with $S3 = 0$, as in panel E. Bottom half: S1—S3 diagram, with $S2 = 0$. The types of stable steady states in each region are annotated as colored circles. Adjoined circles: multistability. See Figure **1** for interpretation of the color scheme. **G.** Simulation results for treatment of a population of cells simultaneously with primary and polarizing signals. **H.** Simulation results for sequential treatment: polarizing signal followed by primary signal. **I.** Simulation results for sequential treatment: primary signal followed by polarizing signal. In G-I, the heterogeneity scores with respect to XSP and YSP are plotted.

Figure 4 Analyses of the core motif with asymmetrical parameters. A and B. One-parameter bifurcation diagram for steady state levels of X and Y as functions of primary signal S1 ($S2 = S3 = 0$). **C.** Bidirectional two-parameter bifurcation diagram with respect to primary signal S1 and polarizing signal S2 or S3. See legend of Figure **3** panels D and E for the interpretation of curves and colored circles. **D-F.** See legend of Figure **3** Panels G-I for simulation conditions.

Figure 5 Analyses of the basal motif with auto-activation relations. A. Bidirectional two-parameter bifurcation diagram with respect to primary signal S1 and polarizing signals S2 and S3 for intermediate weight of auto-activation relations ($\omega = 1.8$). Insets show the zoomed-in view of the cusp regions of the bistable region. **B.** Bidirectional two-parameter bifurcation diagram with respect to primary signal S1 and polarizing signals S2 and S3 for high weight of auto-activation relations ($\omega = 3.2$). The types of stable steady states in each region are annotated as colored circles. Adjoined circles: multistability. See Figure **1** for interpretation of the color scheme. Light blue area: bistable region governing differentiation switch. Light green area: bistable region governing reprogramming switch. Light yellow area: bistable region governing co-expression switch. **C-F.** Various types of heterogeneity scores are plotted for high weight of auto-activation relations ($\omega = 3.2$). **C.** The heterogeneity scores with respect to XSP and YSP. **D.** The heterogeneity scores with respect to XSP and DP. **E.** The heterogeneity scores with respect to YSP and DP. **F.** The heterogeneity scores with respect to XSP, YSP and DP.

Figure 6 Analyses of Prototype Model 1 (heterogeneous differentiation of T_H1 and T_H2 cells). A. Bidirectional two-parameter bifurcation diagram with respect to primary signal TCR and polarizing signals IL-12 and IL-4. **B.** Simulation results for induced differentiation. The heterogeneity scores with respect to T-bet single-positive phenotype and GATA3 single-positive phenotype are shown. **C.** Same legend as Panel A. The GATA-3 auto-activation relation is blocked in the model. **D.** Same legend as Panel B. The GATA-3 auto-activation relation is blocked in the model. In Panels A and C: Adjoined circles: multistability. Blue circle: naïve phenotype. Green circle: T-bet single-positive phenotype. Red circle: GATA3 single positive phenotype. Yellow: DP phenotype.

Figure 7 Analyses of Prototype Model 2 (heterogeneous differentiation of T_H1 and T_H17 cells). A. Two-parameter bifurcation diagram with respect to primary signal TCR and polarizing signal IL-23 + IL1. **B.** Simulation results for induced differentiation. The heterogeneity scores with respect to T-bet single-positive phenotype and DP phenotype are shown. **C.** Two-parameter bifurcation diagram with respect to primary signal TCR and polarizing signal TGF-β + IL-6. **D.** Simulation results for induced differentiation. Heterogeneity scores with respect to T-bet single-positive phenotype and RORγt single-positive phenotype are shown. In Panels A and C: Adjoined circles: multistability. Blue circle: naïve phenotype. Green circle: T-bet single-positive phenotype. Red circle: RORγt single-positive phenotype. Yellow: DP phenotype.

Figure 8 Analyses of Prototype Model 3 (heterogeneous differentiation of iT_{Reg} and T_H17 cells). A. Bidirectional two-parameter bifurcation diagram with respect to primary signal TCR + TGF-β and polarizing signals ATRA/IL2 and IL-6. Adjoined circles: multistability. Blue circle: naïve phenotype. Green circle: Foxp3 single-positive phenotype. Red circle: RORγt single-positive phenotype. Yellow: DP phenotype. **B.** Simulation results of induced differentiation. The heterogeneity scores with respect to Foxp3 single-positive phenotype, RORγt single-positive phenotype and DP phenotype are shown.

Figures

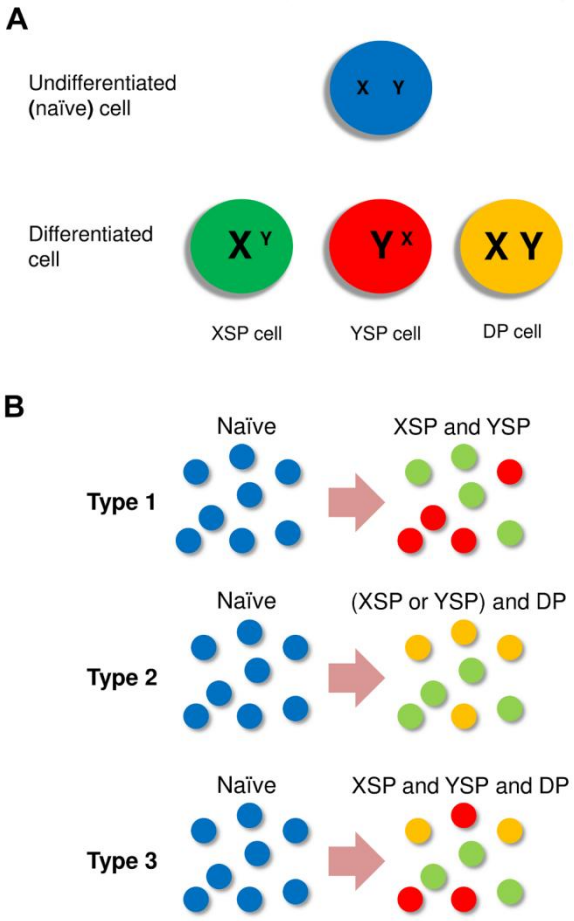

Figure 1. Induced heterogeneous differentiation of $CD4^+$ T cells with respect to a pair of master regulators (X and Y).

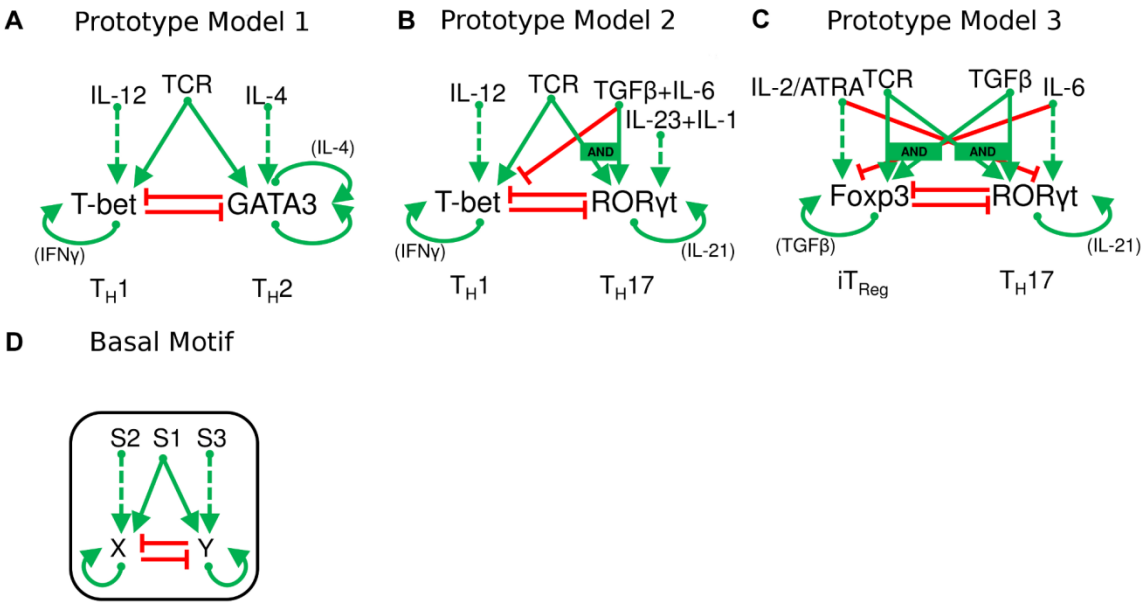

Figure 2. Basal network motif controlling heterogeneous differentiation in the two master regulator paradigm.

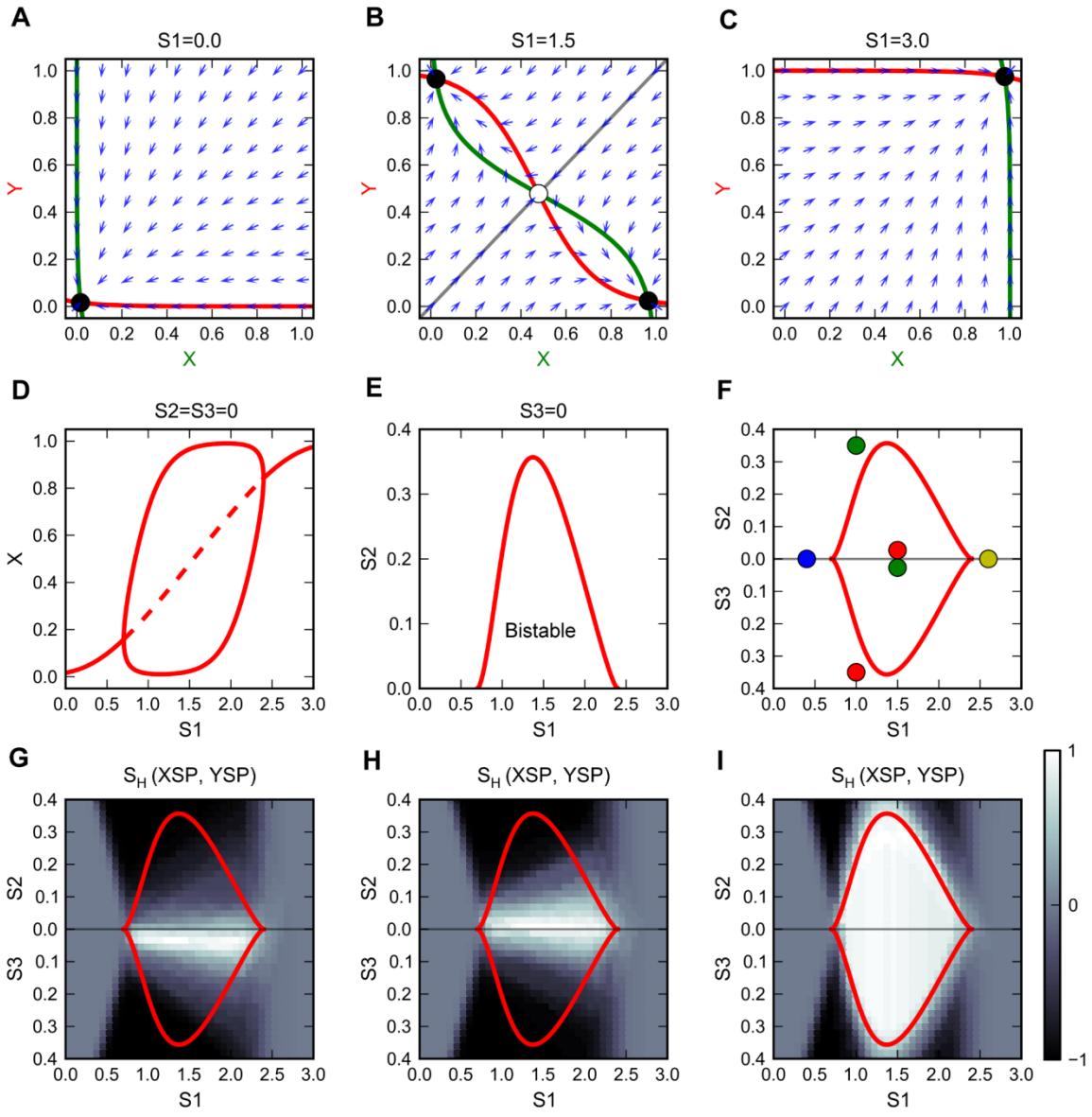

Figure 3. Analyses of the core motif with symmetrical parameters

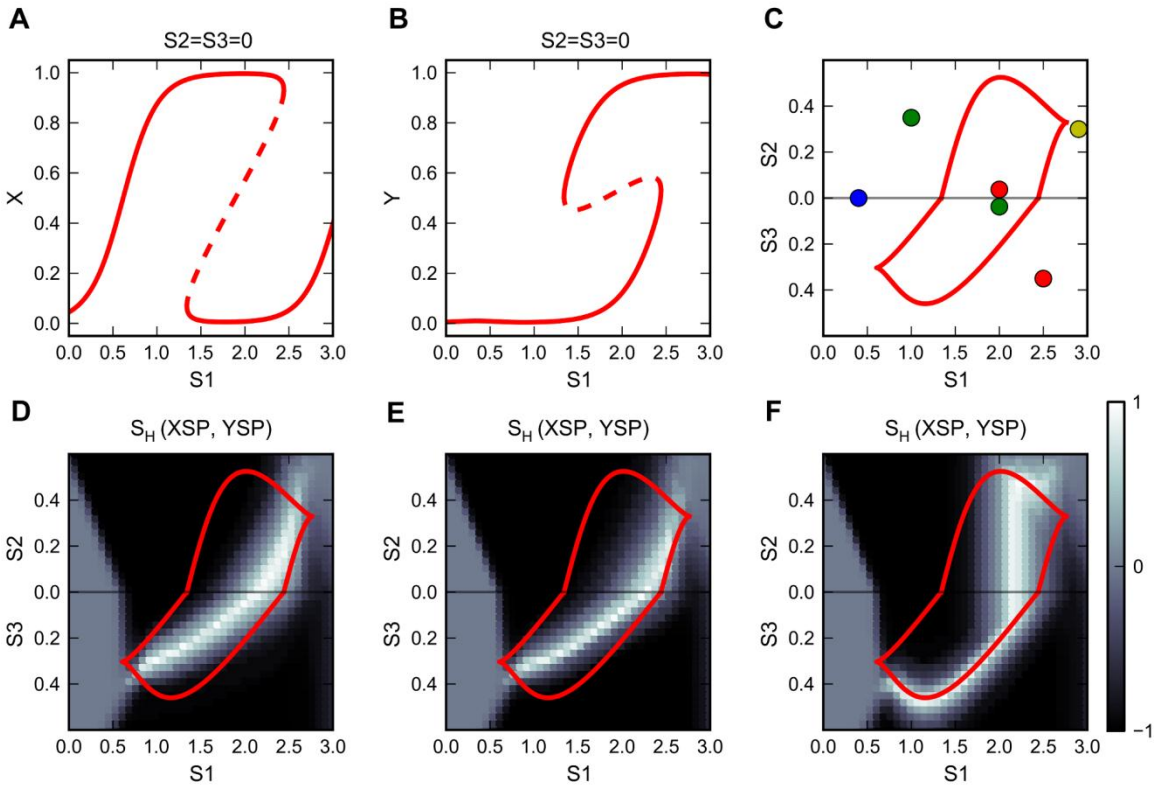

Figure 4. Analyses of the core motif with asymmetrical parameters

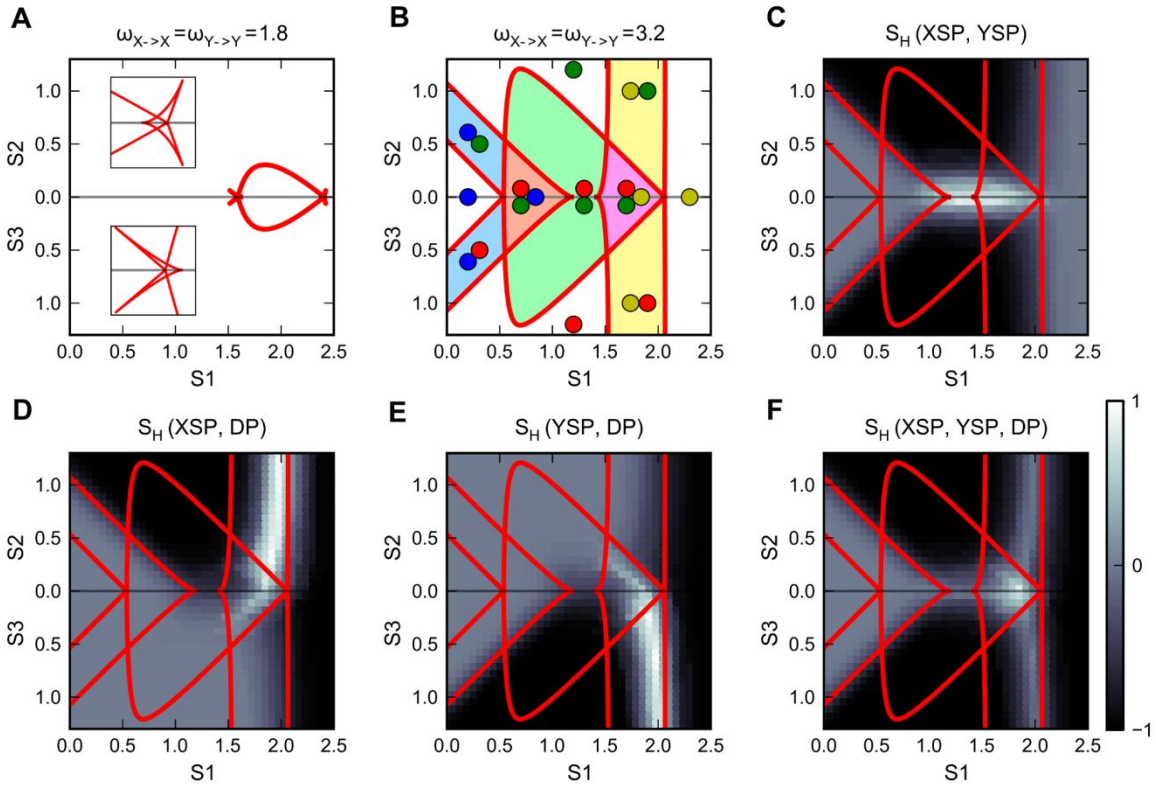

Figure 5. Analyses of the basal motif with auto-activation relations

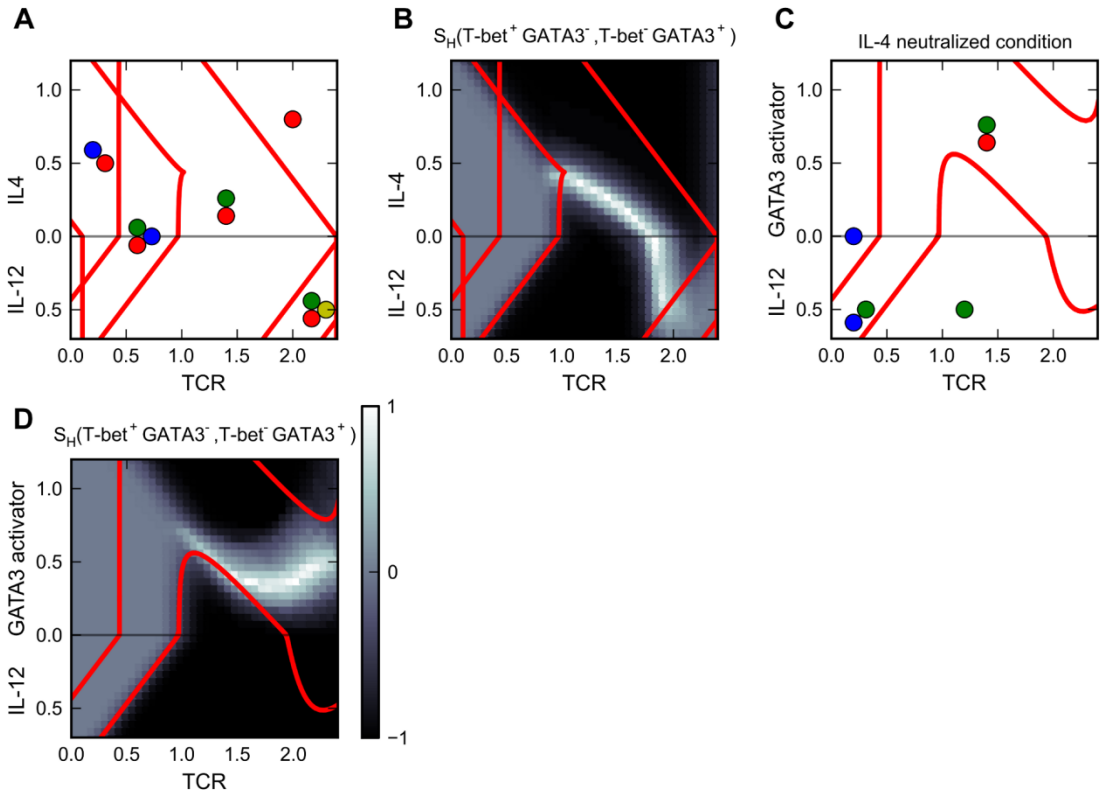

Figure 6. Analyses of Prototype Model 1 (heterogeneous differentiation of T_H1 and T_H2 cells)

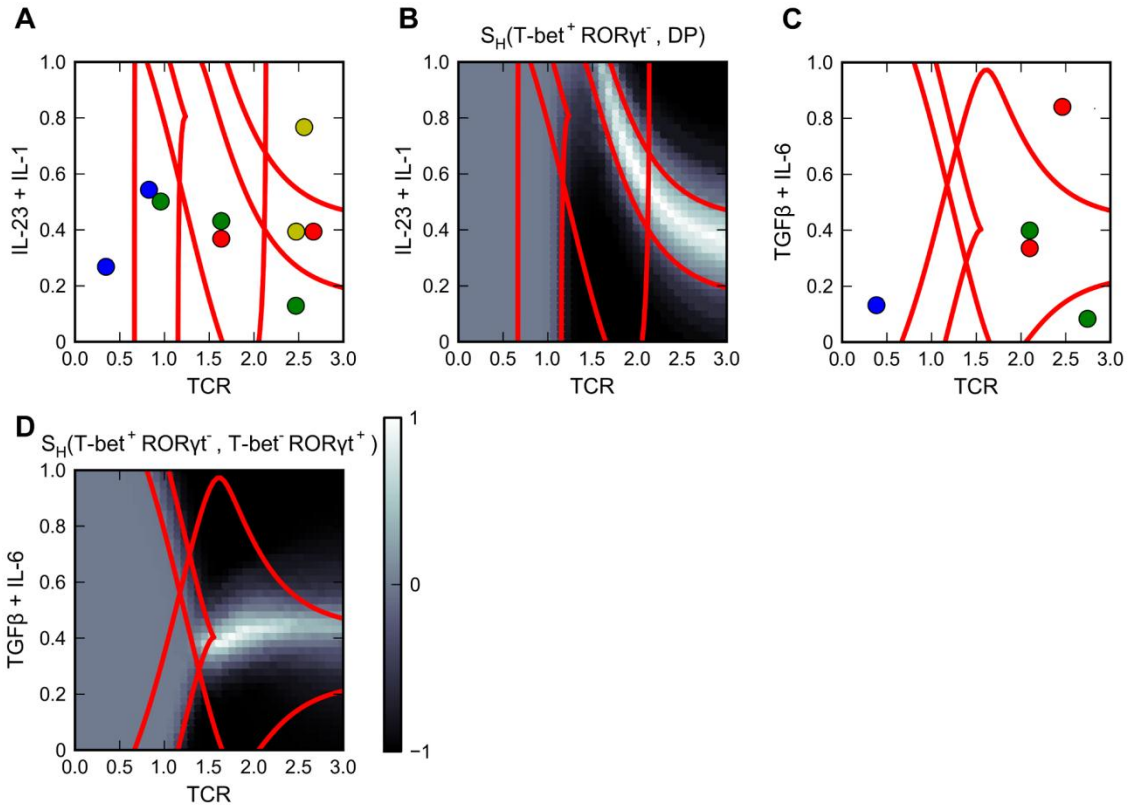

Figure 7. Analyses of Prototype Model 2 (heterogeneous differentiation of T_H1 and T_H17 cells)

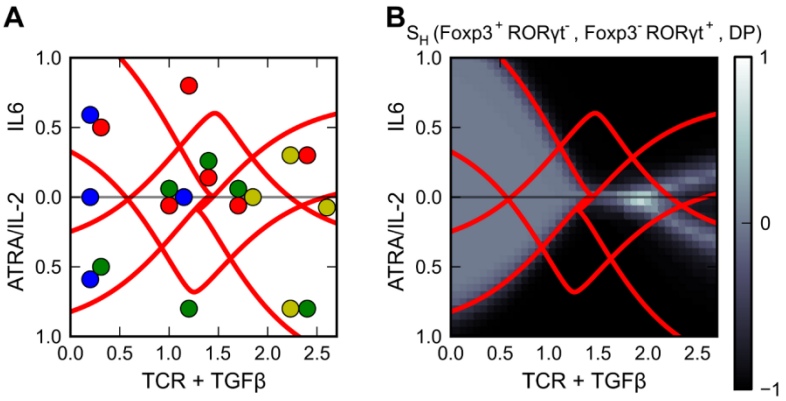

Figure 8. Analyses of Prototype Model 3 (heterogeneous differentiation of iT_{Reg} and T_H17 cells)

Additional Files

Additional file 1

4 supplementary tables and legends for supplementary figures.

Table S 1 Parameter values for an average cell in three different generic models

Parameter name	Description	Generic Model 1	Generic Model 2	Generic Model 3
γ_X	Relaxation rate of X	5	5	5
γ_Y	Relaxation rate of Y	5	5	5
σ_X	Steepness of sigmoidal function for X	5	5	2
σ_Y	Steepness of sigmoidal function for Y	5	5	2
ω_X^o	Basal activation state of X	-0.8	-0.6	-2.4
ω_Y^o	Basal activation state of Y	-0.8	-1	-2.4
$\omega_{X\to X}$	Weight of autoactivation of X	0	0	3.2
$\omega_{Y\to X}$	Weight of inhibition on X by Y	-1.5	-2.5	-1
$\omega_{Y\to Y}$	Weight of autoactivation of Y	0	0	3.2
$\omega_{X\to Y}$	Weight of inhibition on Y by X	-1.5	-1	-1
$\omega_{S1\to X}$	Weight of activation on X by S1	1	1	1
$\omega_{S1\to Y}$	Weight of activation on Y by S1	1	0.8	1
$\omega_{S2\to X}$	Weight of activation on X by S2	1	1	1
$\omega_{S3\to Y}$	Weight of activation on Y by S3	1	1	1
S1	Strength of primary signal S1	0 - 3*	0 - 3	0 - 2.5
S2	Strength of polarizing signal S2	0 - 0.4	0 - 0.6	0 - 1.3
S3	Strength of polarizing signal S3	0 - 0.4	0 - 0.6	0 - 1.3

* S1 is replaced by sigmoidal function $1.5/(1+e^{2\cdot(-1+S1)})$ in Figure S 1A and B to illustrate the effect of primary signal saturation.

Table S 2 Parameter values for an average cell in Prototype Model 1 (T_H1-T_H2)

Parameter name	Description	Value
$\gamma_{\text{T-bet}}$	Relaxation rate of T-bet	5
γ_{GATA3}	Relaxation rate of GATA3	5
$\sigma_{\text{T-bet}}$	Steepness of sigmoidal function for T-bet	4
σ_{GATA3}	Steepness of sigmoidal function for GATA3	6
$\omega^{o}_{\text{T-bet}}$	Basal activation state of T-bet	-1.7
$\omega^{o}_{\text{GATA3}}$	Basal activation state of GATA3	-2
$\omega_{\text{T-bet}\to\text{T-bet}}$	Weight of autoactivation of T-bet	2
$\omega_{\text{GATA3}\to\text{T-bet}}$	Weight of inhibition on T-bet by GATA3	-2
$\omega_{\text{GATA3}\to\text{GATA3}}$	Weight of autoactivation of GATA3	2.5 (0.25)
$\omega_{\text{T-bet}\to\text{GATA3}}$	Weight of inhibition on GATA3 by T-bet	-1
$\omega_{\text{TCR}\to\text{T-bet}}$	Weight of activation on T-bet by TCR	1
$\omega_{\text{TCR}\to\text{GATA3}}$	Weight of activation on GATA3 by TCR	1
$\omega_{\text{IL}-12\to\text{T-bet}}$	Weight of activation on T-bet by IL-12	1
$\omega_{\text{IL}-4\to\text{GATA3}}$	Weight of activation on GATA3 by IL-4	1
TCR	Strength of TCR signal	0 - 2.3
IL-12	Strength of IL-12 signal	0 - 0.7
IL-4	Strength of IL-4 signal	0 - 1.2

Table S 3 Parameter values for an average cell in Prototype Model 2 (T_H1-T_H17)

Parameter name	Description	Value
$\gamma_{\text{T-bet}}$	Relaxation rate of T-bet	5
$\gamma_{\text{RORγt}}$	Relaxation rate of RORγt	5
$\sigma_{\text{T-bet}}$	Steepness of sigmoidal function for T-bet	4
$\sigma_{\text{RORγt}}$	Steepness of sigmoidal function for RORγt	3
$\omega^{o}_{\text{T-bet}}$	Basal activation state of T-bet	-1.7
$\omega^{o}_{\text{RORγt}}$	Basal activation state of RORγt	-2.7
$\omega_{\text{T-bet}\to\text{T-bet}}$	Weight of autoactivation of T-bet	2
$\omega_{\text{RORγt}\to\text{T-bet}}$	Weight of inhibition on T-bet by RORγt	-1
$\omega_{\text{RORγt}\to\text{RORγt}}$	Weight of autoactivation of RORγt	2
$\omega_{\text{T-bet}\to\text{RORγt}}$	Weight of inhibition on RORγt by T-bet	-0.8
$\omega_{\text{TCR}\to\text{T-bet}}$	Weight of activation on T-bet by TCR	2.2
$\omega_{\text{TCR}\to\text{RORγt}}$	Weight of activation on RORγt by TCR	2.2
$\omega_{\text{IL23+IL1}\to\text{RORγt}}$	Weight of activation on RORγt by IL-23+IL-1	1
$\omega_{\text{TGFβ+IL6}\to\text{RORγt}}$	Weight of activation on RORγt by TGFβ+IL-6	1
$\omega_{\text{TGFβ+IL6}\to\text{T-bet}}$	Weight of inhibition on T-bet by TGFβ+IL-6	-1
TCR	Strength of TCR signal	$1/(1+e^{3\cdot(-1+0.8\cdot S1)})$ $0 \le S1 \le 3$
IL23+IL1	Strength of IL-23+IL-1 signal	0 - 1
TGFβ+IL6	Strength of TGFβ+IL-6 signal	0 - 1

Table S 4 Parameter values for an average cell in Prototype Model 3 (iT_{Reg}-T_H17)

Parameter name	Description	Value
γ_{Foxp3}	Relaxation rate of Foxp3	5
$\gamma_{\text{RORγt}}$	Relaxation rate of RORγt	5
σ_{Foxp3}	Steepness of sigmoidal function for Foxp3	2.8
$\sigma_{\text{RORγt}}$	Steepness of sigmoidal function for RORγt	3
$\omega^{o}_{\text{Foxp3}}$	Basal activation state of Foxp3	-2.5
$\omega^{o}_{\text{RORγt}}$	Basal activation state of RORγt	-2.5
$\omega_{\text{Foxp3}\rightarrow\text{Foxp3}}$	Weight of autoactivation of Foxp3	3
$\omega_{\text{RORγt}\rightarrow\text{Foxp3}}$	Weight of inhibition on Foxp3 by RORγt	-1
$\omega_{\text{RORγt}\rightarrow\text{RORγt}}$	Weight of autoactivation of RORγt	3
$\omega_{\text{Foxp3}\rightarrow\text{RORγt}}$	Weight of inhibition on RORγt by Foxp3	-0.8
$\omega_{\text{TCR+TGFβ}\rightarrow\text{Foxp3}}$	Weight of activation on Foxp3 by TCR+TGF-β	2.6
$\omega_{\text{TCR+TGFβ}\rightarrow\text{RORγt}}$	Weight of activation on RORγt by TCR+TGF-β	2.6
$\omega_{\text{ATRA/IL2}\rightarrow\text{Foxp3}}$	Weight of activation on Foxp3 by ATRA/IL-2	1.5
$\omega_{\text{IL6}\rightarrow\text{RORγt}}$	Weight of activation on RORγt by IL-6	1
$\omega_{\text{ATRA/IL2}\rightarrow\text{RORγt}}$	Weight of inhibition on Foxp3 by ATRA/IL-2	-1
$\omega_{\text{IL6}\rightarrow\text{Foxp3}}$	Weight of inhibition on Foxp3 by IL-6	-1.5
TCR+TGFβ	Strength of TCR+TGFβ signal	$1/(1+e^{2.5\cdot(-1+0.8\cdot S1)})$ $0 \le S1 \le 2.6$
ATRA/IL2	Strength of ATRA/IL-2 signal	0 - 1
IL6	Strength of IL-6 signal	0 - 1

Legends for supplementary figures

Figure S 1. Effects of primary signal saturation. A. One-parameter bifurcation diagram for steady state level of X as a function of primary signal S1, which saturates at 1.5 units. Solid curve: stable steady state; dashed curve: unstable steady state. **B.** Bidirectional two-parameter bifurcation diagram with respect to primary signal S1 and polarizing signals S2 and S3. S1 saturates at 1.5 units. Solid curve: locus of bifurcation points in Panel A. The types of stable steady states are annotated as colored circles. Adjoined circles: multistability. See Figure 1 for interpretation of the color scheme.

Figure S 2. Hysteresis effect of the 'reprogramming' bistable switch. A. One-parameter bifurcation diagram for steady state level of X as a function of primary signal S1 in the presence of polarizing signal S2. **B.** One-parameter bifurcation diagram for steady state level of Y as a function of primary signal S1 in the presence of polarizing signal S2. **C.** One-parameter bifurcation diagram for steady state level of X as a function of polarizing signals S2 and S3 in the presence of primary signal S1=1.5. **D.** One-parameter bifurcation diagram for steady state level of Y as a function of polarizing signals S2 and S3 in the presence of primary signal S1=1.5. **E.** Bidirectional two-parameter bifurcation diagram with respect to primary signal S1 and polarizing signals S2 and S3. Horizontal line: reference to diagram shown in Panels A and B. Vertical line: reference to diagrams shown in Panels C and D. The types of stable steady states are annotated as colored circles. Adjoined circles: multistability. See Figure 1 for interpretation of the color scheme.

Figure S 3. Simulation results for the core motif with symmetrical parameters. A. Percentages of naïve cells at the end of the simulations plotted on the bidirectional two-parameter bifurcation diagram. **B.** Percentages of XSP cells at the end of the simulations plotted on the bidirectional two-parameter bifurcation diagram. **C.** Percentages of YSP cells at the end of the simulations plotted on the bidirectional two-parameter bifurcation diagram. **D.** Percentages of DP cells at the end of the simulations plotted on the bidirectional two-parameter bifurcation diagram (compare Panels A-D with Figure 3G). **E.** Overlaid

phase plane portraits. The small cell-to-cell variability make the naïve states (magenta circles) of individual cells lie on different sides of the separatrices (gray curves), thereby resulting different fates of the cells. Green curve: X nullcline. Red curve: Y nullcline. Closed circle: stable steady state. Open circle: unstable steady state.

Figure S 4. Simulation results with different relaxation rates of X and Y. A. Simulation results for the core motif with symmetrical parameters (compare with Figure 3G). **B.** Simulation results for the core motif with asymmetrical parameters (compare with Figure 4D). In each panel, heterogeneity scores with respect to XSP and YSP are shown. In both simulations, the relaxation rate of Y (γ_Y) is changed to 10 (twice of the rate of X).

Figure S 5. Additional bifurcation analyses of the full basal motif. A. One-parameter bifurcation diagram for steady state level of X as a function of primary signal S1 (S2=S3=0) for the case of intermediate weights (=1.5) of auto-activation relations. **B.** One-parameter bifurcation diagram for steady state level of X as a function of primary signal S1 (S2=S3=0) for higher weights (=3.2) of auto-activation relations. **C.** Two-parameter bifurcation diagram with respect to the weights of auto-activation relations and the primary signal S1 (S2=S3=0). Purple curve: locus of the supercritical pitchfork bifurcation points. Orange curve: locus of the subcritical bifurcation points. Red curve: locus of the saddle-node bifurcation points. Gray lines: reference to diagrams shown in Panels A and B. **D.** One-parameter bifurcation diagram for steady state level of X as a function of primary signal S1 in the presence of polarizing signal S2. **E.** One-parameter bifurcation diagram for steady state level of Y as a function of primary signal S1 in the presence of polarizing signal S2. **F.** Bidirectional two-parameter bifurcation diagram with respect to primary signal S1 and polarizing signals S2 and S3. Gray lines: references to diagram shown in Panels D and E. In Panels A, B, D and E: Sold curve: stable steady state; dashed curve: unstable steady state. In Panels C and F, the types of stable steady states are annotated as colored circles. Adjoined circles: multistability. See Figure 1 for interpretation of the color scheme.

Figure S 6. Simulation results of Prototype Model 2 (heterogeneous differentiation of T_H1 and T_H17 cells) with T-bet knocked-out. A. Two-parameter bifurcation diagram with respect to primary signal TCR and polarizing signal IL-23 + IL1. Adjoined circles: multistability. Blue circle: naïve phenotype. Green circle: T-bet single-positive phenotype. Red circle: RORγt single positive phenotype. Yellow: DP phenotype. **B.** Simulation results for induced differentiation. Heterogeneity scores with respect to T-bet single-positive phenotype and RORγt single-positive phenotype are shown. (Bifurcation diagram and simulation results with respect to primary signal TCR and polarizing signal TGF-β + IL-6 are identical to Panels A and B.)

Additional file 2

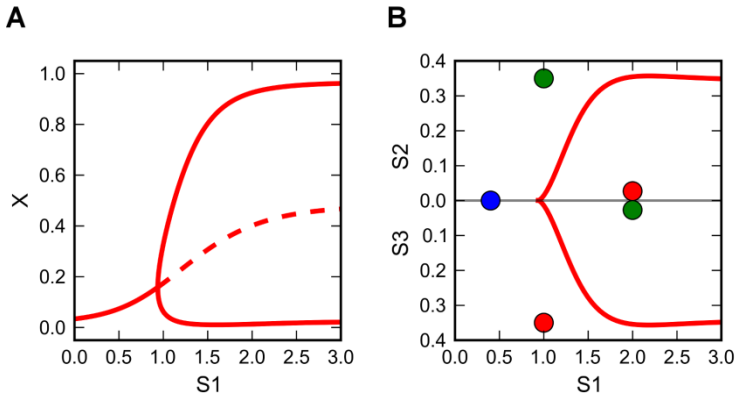

Figure S1. Effects of primary signal saturation.

Additional file 3

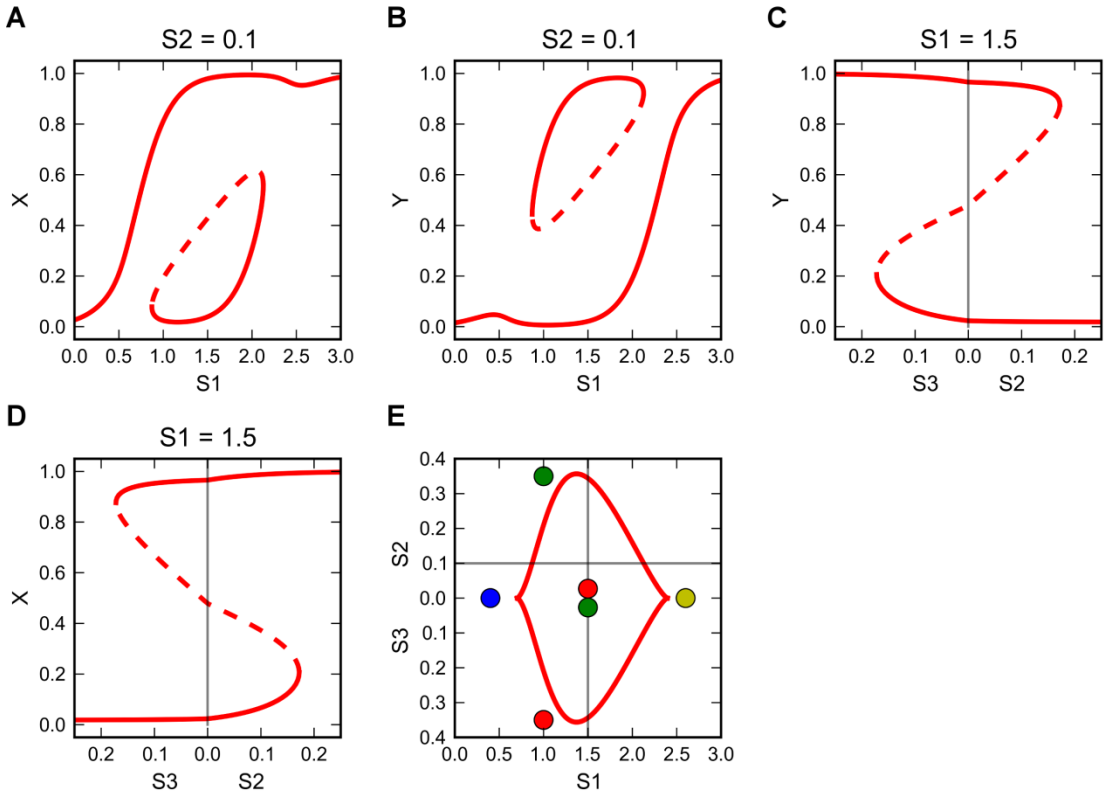

Figure S2. Hysteresis effect of the ‘reprogramming’ bistable switch.

Additional file 4

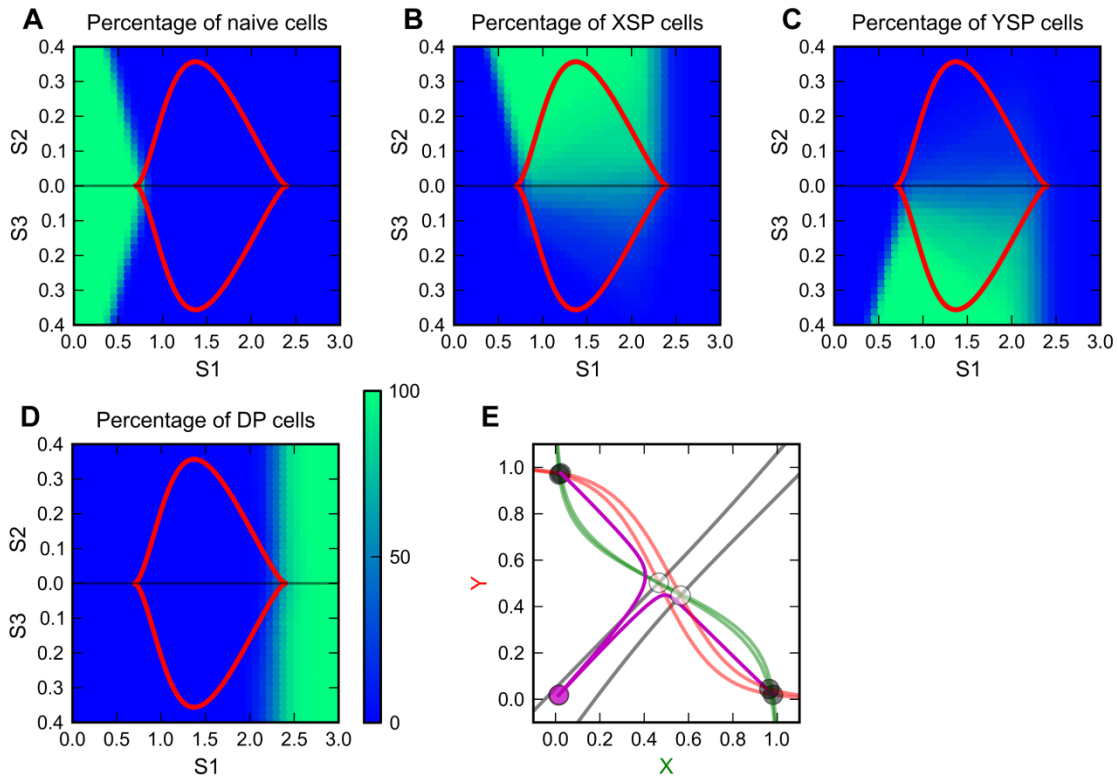

Figure S3. Simulation results for the core motif with symmetrical parameters.

Additional file 5

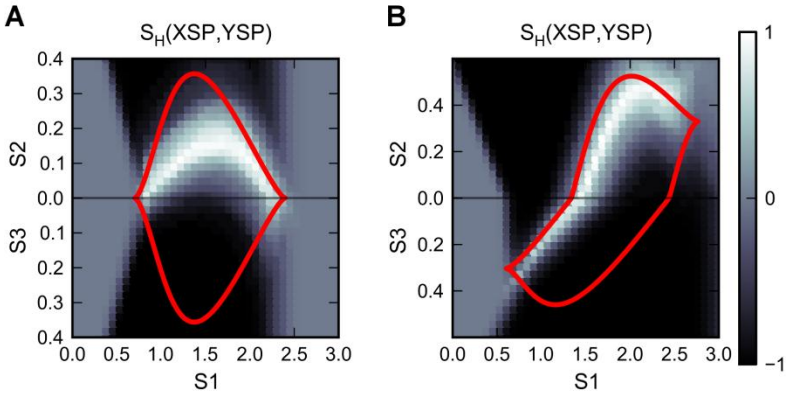

Figure S4. Simulation results with different relaxation rates of X and Y.

Additional file 6

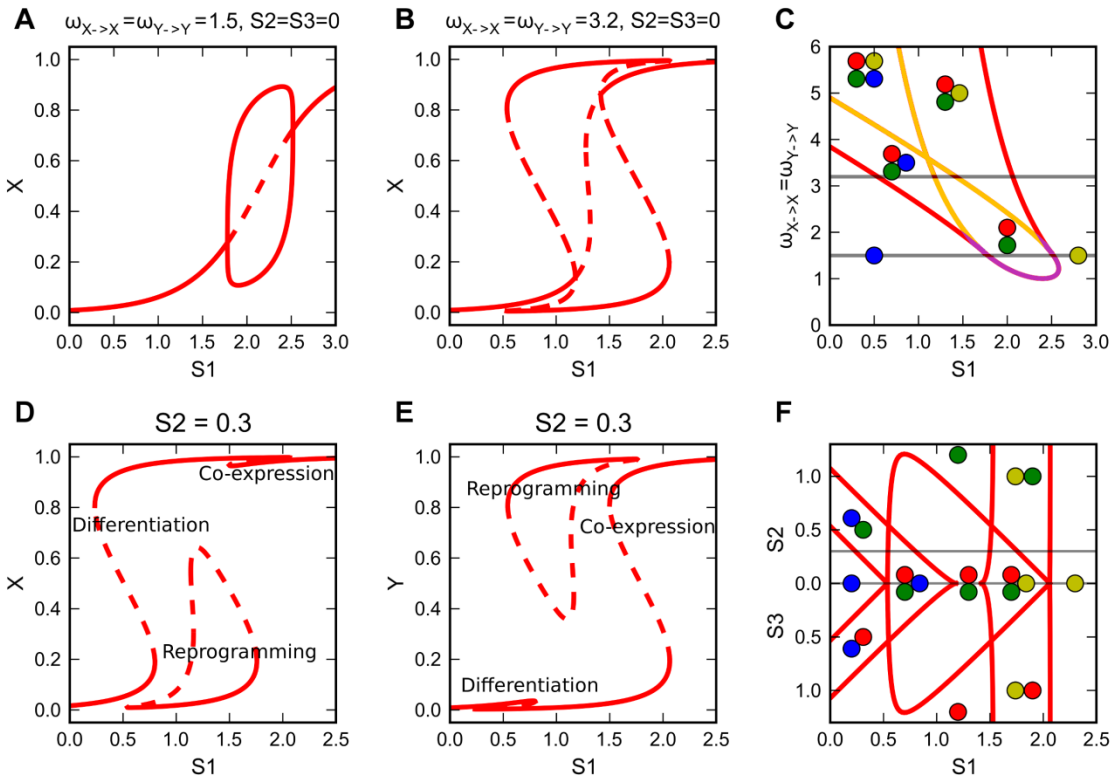

Figure S5. Additional bifurcation analyses of the full basal motif.

Additional file 7

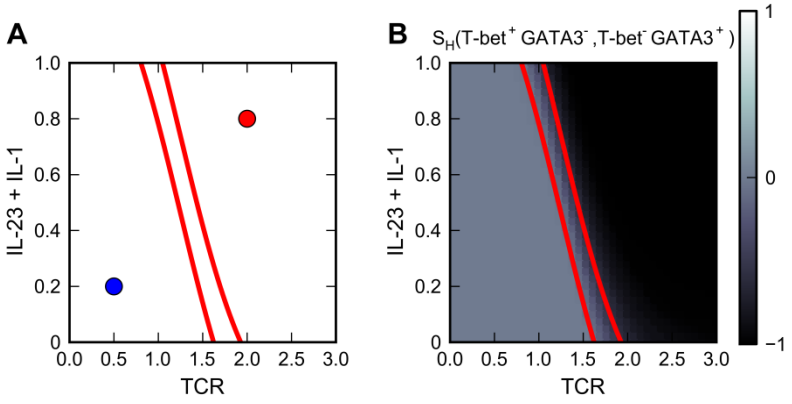

Figure S6. Simulation results of Prototype Model 2 (heterogeneous differentiation of T_H1 and T_H17 cells) with T-bet knocked-out.

CHAPTER 4

A mathematical framework for understanding four-dimensional heterogeneous differentiation of $CD4^+$ T cells

(A manuscript in preparation)

Abstract

At least four distinct lineages of $CD4^+$ T cells play diverse roles in immune system. Both *in vivo* and *in vitro* differentiation of the $CD4^+$ T cells often involve multiple phenotypes of cells. Heterogeneous differentiation of two lineages governed by a mutual-inhibition motif can be studied with a mathematical framework proposed in Chapter 3. Understanding heterogeneous differentiation of $CD4^+$ T cells involving more than two lineages is limited by the lack of a framework for analyzing interconnected mutual-inhibition motifs. In this chapter, I present a mathematical framework for the analysis of multi-stability behavior of multiple state variables with multiple mutual-inhibition motifs. A mathematical model for $CD4^+$ T cells based on this framework can reproduce and predict heterogeneous differentiations.

Introduction

Immune responses are often complex in terms of the types of cells involved and the biochemical activities elicited in pathogenic events. To achieve accurate regulation of various types of responses, the immune system has evolved delicate control mechanisms including the differentiation of various subsets of $CD4^+$ T cells [1]. Subsets of $CD4^+$ T cells play diverse and important regulatory roles in immune responses. The best known subsets of $CD4^+$ T cells are T helper 1 (T_H1), T helper 2 (T_H2), T helper 17 (T_H17) and induced regulatory T (iT_{Reg}) cells [2]. Each subset of $CD4^+$ T cells has a unique key transcription factor, known as a master regulator, which controls the lineage specification. The master regulators for the four subsets are T-bet, GATA3, RORγt and Foxp3 respectively [3-6]. The progenitor cells of all four types of $CD4^+$ cells are known as naïve $CD4^+$ T cells. These cells can be activated by antigen presentation and cytokines, and they differentiate into functional $CD4^+$ T cells upon the activation. The key event of differentiation is the up-regulation of at least one master regulator [7]. The identities and strengths of the environmental cues, i.e. the exogenous signals, determine the lineage of the differentiated cell. For example, interleukin 12 (IL-12) induces naïve T cells to differentiate into T_H1 cells in the presence of antigenic agent that activate their T cell receptors (TCRs) [8].

It is not surprising that most immune responses elicit balanced phenotypes of $CD4^+$ T cells [7,9]. Interestingly, even with the homogeneous treatment with exogenous signals, multiple lineages of $CD4^+$ T cells can be differentiated from a single pool of naïve $CD4^+$ T cells. Such 'induced' heterogeneous differentiation indicates that the balanced immune responses observed *in vivo* may not be due merely to the heterogeneous micro-environments of the cells. Rather, specific regulatory mechanisms may be responsible for the heterogeneous type of differentiation.

Previously, we developed a mathematical framework for analyzing heterogeneous differentiation involving two master regulators [10,11]. However, crosstalk among all four master regulators is important for the specification of $CD4^+$ T cell lineages. Some recent mathematical models for $CD4^+$ T cells have

included signaling networks with more than two master regulators, and they can be used to explain the differentiation of naïve $CD4^+$ T cells into each of the four lineages [12,13]. However, these models do not explain how the naive $CD4^+$ T cells can differentiate heterogeneously into combinations of the four lineages. Moreover, the lack of analytic tools for multi-stability behaviors governed by complex mutual-inhibition relationships has been a challenge to our understanding of this differentiation system. Here, I present a framework that can be specifically used to study multi-stability behavior involving networks with multiple interconnected mutual-inhibition motifs involving three or four master regulators. I use this framework to build a model of $CD4^+$ T cell differentiation with four master regulators and to explain the heterogeneous differentiations that involve these regulators.

Results

A three-fold symmetrical differentiation system

I first analyzed a simple signaling network motif with three master regulators X, Y and Z. Each pair of master regulators interacts by mutual-inhibition, and each master regulator activates its own production. A differentiation signal S1 activates the production of all master regulators (Fig. 1A). For detailed analysis of a two-dimensional system of a similar kind, please refer to our previous studies [10,11]). The basal parameter values used in this study are listed in Supplementary Table 1.

The bifurcation diagram (Fig. 1B) for the differentiation signal S1 reveals that the system has one stable steady state for $0 \leq S1 < 1.8$ (e.g., Fig. 1B vertical line C). This state corresponds to the naïve cell since all three master regulators are expressed at low levels (Fig. 1C, radar plots). When a population of cells was simulated with the indicated amount of signal S1, all cells in the population were still in the naïve state at the end of the simulation (Fig. 1C, bar chart).

At $S1 \approx 2$, there occurs a sub-critical pitchfork bifurcation with three-fold symmetry: the system changes from one naïve state (Fig. 1C) to three single-positive stable steady states (Fig.1D) and four other unstable steady states (not shown, we focus on analyzing stable steady states in this study). In the range of $1.8 < S1 < 4.5$, the system is tri-stable, and the simulated cell population became heterogeneous, containing comparable fractions of three single-positive phenotypes at the end of the simulation (Fig. 1D. bar chart).

At $S1 \approx 5$, two further pitchfork bifurcations occur. Each single-positive state changes to two stable steady states via a super-critical pitchfork bifurcation with two-fold symmetry, forming six stable steady states in total, and at a slightly higher signal strength ($S1 \approx 5.5$) the system undergoes additional pitchfork bifurcations which change these six stable steady states back to three stable steady states. These three new stable steady states correspond to double-positive phenotypes (Fig. 1E). In the range $5.5 < S1 < 7.5$, the system is tri-stable, and the simulated cell population became heterogeneous, containing comparable fractions of three double-positive phenotypes at the end of the simulation (Fig. 1E, bar chart).

At S1 ≈ 7.5, the system undergoes another sub-critical pitchfork bifurcation with three-fold symmetry, changing the three double-positive stable steady states to one triple-positive steady state, and the system is mono-stable S1> 7.5 (Fig. 1F).

An asymmetrical differentiation system

I next analyzed a system with broken symmetry to illustrate how an asymmetrical model differs from a symmetrical one. An asymmetrical model can be obtained by making small perturbations to the model described in the previous subsection. In particular, I changed the basal production parameter for X from -2 to -2.1 and that for Y from -2 to -1.9. Random perturbations of all parameter values give similar results (not shown). Typically, the steady states of an asymmetrical system have profiles similar to the bifurcation diagram shown in Fig. 2A.

Briefly, the asymmetrical model breaks the symmetry of the pitchfork bifurcations obtained with the symmetrical model. Similar to the symmetrical model, the system changes from a mono-stable naïve state (Fig. 2A vertical lines B and Fig. 2B) to a system with three stable steady states (Fig. 2A vertical lines C and Fig. 2C), but two of curves corresponding to the single-positive states are disconnected from the naïve state, forming two broken pieces or 'isolas', each of which has two saddle-node bifurcation points (for best illustration, see left plot of Fig. 2A vertical line C). In terms of cell differentiation, one of the three single-positive phenotypes is favored because of the broken symmetry, and is more abundant in the final state of the simulation (Fig. 2C, bar chart).

For larger values of S1, three double-positive states exist in the system (Fig. 2A vertical lines D and Fig. 2D).

A four-fold symmetrical differentiation system

Using the same strategy, I analyzed a system with four master regulators W, X, Y and Z (Fig. 3A). The parameter values are listed in Supplementary Table 2.

I plotted the bifurcation diagram for state variable W (Fig. 3B). The diagrams for the other three state variables are similar (as in Fig. 1B). The system is mono-stable with one naïve state for $0 \leq S1 < 1.8$ (Fig. 3B vertical line C and Fig. 3C). At $S1 \approx 2$, the system undergoes sub-critical bifurcations with four-fold symmetry, and the system is tetra-stable in the range of $2.5 < S1 < 5.3$, with four single-positive stable steady states (Fig. 3B vertical line D and Fig. 3D). At $S1 \approx 5.5$, the system undergoes a pair of pitchfork bifurcations, one with three-fold symmetry and the other with two-fold symmetry, changing the four stable steady states to six double-positive steady states (Fig. 3B vertical line E and Fig. 3E). At $S1 \approx 9$, the system undergoes another pair of pitchfork bifurcations, changing the six stable steady states to four triple-positive steady states (Fig. 3B vertical line F and Fig. 3F). At $S1 \approx 12$, the system undergoes a pitchfork bifurcation with four-fold symmetry and becomes mono-stable for $S1 > 12$ (Fig. 3B vertical line G and Fig. 3G). Due to the symmetrical nature of the system, in each of these multi-stable regions, comparable fractions of the phenotypes were obtained in the simulation (bar charts in Fig. 3D-F).

As an example for an asymmetrical model with four master regulators, I present a model for $CD4^+$ T cell differentiation in the next subsection.

A system for $CD4^+$ T cell differentiation with four master regulators

I built a model for $CD4^+$ T cell differentiation with the network shown in Fig. 4A. Parameter values for this model are listed in Supplementary Table 3. These values were chosen to give a good fit to the experimental observations listed in Table 1. Basically I performed these experiments by inducing cell differentiation with various exogenous signals (conditions are described in Table 1, and values of signals are listed in Supplementary Table 3) and observing the derived cell populations. The model can reproduce

the experimental results listed in Table 1, and I used my mathematical framework to analyze some of the key observations involving heterogeneous differentiation.

With the T cell receptor signal alone, the system can be bi-stable, containing T-bet-single-positive and GATA3-single-positive states (Fig. 4B, vertical lines D). When a population of cells was treated with TCR signal, a fraction of the population became become T_H1 cells, expressing T-bet, and some others became T_H2 cells, expressing GATA3 (Fig. 4D). When the population was treated with higher strength of TCR signal, a higher fraction of T_H2 cells was obtained. These results are in agreement with experimental results by Yamashita et al [14]. Heterogeneous differentiation of T_H1 and T_H17 can be reproduced by the model as well. As shown in Fig. 4E and F, in the presence of IL-23 and IL-1, four stable steady states (T-bet-positive, GATA3 positive, RORγt-positive and T-bet-RORγt double positive) co-exist with the TCR signal. The simulation results show that the cells were primarily differentiated into T-bet-RORγt double positive phenotype and T-bet-positive phenotype (Fig. 4G), and this is consistent with the observation by Ghoreschi et al. [15].

The list of simulation results and their corresponding experimental evidence are shown in Table 1.

Discussion

Interconnected mutual-inhibition motifs are not unique to $CD4^+$ T cells. Previous studies of generic motifs with four mutually-inhibiting transcription factors suggested that this network can exist in other differentiation systems [16,17], such as olfactory development [18,19]. In these theoretical studies, Olivier et al suggested that the network governs a multi-stable system when the competitions among the master regulators are sufficiently high [16,17]. The framework presented here provides a novel analytic tool for understanding the multi-stability behaviors of this type of system.

The model for a population of $CD4^+$ T cells neglects the fact that T cell differentiation can be influenced by inter-cellular communications. In other words, cytokines secreted by one cell can influence the behaviors of other cells. A consideration of such crosstalk will be the subject of future studies.

The framework presented here is useful to analyze the multi-stability behavior of dynamic systems that have two or more interconnected mutual-inhibition motifs. It has been applied to $CD4^+$ T cells with four master regulators in order explain the heterogeneous differentiations observed experimentally.

Methods

Dynamical Models

In this chapter, I build mathematical models of three different signaling networks motifs (two generic motifs and one motif specific to T cell differentiation). For all of these models, I use a generic form of ordinary differential equations (ODEs) suitable for describing both gene expression and protein interaction networks [20-22]. Each ODE in the model has the form:

$$\frac{dX_i}{dt} = \gamma_i (F(\sigma_i W_i) - X_i)$$
$$F(\sigma W) = 1 \Big/ (1 + e^{-\sigma W})$$
$$W_i = (\omega_i^o + \sum_j^N \omega_{j \to i} X_j)$$
$$i = 1, \ldots, N$$

Here, X_i is the activity or concentration of protein i. On a time scale = $1/\gamma_i$, $X_i(t)$ relaxes toward a value determined by the sigmoidal function, F, which has a steepness set by σ_i. The basal value of F, in the absence of any influencing factors, is determined by ω_i^o. The coefficients $\omega_{j \to i}$ determine the influence of protein j on protein i. N is the total number of proteins in the network.

All variables and parameters are dimensionless. One time unit in the simulations corresponds to approximately 1 day. Basal parameter values (see 'Cell-to-Cell Variability' subsection for details) of each model are listed in supplementary tables.

All simulations and bifurcation analyses were performed with PyDSTool, a software environment for dynamical systems [23].

Bifurcation Diagrams and steady state radar plots

One parameter bifurcation diagrams were plotted by following the steady state solution of the ODEs with change in the value of a control parameter.

In order to analyze the complex multi-stability behavior of a high-dimensional system, we use radar plots to illustrate the steady state of a particular parameter set. This plot depicts the expression level of each key state variable (i.e., master regulator) on one sub-plot, and multiple sub-plots describe multiple steady states. In principle, the radar plot can illustrate unstable steady states as well as stable steady states, but I plot only the stable steady states, which correspond to observable cell phenotypes.

Cell-to-Cell Variability

To account for cell-to-cell variability in a population, I made many simulations of the system of ODEs, in each cell with a slightly different choice of parameter values, to represent slight differences from cell to cell. I assumed that the value of each parameter conforms to a normal distribution with CV = 0.05 (CV = coefficient of variation = standard deviation / mean). I refer to the mean value for each parameter distribution as the 'basal' value of that parameter. In the bifurcation analysis of the dynamical system, I consider an imaginary cell that adopts the basal value for each of its parameters, and I define this cell as the 'average' cell. However, none of the cells in the simulated population is likely to be this average cell, because every parameter value is likely to deviate a little from the basal value, corresponding to a CV of 0.05.

Simulation procedure

In order to simulate the induced differentiation process, I first solved the ODEs numerically with small initial values of master regulator concentrations in the absence of any exogenous signals. After a short period of time, each simulated cell found its own, stable 'naïve' steady state in which all master regulators

are expressed at low level, and this state corresponds to a naïve $CD4^+$ T cell. Next, I changed the exogenous signals to the values listed in Supplementary Tables 1, 2 and 3 and continued the numerical simulation. Each cell arrived at its corresponding 'induced' phenotype, which might vary from cell to cell because of the parametric variability of the population. The expression level of the proteins in the network ranges from 0 unit to 1 unit, and I made the simple definition that a protein is expressed when its level is greater than 0.5 units. I defined the derived population as a 'heterogeneous' population if it contained cells with more than one phenotype.

References

1. Luckheeram RV, Zhou R, Verma AD, Xia B (2012) CD4(+)T cells: differentiation and functions. Clinical & developmental immunology 2012: 925135.

2. Zhu J, Yamane H, Paul WE (2010) Differentiation of effector CD4 T cell populations. Annu Rev Immunol 28: 445-489.

3. Zheng W, Flavell RA (1997) The transcription factor GATA-3 is necessary and sufficient for Th2 cytokine gene expression in CD4 T cells. Cell 89: 587-596.

4. Szabo SJ, Kim ST, Costa GL, Zhang X, Fathman CG, et al. (2000) A novel transcription factor, T-bet, directs Th1 lineage commitment. Cell 100: 655-669.

5. Ivanov, II, McKenzie BS, Zhou L, Tadokoro CE, Lepelley A, et al. (2006) The orphan nuclear receptor RORgammat directs the differentiation program of proinflammatory IL-17+ T helper cells. Cell 126: 1121-1133.

6. Fontenot JD, Gavin MA, Rudensky AY (2003) Foxp3 programs the development and function of CD4+CD25+ regulatory T cells. Nat Immunol 4: 330-336.

7. O'Shea JJ, Paul WE (2010) Mechanisms underlying lineage commitment and plasticity of helper CD4+ T cells. Science 327: 1098-1102.

8. Hsieh CS, Macatonia SE, Tripp CS, Wolf SF, O'Garra A, et al. (1993) Development of TH1 CD4+ T cells through IL-12 produced by Listeria-induced macrophages. Science 260: 547-549.

9. Murphy KM, Stockinger B (2010) Effector T cell plasticity: flexibility in the face of changing circumstances. Nat Immunol 11: 674-680.

10. Hong T, Xing J, Li L, Tyson JJ (2011) A mathematical model for the reciprocal differentiation of T helper 17 cells and induced regulatory T cells. PLoS Comput Biol 7: e1002122.

11. Hong T, Xing J, Li L, Tyson JJ (2012) A simple theoretical framework for understanding heterogeneous differentiation of CD4+ T cells. BMC systems biology 6: 66.

12. Mendoza L (2013) A Virtual Culture of CD4+ T Lymphocytes. Bulletin of mathematical biology 10.1007/s11538-013-9814-9.

13. Naldi A, Carneiro J, Chaouiya C, Thieffry D (2010) Diversity and plasticity of Th cell types predicted from regulatory network modelling. PLoS Comput Biol 6: e1000912.

14. Yamashita M, Kimura M, Kubo M, Shimizu C, Tada T, et al. (1999) T cell antigen receptor-mediated activation of the Ras/mitogen-activated protein kinase pathway controls interleukin 4 receptor function and type-2 helper T cell differentiation. Proc Natl Acad Sci U S A 96: 1024-1029.

15. Ghoreschi K, Laurence A, Yang XP, Tato CM, McGeachy MJ, et al. (2010) Generation of pathogenic T(H)17 cells in the absence of TGF-beta signalling. Nature 467: 967-971.

16. Cinquin O, Demongeot J (2002) Positive and negative feedback: striking a balance between necessary antagonists. J Theor Biol 216: 229-241.

17. Cinquin O, Demongeot J (2005) High-dimensional switches and the modelling of cellular differentiation. J Theor Biol 233: 391-411.

18. Serizawa S, Ishii T, Nakatani H, Tsuboi A, Nagawa F, et al. (2000) Mutually exclusive expression of odorant receptor transgenes. Nature neuroscience 3: 687-693.

19. Ebrahimi FA, Edmondson J, Rothstein R, Chess A (2000) YAC transgene-mediated olfactory receptor gene choice. Developmental dynamics : an official publication of the American Association of Anatomists 217: 225-231.

20. Wilson HR, Cowan JD (1972) Excitatory and inhibitory interactions in localized populations of model neurons. Biophys J 12: 1-24.

21. Mjolsness E, Sharp DH, Reinitz J (1991) A connectionist model of development. J Theor Biol 152: 429-453.

22. Tyson JJ, Novak B (2010) Functional motifs in biochemical reaction networks. Annu Rev Phys Chem 61: 219-240.

23. Clewley R (2012) Hybrid models and biological model reduction with PyDSTool. PLoS Comput Biol 8: e1002628.

24. Messi M, Giacchetto I, Nagata K, Lanzavecchia A, Natoli G, et al. (2003) Memory and flexibility of cytokine gene expression as separable properties of human T(H)1 and T(H)2 lymphocytes. Nat Immunol 4: 78-86.

25. Hosken NA, Shibuya K, Heath AW, Murphy KM, O'Garra A (1995) The effect of antigen dose on CD4+ T helper cell phenotype development in a T cell receptor-alpha beta-transgenic model. J Exp Med 182: 1579-1584.

26. Maruyama T, Li J, Vaque JP, Konkel JE, Wang W, et al. (2011) Control of the differentiation of regulatory T cells and T(H)17 cells by the DNA-binding inhibitor Id3. Nat Immunol 12: 86-95.

27. Zhou L, Lopes JE, Chong MM, Ivanov, II, Min R, et al. (2008) TGF-beta-induced Foxp3 inhibits T(H)17 cell differentiation by antagonizing RORgammat function. Nature 453: 236-240.

28. Mucida D, Park Y, Kim G, Turovskaya O, Scott I, et al. (2007) Reciprocal TH17 and regulatory T cell differentiation mediated by retinoic acid. Science (New York, NY) 317: 256-260.

Tables

Table 1. Experimental results that are in agreement with the model for $CD4^+$ T cells

Conditions of differentiation induction	Induced cell population	Evidence
Exogenous polarizing signals alone	No induction of differentiation	[14]
Low dose of antigenic stimulant (TCR signal) and IL-12	Homogeneous differentiation of T_H1	[14]
Low dose of antigenic stimulant (TCR signal) and IL-4	Homogeneous differentiation of T_H2	[14]
Antigenic stimulant in the presence of IL-4	Heterogeneous differentiation of T_H1 and T_H2	[14,24]
Increasing strengths of TCR signal	A spectrum of heterogeneous populations with increasing percentages of T_H2 cells and decreasing percentage of T_H1 cells.	[25]
Increasing strengths of TCR signal in the presence of IL-4	A spectrum of heterogeneous populations with increasing percentages of T_H2 cells and decreasing percentage of T_H1 cells.	[14]
Blocking GATA3-IL4 feedback by antibodies against IL-4 and inducing with TCR signal	No T_H2 cells are observed	[26]
TCR signal alone	The cell population is dominated by the T_H1 cells	[15]
TCR signal and IL-23+IL-1 signal	Heterogeneous differentiation of T-$bet^+$$ROR\gamma t^-$ cells and T-$bet^+$$ROR\gamma t^+$ cells.	[15]
TCR signal and TGF-β+IL-6 signal	The cell population is dominated by T-$bet^-$$ROR\gamma t^+$ cells	[15]
knocking out T-bet genes and inducing with TCR signal	Homogeneous differentiation of T-$bet^-$$ROR\gamma t^+$ cells with either TGF-β signal or IL-23+IL-1 signal	[15]
TGF-β+TCR signal and IL-6 signal	Heterogeneous differentiation of $ROR\gamma t^+$ and $Foxp3^+$ cells	[27]
TGF-β+TCR signal and ATRA signal	Homogeneous differentiation of $Foxp3^+$ cells	[28]

Figure Legends

Figure 1. Analysis of a motif with three master regulators. **A)** Influence diagram of the model. **B)** Bifurcation diagrams with respect to S1. Solid curves: stable steady states. Dashed curves: unstable steady states. Vertical gray lines: references to stability analysis with specific control parameter values shown in following sub-figures. **C-F)** Radar plots: representation stable steady states. In each radar plot, expression levels of master regulators are plotted on the axes. Bar charts: the phenotypic composition of the cell population at the end of the numerical simulation (t = 7).

Figure 2. Analysis of a motif with three master regulators with broken symmetry. **A)** Bifurcation diagrams with respect to S1. Solid curves: stable steady states. Dashed curves: unstable steady states. Vertical gray lines: references to stability analysis with specific control parameter values shown in following sub-figures. **B-E)** Radar plots: representation stable steady states. In each radar plot, expression levels of master regulators are plotted on the axes. Bar charts: the phenotypic composition of the cell population at the end of the numerical simulation (t = 7).

Figure 3. Analysis of a motif with four master regulators. **A)** Influence diagram of the model. **B)** Bifurcation diagram with respect to S1. Solid curves: stable steady states. Dashed curves: unstable steady states. Vertical gray lines: references to stability analysis with specific control parameter values shown in following sub-figures. **C-G)** Radar plots: representation stable steady states. In each radar plot, expression levels of master regulators are plotted on the axes. Bar charts: the phenotypic composition of the cell population at the end of the numerical simulation (t = 7).

Figure 4. Analysis of the $CD4^+$ T cell model. **A)** Influence diagram of the model. **B)** Bifurcation diagrams with respect to TCR. Solid curves: stable steady states. Dashed curves: unstable steady states. Vertical gray lines: references to stability analysis with specific control parameter values shown in following sub-figures. **C-E and G)** Radar plots: representation stable steady states. In each radar plot, expression levels of master regulators are plotted on the axes. Bar charts: the phenotypic composition of

the cell population at the end of the numerical simulation (t = 7). F) Bifurcation diagrams with respect to TCR in the presence of 5 units of IL23 and 5 units of IL-1.

Figures

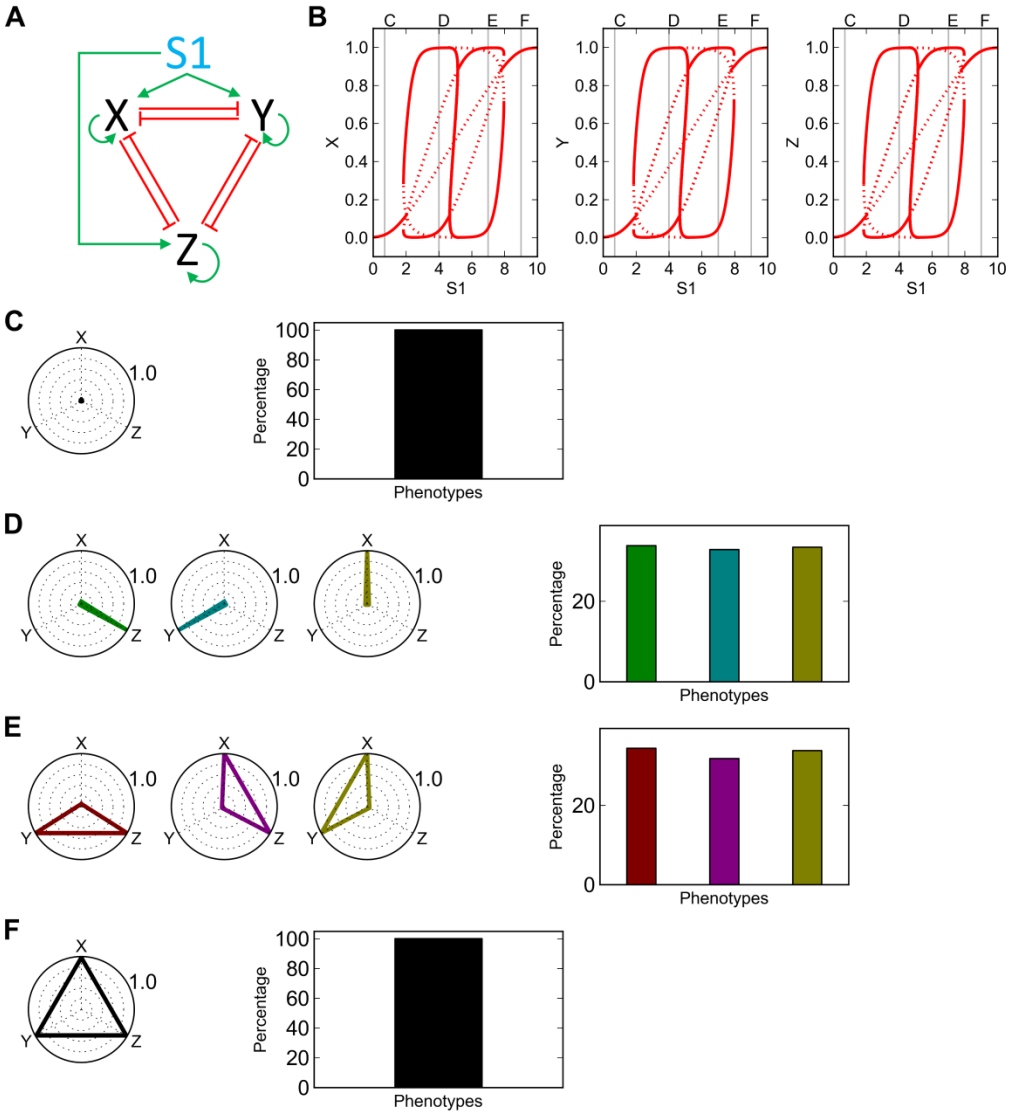

Figure 1. Analysis of a motif with three master regulators

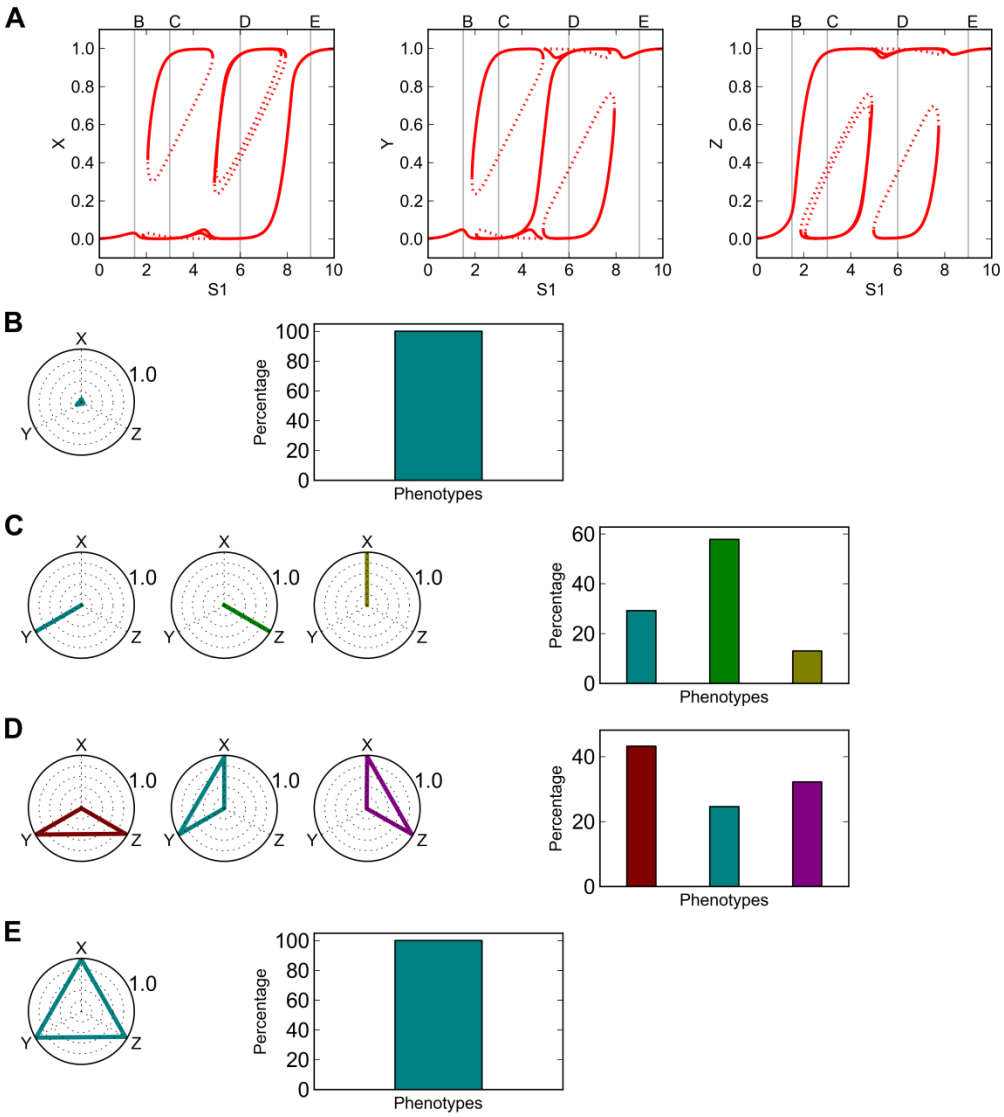

Figure 2. Analysis of a motif with three master regulators with broken symmetry

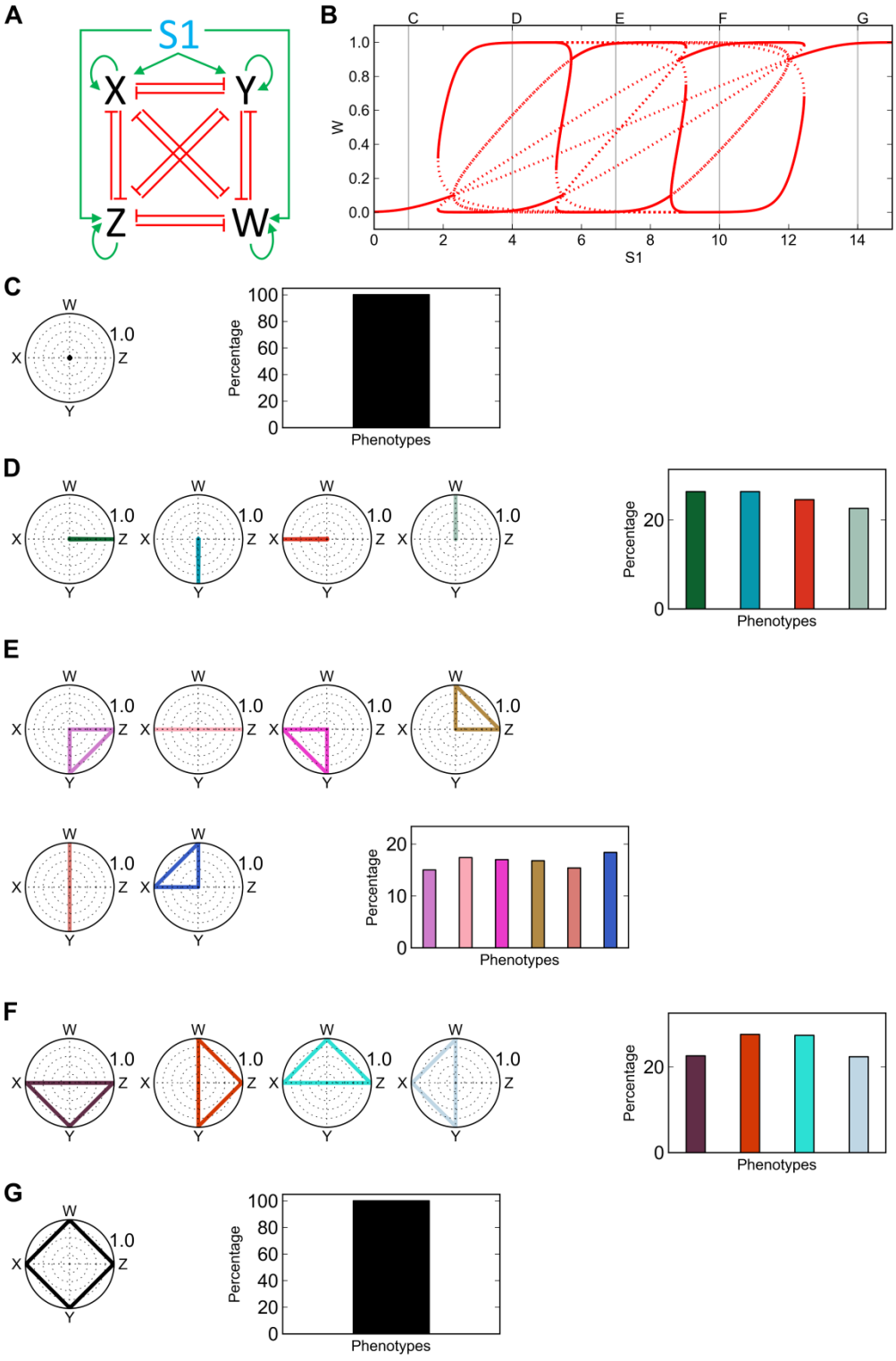

Figure 3. Analysis of a motif with four master regulators.

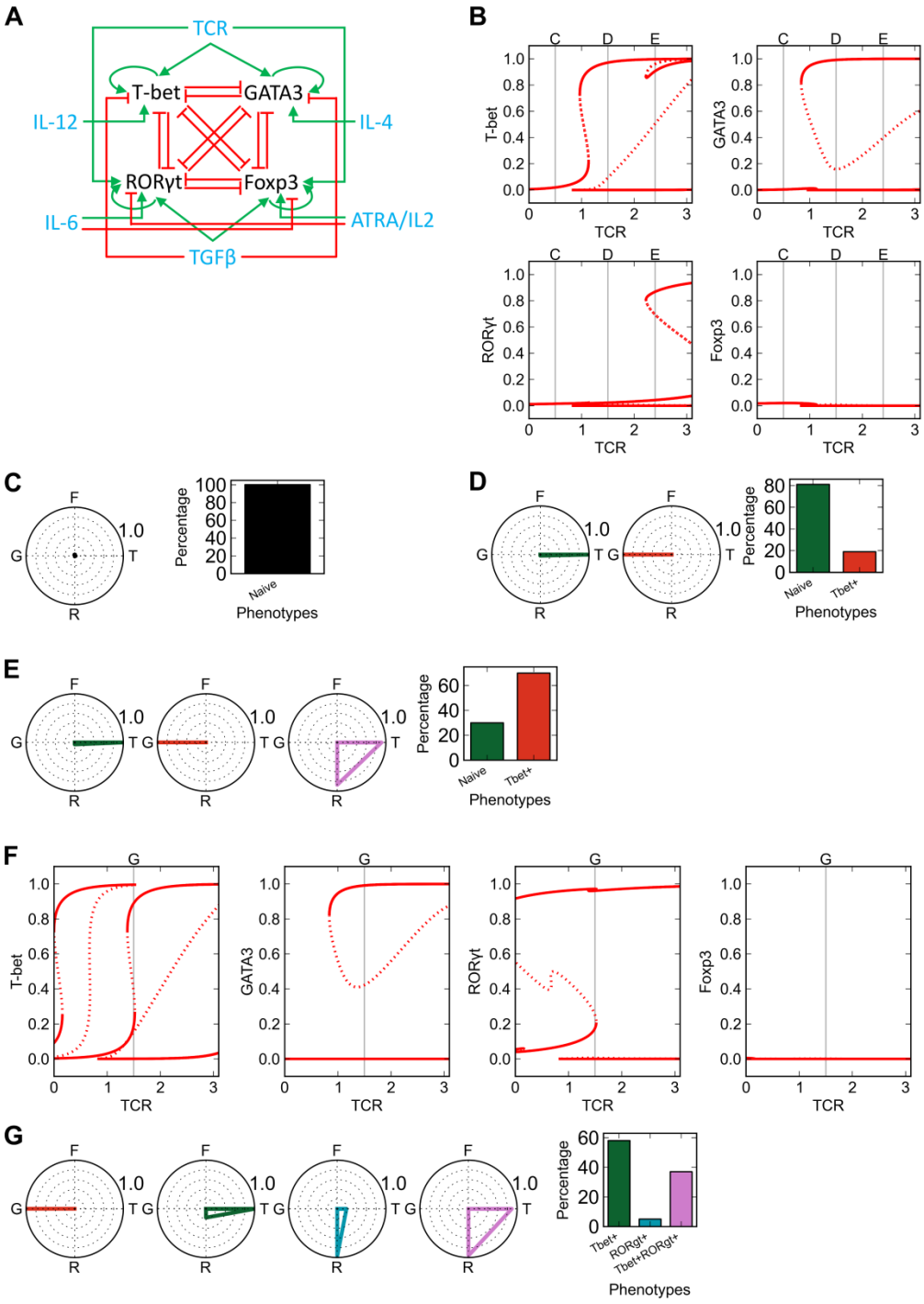

Figure 4. Analysis of the CD4^{+} T cell model

Supplementary Tables

Table S1. Parameter values for the generic model with three master regulators

Parameter	Description	Value
S1	Strength of S1 signal	0 - 10
γ_X	Relaxation rate of X	5
γ_Y	Relaxation rate of Y	5
γ_Z	Relaxation rate of Z	5
σ_X	Steepness of sigmoidal function for X	3
σ_Y	Steepness of sigmoidal function for Y	3
σ_Z	Steepness of sigmoidal function for Z	3
ω_X^o	Basal activation state of X	-2
ω_Y^o	Basal activation state of Y	-2
ω_Z^o	Basal activation state of Z	-2
$\omega_{X\to X}$	Weight of autoactivation of X	0.2
$\omega_{Y\to Y}$	Weight of autoactivation of Y	0.2
$\omega_{Z\to Z}$	Weight of autoactivation of Z	0.2
$\omega_{Y\to X}$	Weight of inhibition on X by Y	-3
$\omega_{X\to Y}$	Weight of inhibition on Y by X	-3
$\omega_{Z\to Y}$	Weight of inhibition on Y by Z	-3
$\omega_{Y\to Z}$	Weight of inhibition on Z by Y	-3
$\omega_{X\to Z}$	Weight of inhibition on Z by X	-3
$\omega_{Z\to X}$	Weight of inhibition on X by Z	-3
$\omega_{S1\to X}$	Weight of activation on X by S1	1
$\omega_{S1\to Y}$	Weight of activation on Y by S1	1
$\omega_{S1\to Z}$	Weight of activation on Z by S1	1

Table S2. Parameter values for the generic model with four master regulators

Parameter	Description	Value
S1	Strength of S1 signal	0 - 15
γ_{W}	Relaxation rate of W	5
γ_{X}	Relaxation rate of X	5
γ_{Y}	Relaxation rate of Y	5
γ_{Z}	Relaxation rate of Z	5
σ_{W}	Steepness of sigmoidal function for W	3
σ_{X}	Steepness of sigmoidal function for X	3
σ_{Y}	Steepness of sigmoidal function for Y	3
σ_{Z}	Steepness of sigmoidal function for Z	3
ω_{W}^{o}	Basal activation state of W	-2
ω_{X}^{o}	Basal activation state of X	-2
ω_{Y}^{o}	Basal activation state of Y	-2
ω_{Z}^{o}	Basal activation state of Z	-2
$\omega_{W\to W}$	Weight of autoactivation of W	0.2
$\omega_{X\to X}$	Weight of autoactivation of X	0.2
$\omega_{Y\to Y}$	Weight of autoactivation of Y	0.2
$\omega_{Z\to Z}$	Weight of autoactivation of Z	0.2
$\omega_{X\to W}$	Weight of inhibition on W by X	-3.5
$\omega_{Y\to W}$	Weight of inhibition on W by Y	-3.5
$\omega_{Z\to W}$	Weight of inhibition on W by Z	-3.5
$\omega_{W\to X}$	Weight of inhibition on X by W	-3.5
$\omega_{Y\to X}$	Weight of inhibition on X by Y	-3.5
$\omega_{Z\to X}$	Weight of inhibition on X by Z	-3.5
$\omega_{W\to Y}$	Weight of inhibition on Y by W	-3.5
$\omega_{X\to Y}$	Weight of inhibition on Y by X	-3.5
$\omega_{Z\to Y}$	Weight of inhibition on Y by Z	-3.5
$\omega_{W\to Z}$	Weight of inhibition on Z by W	-3.5
$\omega_{Y\to Z}$	Weight of inhibition on Z by Y	-3.5
$\omega_{X\to Z}$	Weight of inhibition on Z by X	-3.5
$\omega_{S1\to W}$	Weight of activation on W by S1	1
$\omega_{S1\to X}$	Weight of activation on X by S1	1
$\omega_{S1\to Y}$	Weight of activation on Y by S1	1

$\omega_{S1\to Z}$	Weight of activation on Z by S1	1

Table S3. Parameter values for $CD4^+$ T cell model

Parameter name	Description	Value
TCR	Strength of TCR signal	0 - 3
TGF-β	Strength of TGF-β signal	0 or 5
IL-12	Strength of IL-12 signal	0 or 5
IL-4	Strength of IL-4 signal	0 or 5
IL-6	Strength of IL-6 signal	0 or 5
IL-23	Strength of IL-23 signal	0 or 5
IL-1	Strength of IL-1 signal	0 or 5
ATRA	Strength of ATRA signal	0 or 5
$\gamma_{\text{T-bet}}$	Relaxation rate of T-bet	5
γ_{GATA3}	Relaxation rate of GATA3	5
$\gamma_{\text{RORγt}}$	Relaxation rate of RORγt	5
γ_{Foxp3}	Relaxation rate of Foxp3	5
$\sigma_{\text{T-bet}}$	Steepness of sigmoidal function for T-bet	2.5
σ_{GATA3}	Steepness of sigmoidal function for GATA3	3.3
$\sigma_{\text{RORγt}}$	Steepness of sigmoidal function for RORγt	2
σ_{Foxp3}	Steepness of sigmoidal function for Foxp3	2
$\omega^{\text{o}}_{\text{T-bet}}$	Basal activation state of T-bet	-2
$\omega^{\text{o}}_{\text{GATA3}}$	Basal activation state of GATA3	-2
$\omega^{\text{o}}_{\text{RORγt}}$	Basal activation state of RORγt	-2
$\omega^{\text{o}}_{\text{Foxp3}}$	Basal activation state of Foxp3	-2
$\omega_{\text{T-bet}\to\text{T-bet}}$	Weight of autoactivation of T-bet	2
$\omega_{\text{GATA3}\to\text{GATA3}}$	Weight of autoactivation of GATA3	2
$\omega_{\text{RORγt}\to\text{RORγt}}$	Weight of autoactivation of RORγt	2
$\omega_{\text{Foxp3}\to\text{Foxp3}}$	Weight of autoactivation of Foxp3	2
$\omega_{\text{GATA3}\to\text{T-bet}}$	Weight of inhibition on T-bet by GATA3	-3.5
$\omega_{\text{RORγt}\to\text{T-bet}}$	Weight of inhibition on T-bet by RORγt	-1.5
$\omega_{\text{Foxp3}\to\text{T-bet}}$	Weight of inhibition on T-bet by Foxp3	-3.5
$\omega_{\text{T-bet}\to\text{GATA3}}$	Weight of inhibition on GATA3 by T-bet	-2.5
$\omega_{\text{RORγt}\to\text{GATA3}}$	Weight of inhibition on GATA3 by RORγt	-3.5
$\omega_{\text{Foxp3}\to\text{GATA3}}$	Weight of inhibition on GATA3 by Foxp3	-3.5

$\omega_{\text{T-bet}\rightarrow\text{RORγt}}$	Weight of inhibition on RORγt by T-bet	-0.3
$\omega_{\text{GATA3}\rightarrow\text{RORγt}}$	Weight of inhibition on RORγt by GATA3	-3.5
$\omega_{\text{Foxp3}\rightarrow\text{RORγt}}$	Weight of inhibition on RORγt by Foxp3	-3.5
$\omega_{\text{T–bet}\rightarrow\text{Foxp3}}$	Weight of inhibition on Foxp3 by T-bet	-3.5
$\omega_{\text{RORγt}\rightarrow\text{Foxp3}}$	Weight of inhibition on Foxp3 by RORγt	-3.5
$\omega_{\text{GATA3}\rightarrow\text{Foxp3}}$	Weight of inhibition on Foxp3 by GATA3	-3.5
$\omega_{\text{TCR}\rightarrow\text{T-bet}}$	Weight of activation on T-bet by S1	1
$\omega_{\text{TCR}\rightarrow\text{GATA3}}$	Weight of activation on GATA3 by S1	0.98
$\omega_{\text{TCR}\rightarrow\text{RORγt}}$	Weight of activation on RORγt by S1	0.3
$\omega_{\text{TCR}\rightarrow\text{Foxp3}}$	Weight of activation on Foxp3 by S1	0.3
$\omega_{\text{TGF-β}\rightarrow\text{T–bet}}$	Weight of inhibition on T-bet by TGF-β	-0.8
$\omega_{\text{TGFβ}\rightarrow\text{GATA3}}$	Weight of inhibition on GATA3 by TGF-β	-0.8
$\omega_{\text{TGFβ}\rightarrow\text{RORγt}}$	Weight of activation on RORγt by TGF-β	0.11
$\omega_{\text{TGF-β}\rightarrow\text{Foxp3}}$	Weight of activation on Foxp3 by TGF-β	0.15
$\omega_{\text{IL–1}\rightarrow\text{T-bet}}$	Weight of activation on T-bet by IL-1	0.18
$\omega_{\text{IL1}\rightarrow\text{RORγt}}$	Weight of activation on RORγt by IL-1	0.1
$\omega_{\text{IL–12}\rightarrow\text{T-bet}}$	Weight of activation on T-bet by IL-12	0.1
$\omega_{\text{IL–12}\rightarrow\text{GATA3}}$	Weight of inhibition on GATA3 by IL-12	-1
$\omega_{\text{IL–4}\rightarrow\text{T-bet}}$	Weight of inhibition on T-bet by IL-4	-1
$\omega_{\text{IL–4}\rightarrow\text{GATA3}}$	Weight of activation on GATA3 by IL-4	0.1
$\omega_{\text{IL6}\rightarrow\text{RORγt}}$	Weight of activation on RORγt by IL-6	0.03
$\omega_{\text{IL6}\rightarrow\text{Foxp3}}$	Weight of inhibition on Foxp3 by IL-6	-0.1
$\omega_{\text{ATRA}\rightarrow\text{RORγt}}$	Weight of inhibition on RORγt by ATRA	-1
$\omega_{\text{ATRA}\rightarrow\text{Foxp3}}$	Weight of activation on Foxp3 by ATRA	0.02
$\omega_{\text{IL23}\rightarrow\text{RORγt}}$	Weight of activation on RORγt by IL-23	0.03

CHAPTER 5

Dynamic influence of lipopolysaccharide on differentiation and proliferation of $CD4^+$ T cells under the inducing condition of induced regulatory T cells

(A manuscript in preparation)

Abstract

The antigen-presenting-cell-independent influence of lipopolysaccharide (LPS) on the $CD4^+$ T cell differentiation and proliferation has important implications on how endotoxin may modulate adaptive immune responses. To test this proposal, we examined the effects of varying dosages of LPS on T helper cell differentiation and proliferation *in vitro*. We observed that LPS inhibits the expression of Foxp3 under the inducing condition of iT_{Reg} cells**.** The timing of engagement of the LPS signal is critical for this suppressive effect. In addition, LPS promotes the proliferation of $CD4^+$ T cells under the same condition, but not under non-inducing conditions. These results give novel insights on how microbial products can directly change the profile of $CD4^+$ cells and skew the host adaptive immune system into a pro-inflammatory state.

Introduction

Lipopolysaccharide (LPS) is the major molecule constituting the outer membrane of Gram-negative bacteria [1]. When massively released into the host during the course of an infection, it acts as a potent virulence factor responsible for septic shock in mammals [2]. LPS is known to be sensed by toll-like receptor 4 (TLR4) expressed on the surface of antigen-presenting cells (APCs), such as dendritic cells and macrophages [3]. The activation of these innate immune cells elicits cytokine production and secretion, which in turn provokes the adaptive immune responses, including $CD4^+$ T cell activation, differentiation and proliferation [4]. Recent evidences indicate that TLR4 is also expressed by $CD4^+$ T cells [5-9]. However, less is known about the direct influence of LPS on $CD4^+$ T cell responses.

Activities of various subsets of $CD4^+$ T cells are important both for orchestrating the immune responses against pathogenic microorganisms and for controlling autoimmunity [10]. Particularly, a subset of $CD4^+$ T cells exhibiting characteristics of regulatory T cells, known as induced regulatory T (iT_{Reg}) cells, were shown to perform important modulating functions in the immune system [11,12]. A previous study has shown that LPS can directly promote the suppressive function of natural regulatory T (nT_{Reg}) cells and enhance their survival and proliferation [6], but it is unclear about the effect of LPS on iT_{Reg} cells, which may be functionally distinct from nT_{Reg} cells [12,13].

In this study, we show that LPS modulates, in a dose-dependent manner, the differentiation of iT_{Reg} cells by inhibiting the expression of Foxp3 in $CD4^+$ T cells. In the meantime, LPS also dose-dependently modulates the proliferation of T helper cells. These phenomena have important implications on how direct effects of endotoxin can break the balance between effector $CD4^+$ T cells and iT_{Reg} cells and the balance between nT_{Reg} cells and iT_{Reg} cells.

Methods

Isolation of naïve $CD4^+$ T cells and cell culture

Splenocytes from C57BCL/6 or 129/Sv mice were pooled, and T cells were purified using a $CD4^+$ T cell isolation kit (Miltenyi), then further sorted into naïve $CD4^+$ (i.e. $CD4^+CD62L^+$) cells with CD62L microbeads (Miltenyi). Naïve $CD4^+$Cells were cultured in wells of 96-well plates (2×10^5 cells/well) for 5 days in complete RPMI buffer (Sigma), with 5 μg/ml plate-coated anti-CD3 (eBioscience), 0.5 μg/ml anti-CD28 (eBioscience), 10 μg/ml anti-IFN (Bio X Cell), 10 μg/ml anti-IL4 (Bio X Cell), with or without 10 ng/ml recombinant human TGFβ (R&D systems), and 100 pg/ml, 10 ng/ml or 1 μg/ml LPS (Sigma).

Flow cytometry

All cells were fixed and permeabilized with fixation/permeabilization buffer (eBioscience). Intracellular staining was performed with Flow Cytometry Staining buffer containing FBS, and sodium azide (0.09%) (eBioscience), and PE-conjugated Foxp3 antibody (eBioscience). Cells were analyzed with FACSCanto (BD Biosciences), and data were analyzed with FCM flow cytometry analysis library. The total number of T cells in the culture was measured with AccuCheck Counting Beads (Invitrogen).

Statistical test

All experiments were carried out at least 3 times, and all the results were reported as means ± standard errors. Statistical analysis was done using two-tailed unpaired Student's t test. Significance was defined when P values were <0.05.

Results

LPS inhibits iT_{Reg} differentiation in a dose-dependent manner

In the presence of TGF-β, a majority of naïve $CD4^+$ cells became Foxp3-positive after 5-day incubation (Figure 1A and B), and this observation is in agreement of previous studies [14,15]. In order to examine whether LPS has significant effects on the differentiation of iT_{Reg} cells, we induced iT_{Reg} differentiation with or without various doses of LPS (10ng/ml and 1μg/ml). After 5-day incubation, cells with high dose LPS (1μg/ml) have significantly lower percentages of $Foxp3^+$ cells (Figure 1C), whereas low dose LPS (10ng/ml) did not have a significant effect on the percentages of $Foxp3^+$ cells upon the induction by TGF-β (Figure 1D).

Simultaneous engagement of LPS signaling and the TCR/TGFβ signaling is important for the suppressive effect of LPS

We next examined the importance of the timing of LPS treatment on the inhibition of iT_{Reg} differentiation. Neither pre-treatment of high-dose LPS 6-hour before induction nor post-treatment of high-dose LPS 1-day after the induction had significant effect on the percentages of $Foxp3^+$ cells (Figure 2). This suggests that the simultaneous engagement of LPS signaling and TCR/TGFβ signaling is important for the suppressive effect of LPS on iT_{Reg} differentiation.

The suppressive effect of LPS is more pronounced when the TGF-β is removed from the media after differentiating the cells for two days

To examine how the time course of differentiation signal TGF-β can influence the suppressive effect of LPS, we incubated cells for 2 days in TGF-β plus LPS, and then re-suspended the cells in TGF-β-free

media, keeping the LPS concentration constant. When TGF-β was removed from the media, the frequency of $Foxp3^+$ cells was not reduced in the LPS-free or low-dose LPS conditions, but high-dose LPS had much more pronounced suppressive effect on the percentages of the $Foxp3^+$ cells in the populations (Figure 3, yellow bars, compare left panel and middle panel). This suggests that the suppressive effect of LPS on iT_{Reg} differentiation might be sensitive to the concentrations of the TGF-β throughout the inhibition process, even though the presence TGF-β is not important for the iT_{Reg} differentiation after the initial induction of the differentiation. Additionally, when the cells were transferred to wells without anti-CD3 after 2-day incubation, the suppressive effect of LPS is significant, but not as pronounced as in the TGF-β free condition in wells with anti-CD3 (Figure 3, yellow bars, right panel).

High-dose LPS may promote $CD4^+$ T cell proliferation under iT_{Reg} inducing condition, but not under non-inducing condition

We next examined whether LPS can affect $CD4^+$ T cell proliferation under iT_{Reg} inducing condition. As shown in Figure 3 and Figure 4, high-dose LPS significantly increased the frequency (Figure 3, red bars) and the total number (Figure 4, red bars) of live cells under iT_{Reg} inducing condition. However, when the naïve $CD4^+$ T cells were incubated in high-dose LPS under non-inducing condition, there is no significant change on the total number of live cells (Figure 4).

Effect of LPS on iT_{Reg} cell proliferation may be independent of its suppressive effect on Foxp3 expression.

To show if the observed effects of LPS on iT_{Reg} differentiation and proliferation are correlated, we used the splenocytes from129/Sv mice. Consistent with the previous observation with C57BL/6 mice, LPS increased the total number of the $CD4^+$ cells. However, no significant change in the frequency of Foxp3

expressing cells was observed with 129 mice (Figure 5). This suggests that the effect of LPS on iT_{Reg} proliferation may be independent of its suppressive effect of Foxp3 expression.

Discussion

Although regulation of $CD4^+$ T cells by LPS has been previously considered to be dependent on antigen-presenting cells (APCs) [16], recent evidences and this study suggest that LPS can directly influence the differentiation and proliferation of $CD4^+$ T cells in the absence of APCs. Particularly, we found that LPS directly inhibit the expression of Foxp3 in TCR-activated $CD4^+$ T cells. Consequently, even though LPS enhanced $CD4^+$ T cell proliferation, it did not increase the number of $Foxp3^+$ cells (Figure 3 and Figure 4). Caramalho et al. previously demonstrated that LPS promotes the suppressive activity and the survival/proliferation of nT_{Reg} cells [6]. Our finding implies that the effect of LPS on iT_{Reg} cells may be distinct from nT_{Reg} cells, in that LPS may enhance nT_{Reg} activity but inhibit iT_{Reg} activity. Given the possible functional differences of these two types of cells [13], the study suggests one possible way in which microbial products can break the balance of the adaptive immune system in an early stage of inflammation.

It has been demonstrated that low-dose LPS has significant influence on the activation of macrophages [17]. In contrast, the doses of LPS as low as picogram range failed to show significant effect on the Foxp3 expression or the proliferation of $CD4^+$T cells under iT_{Reg} inducing condition. Given the influence of APC activation on $CD4^+$ T cells, these results suggest that of LPS may play a key dose-dependent role in the differential APC-dependent and APC-independent modulation of $CD4^+$ T cells.

Our results also indicate that the timing of the engagement of the LPS signal is critical for its inhibitory activity on Foxp3 expression. This might be because LPS treatment is most effective in early stages of the differentiation process. Interestingly, although TLR4 expression is found in naïve $CD4^+$ T cells, its cell surface expression only occurs in activated $CD4^+$ T cells [18], indicating significant variations of the capability for the cells to process LPS signals during the course of differentiation.

The proliferation of cells was examined by measurements of cell numbers in our study. It would be beneficial to confirm this observation by CFSE assay for the measurement of proliferation rate. In order

to dissect the effects on cell proliferation and survival, it would also be informative to pinpoint the rate of apoptosis of the cells during the course of LPS treatment. In addition, we found that LPS enhanced the proliferation of activated $CD4^+$ T cells, but not of the $Foxp3^+$ cells, suggesting the possibility that LPS may promote the proliferation of other subsets of $CD4^+$ T cells in the presence of TGFβ, so it would be interesting to test if LPS can enhance the proliferation of those T helper cells, especially T_H17, which requires TGF-β for its differentiation.

References

1. Raetz CR, Reynolds CM, Trent MS, Bishop RE (2007) Lipid A modification systems in gram-negative bacteria. Annu Rev Biochem 76: 295-329.

2. Seydel U, Hawkins L, Schromm AB, Heine H, Scheel O, et al. (2003) The generalized endotoxic principle. Eur J Immunol 33: 1586-1592.

3. Akira S, Hemmi H (2003) Recognition of pathogen-associated molecular patterns by TLR family. Immunol Lett 85: 85-95.

4. Iwasaki A, Medzhitov R (2004) Toll-like receptor control of the adaptive immune responses. Nat Immunol 5: 987-995.

5. Kabelitz D (2007) Expression and function of Toll-like receptors in T lymphocytes. Curr Opin Immunol 19: 39-45.

6. Caramalho I, Lopes-Carvalho T, Ostler D, Zelenay S, Haury M, et al. (2003) Regulatory T cells selectively express toll-like receptors and are activated by lipopolysaccharide. J Exp Med 197: 403-411.

7. Gelman AE, Zhang J, Choi Y, Turka LA (2004) Toll-like receptor ligands directly promote activated CD4+ T cell survival. J Immunol 172: 6065-6073.

8. Fukata M, Breglio K, Chen A, Vamadevan AS, Goo T, et al. (2008) The myeloid differentiation factor 88 (MyD88) is required for CD4+ T cell effector function in a murine model of inflammatory bowel disease. J Immunol 180: 1886-1894.

9. Tomita T, Kanai T, Fujii T, Nemoto Y, Okamoto R, et al. (2008) MyD88-dependent pathway in T cells directly modulates the expansion of colitogenic CD4+ T cells in chronic colitis. J Immunol 180: 5291-5299.

10. Zhu J, Paul WE (2008) CD4 T cells: fates, functions, and faults. Blood 112: 1557-1569.

11. DiPaolo RJ, Brinster C, Davidson TS, Andersson J, Glass D, et al. (2007) Autoantigen-specific TGFbeta-induced Foxp3+ regulatory T cells prevent autoimmunity by inhibiting dendritic cells from activating autoreactive T cells. J Immunol 179: 4685-4693.

12. Wen K, Li G, Yang X, Bui T, Bai M, et al. (2012) CD4+ CD25- FoxP3+ regulatory cells are the predominant responding regulatory T cells after human rotavirus infection or vaccination in gnotobiotic pigs. Immunology 137: 160-171.

13. Curotto de Lafaille MA, Lafaille JJ (2009) Natural and adaptive foxp3+ regulatory T cells: more of the same or a division of labor? Immunity 30: 626-635.

14. Chen W, Jin W, Hardegen N, Lei KJ, Li L, et al. (2003) Conversion of peripheral CD4+CD25- naive T cells to CD4+CD25+ regulatory T cells by TGF-beta induction of transcription factor Foxp3. J Exp Med 198: 1875-1886.

15. Zhou L, Lopes JE, Chong MMW, Ivanov II, Min R, et al. (2008) TGF-beta-induced Foxp3 inhibits T(H)17 cell differentiation by antagonizing RORgammat function. Nature 453: 236-240.

16. Tough DF, Sun S, Sprent J (1997) T cell stimulation in vivo by lipopolysaccharide (LPS). J Exp Med 185: 2089-2094.

17. Glaros TG, Chang S, Gilliam EA, Maitra U, Deng H, et al. (2013) Causes and consequences of low grade endotoxemia and inflammatory diseases. Front Biosci (Schol Ed) 5: 754-765.

18. Komai-Koma M, Jones L, Ogg GS, Xu D, Liew FY (2004) TLR2 is expressed on activated T cells as a costimulatory receptor. Proc Natl Acad Sci U S A 101: 3029-3034.

Figure Legends

Figure 1. High dose of LPS inhibits iT_{Reg} differentiation. Naïve $CD4^+$ Cells were stimulated with 5 μg/ml plate-coated anti-CD3, 0.5μg/ml anti-CD28, 10 μg/ml anti-IFN , 10 μg/ml anti-IL4, with or without 10 ng/ml recombinant human TGFβ and 10 ng/ml or 1μg/ml LPS. Frequency of Fopx3+ cells were counted with respect to the total number of live T cells analyzed in a flow cytometry experiment. **A-D**: histograms of the PE-Foxp3 channel. Vertical lines are the gating threshold.

Figure 2 Simultaneous engagement of LPS signaling and the TCR/TGFβ signaling is important for the suppressive effect of LPS. Naïve $CD4^+$ Cells were stimulated with 5 μg/ml plate-coated anti-CD3, 0.5μg/ml anti-CD28, 10 μg/ml anti-IFN, 10 μg/ml anti-IL4, with or without 10 ng/ml recombinant human TGFβ and 1μg/ml LPS. For the post-treatment group, LPS was added to the media 24 hours after the start of the incubation. For the pre-treatment group, cells were incubated with LPS 6 hours prior to incubation with other stimulants. Frequency of $Fopx3^+$ cells were counted with respect to the total number of live T cells analyzed in a flow cytometry experiment.

Figure 3 The suppressive effect of LPS is more pronounced when the TGF-β is removed from the media after differentiating the cells for two days. Naïve $CD4^+$ Cells were stimulated with 5 μg/ml plate-coated anti-CD3, 0.5μg/ml anti-CD28, 10 μg/ml anti-IFN, 10 μg/ml anti-IL4, with or without 10 ng/ml recombinant human TGFβ and 100 pg/ml, 10 ng/ml or 1μg/ml LPS for 2 days. Left panel: cells were subsequently re-suspended in media containing the same stimulants as those in the start media and incubated for additional 3 days. Middle panel: cells were subsequently re-suspended in media without TGF-β and incubated for additional 3 days. Right panel: cells were subsequently re-suspended in media

without TGF-β, transferred to wells without plate-bound anti-CD3 and incubated for additional 3 days. Frequency of Fopx3$^+$ cells was calculated with respect to the total number of live T cells analyzed in a flow cytometry experiment. Frequency of live T cells was calculated with respect to the total number of events of the flow cytometry analysis.

Figure 4 High dose LPS may promote CD4$^+$ T cell proliferation under iT$_{Reg}$ inducing condition, but not under non-inducing condition. Naïve CD4$^+$ Cells were stimulated with 5 μg/ml plate-coated anti-CD3, 0.5 μg/ml anti-CD28, 10 μg/ml anti-IFN, 10 μg/ml anti-IL4, with or without 10 ng/ml recombinant human TGFβ and/or 1 μg/ml LPS. Frequency of Fopx3$^+$ cells were counted with respect to the total number of live T cells analyzed in a flow cytometry experiment. The total numbers of cells in the wells were measured by AccuCheckcounting beads.

Figure 5 Effect of LPS on iT$_{Reg}$ cell proliferation may be independent of its suppressive effect on Foxp3 expression. Naïve CD4$^+$ Cells from 129/Sv mice were stimulated with 5 μg/ml plate-coated anti-CD3, 0.5 μg/ml anti-CD28, 10 μg/ml anti-IFN, 10 μg/ml anti-IL4, with or without 10 ng/ml recombinant human TGFβ and/or 1 μg/ml LPS. Frequency of Fopx3$^+$ cells were counted with respect to the total number of live T cells analyzed in a flow cytometry experiment. The total numbers of cells in the wells were measured by AccuCheck counting beads.

Figures

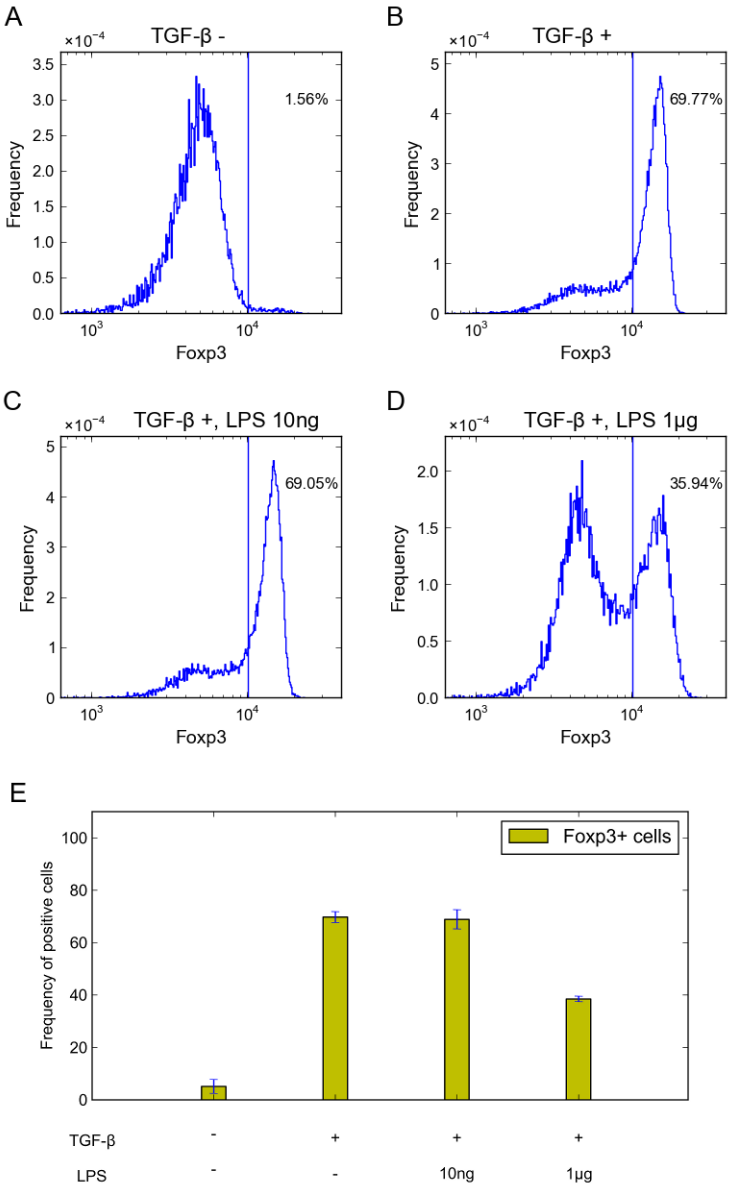

Figure 1. High dose of LPS inhibits iT_{Reg} differentiation

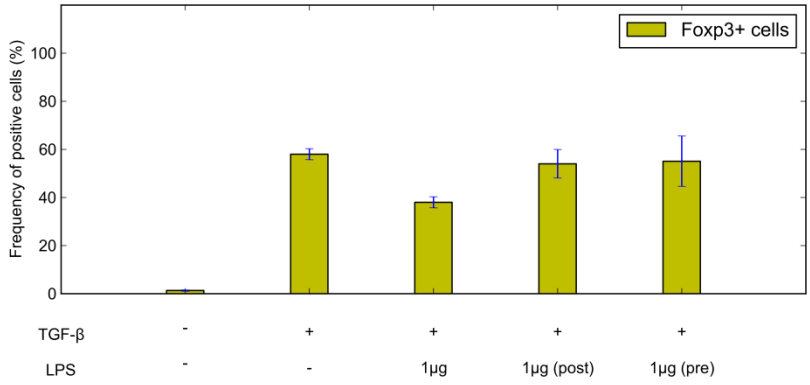

Figure 2. Simultaneous engagement of LPS signaling and the TCR/TGFβ signaling is important for the suppressive effect of LPS

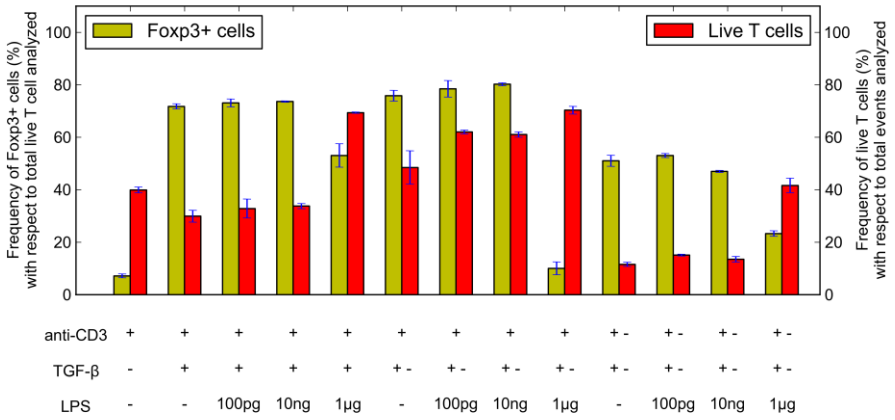

Figure 3. The suppressive effect of LPS is more pronounced when the TGF-β is removed from the media after differentiating the cells for two days

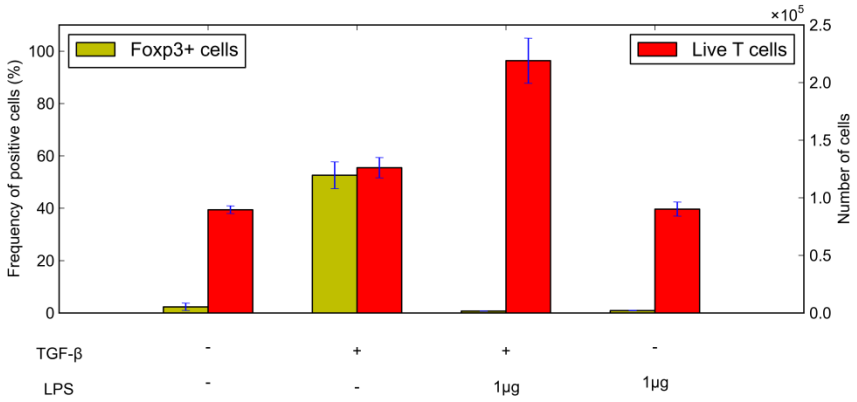

Figure 4. High dose LPS may promote $CD4^+$ T cell proliferation under iT_{Reg} inducing condition, but not under non-inducing condition

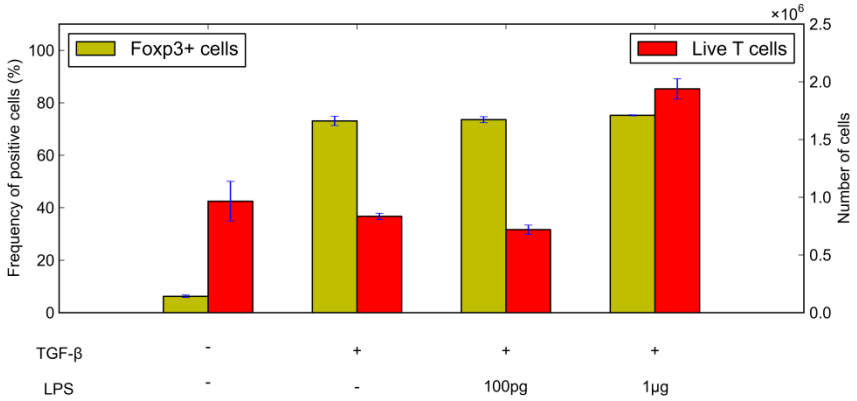

Figure 5. Effect of LPS on iT_{Reg} cell proliferation may be independent of its suppressive effect on Foxp3 expression

CHAPTER 6

Conclusions

Understanding how $CD4^+$ T cells differentiate is critical to unravel the mysteries of how the entire immune system is regulated. However, the diversity and plasticity of $CD4^+$ T cells, together with their complex signaling pathways, render it difficult to understand and study these cells. Therefore, new experimental results and theoretical analysis are needed to advance this field.

We first took a systems-approach to answer the question of how $CD4^+$ T cells diversify in the response to pathogenic challenges. In Chapter 2, we presented a mathematical model of T_H17-iT_{Reg} differentiation, in which three phenotypes of cells can be heterogeneously differentiated from a population of naïve $CD4^+$ T cells. The model suggests that mutual inhibition between the two master regulators and the underlying pitchfork bifurcation may be responsible for this type of phenomena. In Chapter 3, we demonstrated that a simple signaling network motif can be responsible for generating all possible types of heterogeneous populations with respect to a pair of master regulators controlling $CD4^+$ T cell differentiation. The motif involves the mutual inhibition between two master regulators, the auto-activation of these regulators, and various signals that can influence the expression of the two regulators. In Chapter 4, we presented a framework that can help to study heterogeneous differentiation involving more than two master regulators. The framework enables us to analyze multi-stability behavior in high dimensions. We used the framework to analyze generic networks with more than one interconnected mutual inhibition motifs and build a model that includes four master regulators of $CD4^+$ T cells. These studies provide a mathematical basis for how naïve $CD4^+$ T cells can integrate multiple types of signals to differentiate into populations of diverse phenotypes with the intrinsic dynamic properties governed by their signaling pathways.

The predictions of these models need to be validated experimentally in future works. All predictions we made are under testable *in vitro* conditions, and the experimental results obtained can be used for further optimization of the models. The framework presented here take us one step further towards linking a model of intracellular signaling pathways to the models of populations of immune cells. However, in order to make the mathematical models more realistic for simulating the immune system, we have to take a few more factors into account. First, intercellular communication has to be considered. This includes not only the cross-talk among $CD4^+$ T cells but also communication between $CD4^+$ T cells and other immune cells, such as dendritic cells, $CD8^+$ T cells and macrophages. To model the intercellular communication, experimental data on the extracellular concentrations of cytokines are necessary. Secondly, cell death and proliferation have to be considered, because regulation of cell death and proliferation is critical to maintain the homeostasis of immune system. The rate of cell death and proliferation for each phenotypes under different conditions have to be estimated in order to build a reasonable model. Thirdly, spatial dynamics of immune cells and pathogens have to be considered. The spatial distribution and movement of the immune cells and pathogens are important when we need to understand the progression of a pathogenic event or different types of immune disease. All these extensions can be achieved by scaling up our ODE models except perhaps the consideration of cell movement. It is more feasible to use agent-based modeling strategy to simulate the cell movement, so coupling of ODE models and agent-based models may be needed for simulating the immune system with all these factors included. Our current models are useful for predicting how genetic variations or external perturbations can affect population of $CD4^+$ T cells. When the additional factors are considered, we will be able to use mathematical models to predict the outcome of perturbations in the scope of the entire immune system and suggest possible ways to overcome the immune diseases.

In addition to the mathematical models for heterogeneous differentiation, we asked how LPS can influence the differentiation of $CD4^+$ T cells. In Chapter 5, we showed that LPS modulates the differentiation of iT_{Reg} cells by inhibiting the expression of Foxp3 in $CD4^+$ T cells under iT_{Reg} inducing

condition. LPS also enhances the proliferation of $CD4^+$ T cells under this condition. These phenomena imply that endotoxin can break the balance between effector CD4+ T cells and iT_{Reg} cells and that between nT_{Reg} cells and iT_{Reg} cells in a direct manner. Identification of key signaling molecules involved in these behaviors is warranted in future studies.